RL-TR-91-369
Final Technical Report
December 1991

FIBER OPTIC BASED SIGNAL PROCESSING

PCO Inc.

Dr. Bor U. Chen, et al.

APPROVED FOR PUBLIC RELEASE; DISTRIBUTION UNLIMITED.

Rome Laboratory
Air Force Systems Command
Griffiss Air Force Base, NY 13441-5700

This report has been reviewed by the Rome Laboratory Public Affairs Office (PA) and is releasable to the National Technical Information Service (NTIS). At NTIS it will be releasable to the general public, including foreign nations.

RL-TR-91-369 has been reviewed and is approved for publication.

APPROVED: Paul Sierak

PAUL F. SIERAK
Project Engineer

FOR THE COMMANDER: John A. Graniero

JOHN A. GRANIERO
Technical Director
Directorate of Communications

If your address has changed or if you wish to be removed from the Rome Laboratory mailing list, or if the addressee is no longer employed by your organization, please notify RL(C3DB) Griffiss AFB, NY 13441-5700. This will assist us in maintaining a current mailing list.

Do not return copies of this report unless contractual obligations or notices on a specific document require that it be returned.

REPORT DOCUMENTATION PAGE

Form Approved
OMB No. 0704-0188

1. AGENCY USE ONLY (Leave Blank)	2. REPORT DATE	3. REPORT TYPE AND DATES COVERED
	December 1991	Final Jun 85 - Apr 91

4. TITLE AND SUBTITLE
FIBER OPTIC BASED SIGNAL PROCESSING

5. FUNDING NUMBERS
C - F30602-87-C-0015
PE - 62702F
PR - 4519
TA - 21
WU - 71

6. AUTHOR(S)
Dr. Bor U. Chen, et al.

7. PERFORMING ORGANIZATION NAME(S) AND ADDRESS(ES)
PCO Inc.
20200 Sunburst Street
Chatsworth CA 91311-6289

8. PERFORMING ORGANIZATION REPORT NUMBER
N/A

9. SPONSORING/MONITORING AGENCY NAME(S) AND ADDRESS(ES)
Rome Laboratory (C3DB)
Griffiss AFB NY 13441-5700

10. SPONSORING/MONITORING AGENCY REPORT NUMBER
RL-TR-91-369

11. SUPPLEMENTARY NOTES
Rome Laboratory Project Engineer: Paul F. Sierak/C3DB/(315) 330-4092

12a. DISTRIBUTION/AVAILABILITY STATEMENT
Approved for public release; distribution unlimited.

12b. DISTRIBUTION CODE

13. ABSTRACT (Maximum 200 words)

The objective of this project was to determine the theoretical performance and design latitude available from optical fiber based signal processors in accomplishing filtering, coded sequence generation, and matrix multiplication functions. Towards this goal the contractor has completed the study, design, fabrication and testing aspects of the coded sequence generator. The study and design facets of the filter and matrix multiplier functions also have been accomplished but the fabrication and testing aspects of the processors have not been done. This report extends the art of fiber based signal processors, points the way towards further work and has produced a significant patent (included) and numerous open literature publications.

14. SUBJECT TERMS	15. NUMBER OF PAGES
Fiber Optics, Signal Processing, Filters, Coded Signal Generator, Matrix/Vector Multipliers	198
	16. PRICE CODE

17. SECURITY CLASSIFICATION OF REPORT	18. SECURITY CLASSIFICATION OF THIS PAGE	19. SECURITY CLASSIFICATION OF ABSTRACT	20. LIMITATION OF ABSTRACT
UNCLASSIFIED	UNCLASSIFIED	UNCLASSIFIED	UL

TABLE OF CONTENTS

1.0 INTRODUCTION AND SUMMARY
- 1.1 Introduction and Background
- 1.2 Summary

2.0 THEORETICAL PERFORMANCE ASSESSMENT
- 2.1 Frequency Domain Functions
  - 2.1.1 Band-Pass Filter
    - 2.1.1.1 Tapped Transversal Filter
    - 2.1.1.2 Non-Recirculating Feed-Forward Lattice Filter
    - 2.1.1.3 Recirculating Feed-Backward Lattice Filter
    - 2.1.1.4 Cascaded Transversal Filter
    - 2.1.1.5 Cascaded Recirculating Filter
    - 2.1.1.6 Comparison
  - 2.1.2 Notch Filter
    - 2.1.2.1 Tapped Transversal Filter
    - 2.1.2.2 Recirculating Filter
    - 2.1.2.3 Non-Recirculating Lattice Filter
    - 2.1.2.4 Recirculating Lattice Filter
- 2.2 Time Domain Functions
  - 2.2.1 Coded Sequence Generator
    - 2.2.1.1 Single Tapped Delay Line
    - 2.2.1.2 Non-Recirculating Lattice
    - 2.2.1.3 Recirculating Lattice
  - 2.2.2 Matched Filter
- 2.3 Numerical Functions
  - 2.3.1 Matrix-Vector Multiplier
    - 2.3.1.1 Recirculating Lattice
    - 2.3.1.2 Non-Recirculating Lattice
    - 2.3.1.3 Recommended Structure
  - 2.3.2 Matrix-Matrix Multiplication
    - 2.3.2.1 Recirculating Lattice
    - 2.3.2.2 Non-Recirculating Lattice
    - 2.3.2.3 2-Dimensional Lattice
    - 2.3.2.4 WDM Techniques
- 2.4 Summary of Theoretical Performance Assessment

3.0 REALIZABLE PERFORMANCE ASSESSMENT
- 3.1 Frequency Response
- 3.2 Center Frequency
- 3.3 Pass-Band Width
- 3.4 Quality Factor
- 3.5 Dynamic Range

TABLE OF CONTENTS (cont.)

3.6 Power Budget
3.6.1 Power Conserving Configurations
3.6.2 Power Discarding Configurations
3.7 Noise Performance
3.8 Programmability
3.8.1 Tap Separation
3.8.2 Tap Strength
3.8.3 Tap Number
3.9 Summary of Realizable Performance Assessment

4.0 KEY COMPONENT CHARACTERIZATION
4.1 Fibers
4.2 Couplers and Taps
4.3 Polarization Control Components
4.4 Wavelength Selective Components
4.5 External Modulators
4.6 Spatial Light Modulators

5.0 COMPONENT BREADBOARDING
5.1 Component Design Specifications
5.2 Component Test Plan
5.3 Component Test Verification

6.0 PROCESSOR DESIGN/PLAN
6.1 Band-Pass Filter
6.1.1 Architecture
6.1.2 Predicted Performance
6.2 Coded Sequence Generator
6.2.1 Architecture
6.2.2 Predicted Performance
6.3 Matrix-Vector Multiplier
6.3.1 Architecture
6.3.2 Predicted Performance

7.0 SYSTEM BREADBOARD EXPERIMENT
7.1 Test Results -- Coded Sequence Generator

TABLE OF CONTENTS (cont.)

APPENDIX A BIBLIOGRAPHY OF FIBER OPTIC SIGNAL PROCESSING

APPENDIX B CALCULATION OF FILTER CHARACTERISTICS

APPENDIX C CASCADED RECIRCULATING TRANSMISSION LINE WITHOUT BENDING LOSS LIMITATIONS (PATENT NO. 4,934,777)

APPENDIX D CHARACTERIZATION STUDY OF OPTICAL FIBERS

APPENDIX E COMPONENT TEST RESULTS

APPENDIX F CODED SEQUENCE GENERATOR - SYSTEM TEST REPORT

APPENDIX G CODED SEQUENCE GENERATOR - OPERATING INSTRUCTIONS AND USER'S NOTES

1.0 INTRODUCTION AND SUMMARY

Fiber Optic Based Signal Processing (Contract No. F 30602-87-C-0015) is a study program with the objective of determining the theoretical performance and design latitude available from optical fiber based signal processors in accomplishing filtering, coded sequence generation, and matrix multiplication functions. To verify the design objectives, three separate processors will be constructed using commercially available components and necessary key components to be developed under this program.

The technical effort is divided into five major tasks. Task 1 (Statement-of-Work, SOW 4.1.1) is to conduct a study of the theoretical performance available from optical fiber based signal processors in accomplishing filtering, coded sequence generation, and matrix multiplication functions. Task 2 is to delineate the realizable performance of processing functions using available optical componentry and to determine the implementation latitude of each of the signal processing functions, given presently available optical componentry. Task 3 (SOW 4.1.3) is to identify key componentry improvements that have potential for significant impact on fiber based signal processor performance. The key componentry identified

in Task 3 will be breadboarded to verify the feasibility in Task 4 (SOW 4.1.3.1). Task 5 (SOW 4.1.4, 4.1.5, and 4.1.6) is to design and investigate through breadboarding three separate models of fiber optic based signal processors to accomplish individually the functions of filtering, coded sequence generation, and matrix multiplications. The test results will be compared with the designed specifications.

1.1 INTRODUCTION AND BACKGROUND

Electric signal processing techniques are effective below frequencies of 1 to 2 GHz but are of limited applicability at higher frequencies. The emergence of optical fiber technology has resulted in the evolution of a number of fiber based applications, not all of which are directly related to optical communications as originally perceived. For example, single mode fiber is an excellent frequency-independent delay medium (0.2 km/μs), with demonstrated modulation bandwidth (>100 GHz.km) and low loss (<0.2 dB/km). As a result, it can form the basis for signal processing elements offering an order of magnitude increase in bandwidth over electric devices. Signal processing devices based on optical fiber are schematically, structurally, and operationally similar to their electrical counterparts. Their design, architectures, and analysis are

also essentially equivalent. The principal differences in a fiber optic based architecture are the intensity summation inherent in its basic incoherent delay line structure and its positivity.

Using basic tapped and recirculating delay lines, together with more complex feed-forward and feed-backward lattices, a range of processing operations have already been demonstrated. Tapped delay line has been used for basic transversal frequency filtering operations at frequencies around 1 GHz and for time domain operations (convolution, correlation, matched filter and coded sequence generation) at speeds around 1 Gbit/s. Recirculating delay lines are capable of temporary data storage and data rate transformations and have been demonstrated as frequency filters around 1 GHz. Fiber-lattice structures have performed as Toeplitz matrix multipliers at 100 MHz and as broad-band filters at frequencies in excess of 1 GHz.

Extension to frequencies of 10 GHz and above are straightforward in principle. Unfortunately, all systems demonstrated to date have operated at frequencies much lower than expected. In practice, higher frequencies require the

use of shorter fiber lengths, more compact designs, and faster opto-electronic interfaces. In addition, bending loss of the fiber places a lower limit on the loop length in recirculated structures, which in turn places a limit on the frequency of operation. The quality factor and sidelobe level performances in Finite Impulse Response systems are also limited by the number of feasible taps and stages. Therefore, to operate at higher speeds alternative architectures and low loss components must be developed. Additionally, the use of switchable components may expand the capabilities of processors by using functional programmability. More general matrix multiplication may also be implemented by the use of such components.

1.2 SUMMARY

Detailed discussion on the accomplishment of program Tasks is reported in Section 2 through Section 7. There are a number of significant contributions achieved under this program.

This program provided, for the first time, an organized and thorough study of fiber optic based signal processors. The theoretical performance and design latitude available for processing functions of filtering, coded sequence generation,

and matrix multiplication were investigated. As a result of the study, comprehensive Component and System Design Plans were generated. Three separate processors were designed to perform the following functions:

- Band-pass filtering at 4.75 GHz center frequency with simultaneous high quality factor and low sidelobe level.
- Adjustable 4 bit coded sequence generation at 2 Gbit/s pulse rate.
- Matrix-vector multiplication with a general 2 x 2 matrix at 0.5 Gbit/s rate.

The major limiting factor in extending processor performance is the upper frequency limit imposed by bend loss considerations in small diameter fiber loops. The problem can be overcome by an invention conceived during the performance of this program. A patent entitled "Cascaded Recirculating Transmission Line Without Bending Loss Limitation," Number 4,934,777, was awarded.

A range of novel optical fiber and waveguide directional coupler components has been developed under this program. These couplers are suitable for incorporation in a variety of

optical tapped delay line signal processing system configurations. Components developed included polished polarization-maintaining couplers fabricated in high-birefringence fiber and high speed switched $LiNbO_3$ couplers. The polished polarization maintaining couplers fabricated exhibit polarization extinction comparable with or superior to that available from state-of-the-art components. The high speed switch $LiNbO_3$ couplers can be used for processor applications requiring high speed reconfiguration of coupling parameters. The component breadboarding phase of the program has confirmed the feasibility of manufacture of monolithic arrays of evanescent wave coupler elements with uniform characteristics, suitable for the assembly of multi-stage processor systems, and has resulted in the derivation of a novel fabrication topology for recursive lattice structures, permitting assembly of superficially asymmetric structures from two identical elements.

The breadboard system of 4 bit coded sequence generator at 1 Gbit/s pulse rate exhibits performance in excellent agreement with design requirement. The quasi-monolithic construction approach adopted in this case represents a new departure for multiple coupler assemblies, permitting manufacture of

multiple individual coupler elements on a single fiber length at separations considerably less than the mechanical dimensions of an individual mechanical assembly. An output pulse repetition rate of 2 GHz has been demonstrated here, based on an incremental fiber delay length of 103 mm. This dimension is obviously capable of significant further reduction. Given current technology, it appears perfectly feasible to reduce the incremental delay by a factor of 10 , to the order of 10 mm, giving an output pulse repetition rate of 20 GHz.

The breadboarding work for band-pass filter and matrix-vector multiplier, however, suffered from a number of setbacks. First, the 4.75 GHz transmitter and receiver pair required for the characterization of band-pass filter was not available to PCO from the government. The technical process was further jeopardized by the leave of a key technical staff member, who was the only qualified person at PCO to complete the experiment. At that time, PCO had already incurred costs of engineering/technician hours more than the contract provided. As a result, the breadboarding working for band-pass filter and matrix-vector multiplier was suspended.

2.0 THEORETICAL PERFORMANCE ASSESSMENT

The objective of this task is to conduct a study to determine the theoretical performance relationships which characterize optical fiber based signal processors in accomplishing the following six signal processing functions: band-pass filter, notch or comb filter, matched filter, coded sequence generator, matrix-vector multiplier, and matrix-matrix multiplier. Under this Task, we have conducted an extensive literature survey covering fiber optical processors in these six categories. More than 250 published papers were identified and reviewed. A list of most significant publications related to this program is listed in Appendix A. Most of these papers dealing with these and related subjects are generally component oriented. The survey has resulted in the collation of significant bibliography on the subject, with a subject breakdown as follows:

General Signal Processing Theory	56
Band-Pass Filter	22
Notch Filter	13
Matched Filter/Correlator	18
Coded Sequence Generator	17
Matrix Operations	17
Noise	10

Optical Fiber	20
Fiber Modulator	14
Fiber Coupler/Tap	34
Miscellaneous Techniques	27

Fiber optical processors can be configured to be "recursive" (or "feed-backward") or "non-recursive" (or "feed-forward"). For recursive type processors, signals tapped from the main fiber path are returned to the earlier stages of the process. On the other hand, tapped signals for non-recursive processors can only propagate in the forward direction. More complicated structures using combination of recursive and non-recursive processor have also been demonstrated. Processors based on fiber optic delay line structure exhibit either finite impulse response (FIR) or infinite impulse response (IIR) depending on whether a single input impulse generates a finite or infinite output pulse train. Recursive systems are inherently IIR.

A number of fiber optical technological approaches to the processor design have been identified. Each of these technological approaches has its characteristic advantages and limitations, which must be considered in the processor system

design. As a result of the literature survey, a matrix of signal processing functions and available fiber optic technologies is generated Table 2.1. "*" is used to indicate that the specific fiber optical technology can be used to realize the signal processing functions listed. "?" is used to indicate that the possibility exists to use the fiber optical technology to demonstrate certain signal processing functions.

FIBER OPTICAL TECHNOLOGY	BAND-PASS FILTER	NOTCH/ COMB FILTER	MATCHED FILTER	CODE GEN.	M-V MULT.	M-M MULT.
Tapped D.L. FIR	*	*	*	*	?	
Fiber Bundle FIR	*	?	*	*	?	
Phase Mod. Tap FIR	*	*	?	?	?	
Recirc. Delay L IIR	?	*				
Non Rec. 1D Latt FIR	*	?		?	?	
Rec. 1D Latt IIR	*	*	*	*	*	
Mixed 1D Latt IIR						
Non Rec. 2D Latt FIR						?
Rec. 2D Latt IIR						*
Mixed 2D Latt IIR						?
Star Coupler FIR	*	?	?	?	?	
Concat. Bundle FIR	*	?	?	?	?	

TABLE 2.1.

SIGNAL PROCESSING FUNCTIONS
AND AVAILABLE FIBER OPTIC TECHNOLOGIES

Based on the technology/function matrix, theoretical models have been identified and/or derived. The six signal processing functions identified in SOW 4.1.1 can be categorized into three groups: frequency domain functions, time domain functions, and numerical processors. Band-pass filter and notch or comb filter are in the frequency domain. Coded sequence generator and matched filter are in the time domain. The matrix-vector multiplier and matrix-matrix multipliers are numerical processors.

2.1 FREQUENCY DOMAIN FUNCTIONS

2.1.1 BAND-PASS FILTER

Band-pass Filter response can be achieved via a number of alternative architectures. The resultant devices can, however, be characterized in common terms. The fundamental parameter is frequency response, i.e., the complex transfer function relating output to input as a function of frequency. For digital systems, where signals propagate with well-defined time delays, frequency response can be obtained from the Fourier transform of the impulse response. In most cases considered during this study, this function can be obtained in analytical form with functional dependence on structural

parameters; analytic expressions for frequency response in terms of system parameters were collated in the May 1987 monthly report. From the frequency response, other parameters such as dynamic range, quality factor, power efficiency, and sidelobe ratio of any filter can generally be obtained.

Filter architectures are discussed in the System Design Plan, which was submitted and approved as part of the contract requirement, CDRL-A004. The general conclusions are summarized here.

2.1.1.1 TAPPED TRANSVERSAL FILTER

Fig. 2.1 shows the basic structure of a tapped transversal filter. The unweighted tapped transversal filter, with $W_1=W_2=...W_N$, exhibits a characteristic Sin(Nx)/Sin(x) response, with a quality factor equal to the number of taps, N, a first sidelobe level of -13 dB and (N-2) sidelobes between response maxima. A higher quality factor can only be obtained by increasing the number of taps while sidelobe ratio is enhanced by suitable tap weighting.

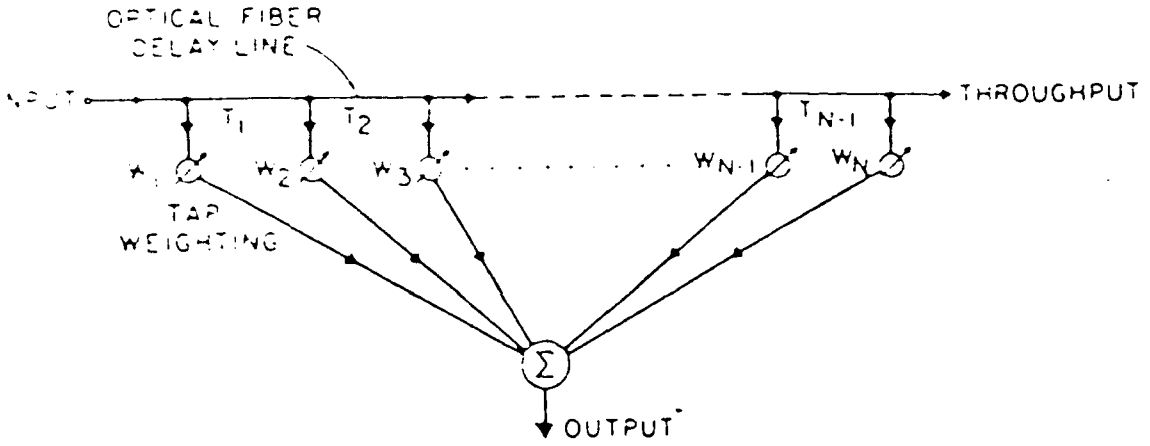

Figure 2.1 Basic Structure of a Tapped Transversal Filter

2.1.1.2 NON-RECIRCULATING FEED-FORWARD LATTICE FILTER

Fig. 2.2 shows the schematics of the N-th order non-recirculating feed-forward lattice filter. The basic lattice element is a 2 x 2 directional coupler with coupling coefficient a. The N-th order lattice filer infers that there is a total of N number of 2 x 2 lattice element in the filter design.

The center frequency of this lattice filter structure equals the reciprocal of the characteristic delay time T, defined by the length difference between inter-stage fibers, regardless of absolute line length. Bandwidth depends inversely on the order of the lattice and the coupling coefficients. Sidelobe level depends similarly on system coupling details.

2.1.1.3 RECIRCULATING FEED-BACKWARD LATTICE FILTER

Fig. 2.3 shows the schematic of N-th order recirculating feed-backward lattice filter. The center frequency of this lattice filter structure equals the reciprocal of the characteristic loop delay time T. Since this is defined by the absolute loop length, rather than by the difference of two lengths as in the non-recursive case, it is difficult to implement a high center frequency filter. The minimum practical loop delay length is

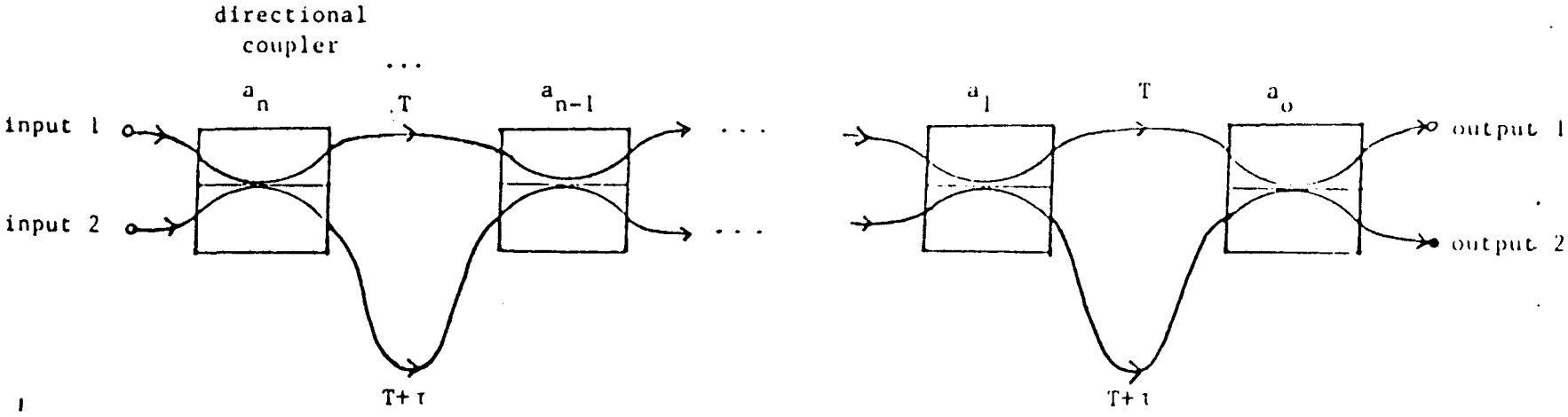

Figure 2.2 Nth-Order Non-Recirculating Feed-Forward Lattice Filter

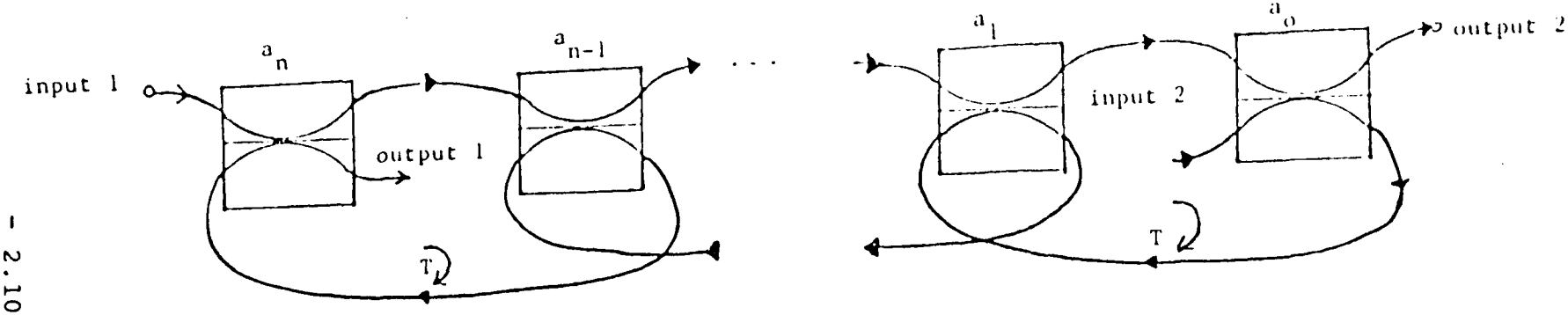

Figure 2.3 Nth-Order Recirculating Feed-Backward Lattice Filter

of the order of 120 mm, equivalent to a limiting frequency of 1.6 GHz. With suitable coupling coefficients, the recirculating lattice can exhibit very narrow bandwidth. With all coupling coefficients equal, the stop-band is monotonic in shape, with no intervening side-lobe maxima. Further calculations indicate a maximal stop-band depth for coupling coefficients of the order of 0.9, the depths around -60 dB can be achieved with a 3rd order filter.

2.1.1.4 CASCADED TRANSVERSAL FILTER

Fig. 2.4 shows schematics of cascaded transversal filters fabricated with N number of (A) 2 x 2 couplers, (B) 3 x 3 couplers, (C) j x j ($j \geq 2$) couplers. T_i is the tap period of the i^{th} coupler unit. This design comprises cascaded multiple stages, each comprising a parallel coupled fiber bundle of progressively increasing delays. A typical implementation comprises n bundles each containing j-fibers, coupled using j x j star couplers.

2.1.1.5 CASCADED RECIRCULATING FILTER

Consideration of the cascaded transversal filter led to evolution of a novel design, the Cascaded Recirculating Filter, as shown in Fig. 2.5. The filter design comprises an

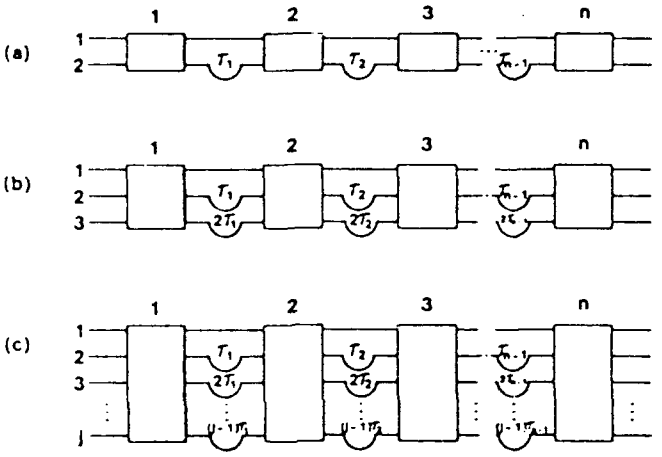

Figure 1. A single cascaded filter fabricated with n 2 × 2 couplers (a), 3 × 3 couplers (b), or $j \times j$ ($j \geq 2$) couplers (c). τ_i is the tap period of the ith coupler unit.

Figure 2.4 Cascaded Transversal Filter. A single cascaded filter fabricated with n 2 x 2 couplers (a), 3 x 3 couplers (b), or j x j (j ≥ 2) couplers (c). τ_i is the tap period of the ith coupler unit.

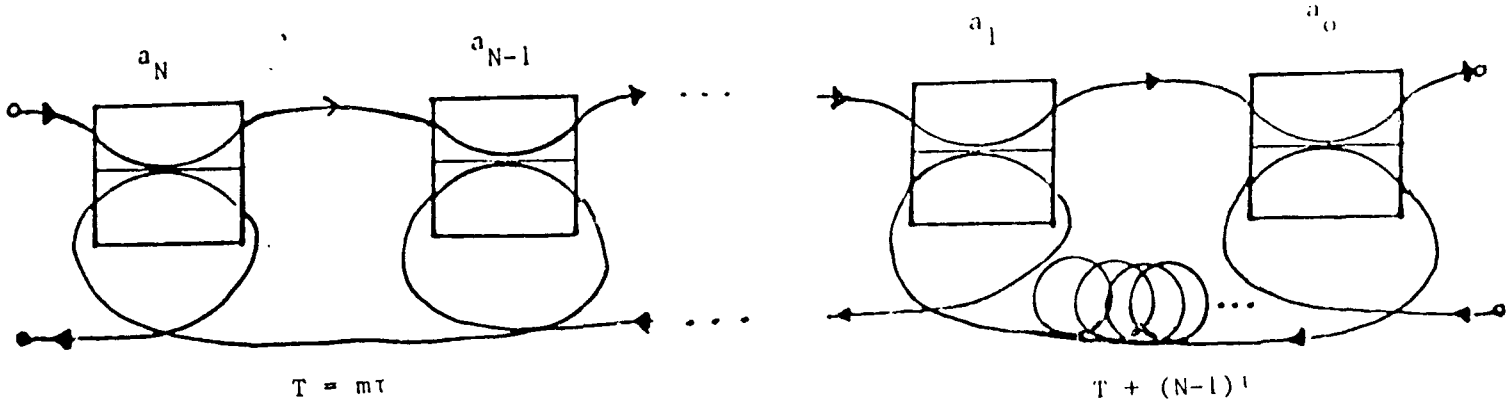

Figure 2.5 The Nth-Order Cascade Recirculating Filter. T is the basic delay time and τ is the fundamental delay time. m is an interger. a_0, a_1, ...a_N are the coupling coefficients of couplers.

N-stage recirculating lattice with loop delays increasing by a common incremental period t; the loop delays can be expressed as T+n•t, where n=o, 1,2,...N-1, N is the lattice order, and T is the basic delay time equal to m•t, where m is an integer. Since the center frequency is determined by t, i.e., the delay difference between two adjacent stages, rather than a loop length, it can be configured to be very short, giving a potentially very high fundamental center frequency, thus overcoming the minimum bending radius problem. Analysis reveals that this structure is capable of exhibiting narrow pass-band (high quality factor) and low sidelobe level simultaneously, a significant advance over previous designs.

2.1.1.6 COMPARISON

Table 2.2 summarizes qualitatively the pertinent characteristics of the classes of filter considered here.

	Center Frequency	Weight Taps	Sidelobe Level	No. of Couplers	Q	Power Eff.
Tapped Transversal	High	Yes	Low	More	Low	Low
Non-Recirculating	High	No	Low	More	Low	Low
Recirculating Lattice	Low	No	V. Low	Less	V. High	Low
Cascaded Transversal	High	No	Low	More	Norm	Norm
Cascaded Recirculating	V. High	No	Low	Less	V. High	Low

Table 2.2. Band-Pass Filter Assessment

2.1.2 NOTCH FILTER

Notch filter response is a special case of band-pass filtering, with tap number reduced to two. Under these circumstances, the response comprises alternating maxima and minima, with no intervening sidelobe structure. Experimental demonstration has been made in tapped transversal filter (Fig. 2.1), recirculating delay-line (Fig. 2.6), and non-

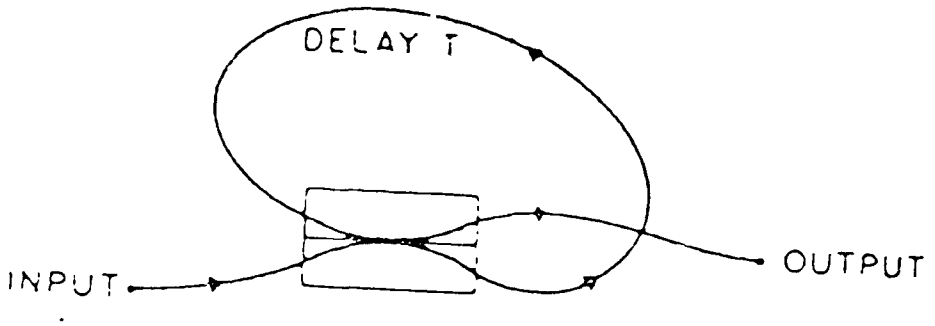

Figure 2.6 Recirculating Fiber Optic Delay Line

recirculating lattice filter (Fig. 2.2) and recirculating lattice filter (Fig. 2.5).

2.1.2.1 TAPPED TRANSVERSAL FILTER

A transversal filter with just two taps exhibits theoretical notch filter performance, as readily seen by consideration of the characteristic equations.

2.1.2.2 RECIRCULATING FILTER

The single loop recirculating delay line with coupling coefficient 0.38 possesses an impulse response comprising principally two equal height pulses, and thus exhibits notch/comb characteristics.

2.1.2.3 NON-RECIRCULATING LATTICE FILTER

The two-coupler, non-recirculating lattice filter with both coupling coefficients equal to 0.5 exhibits notch behavior, demonstrable using the theoretical equations.

2.1.2.4 RECIRCULATING LATTICE FILTER

The two-coupler recirculating lattice with coupling coefficients 0.38 and 0.95 achieves theoretically infinite notch depth filtering.

2.2 TIME DOMAIN FUNCTIONS

2.2.1 CODED SEQUENCE GENERATOR

Application of fiber optic delay lines to coded sequence generation is simple in principle, any weighted tapped configuration being generally applicable. The concepts are readily derived in the time domain. Fig. 2.7 illustrates the structure of a four bit code sequencing generator.

2.2.1.1 SINGLE TAPPED DELAY LINE

If a single pulse is input into a single tapped delay line possessing N equi-spaced taps, as shown in Fig. 2.1, the summed tap output comprises N pulses separated by the characteristic delay time, with amplitudes directly corresponding to the tap weight profile.

2.2.1.2 NON-RECIRCULATING LATTICE

The basic non-recirculating (non-recursive) lattice element is shown in Fig. 2.8 (b). If a single pulse is input into one of the input ports of a 2 x 2 directional coupler, time-correlated output pulses appear at each output port. A coupled loop system containing N couplers divides a single input pulse into 2(N-1) pulses. In an equal-delay structure

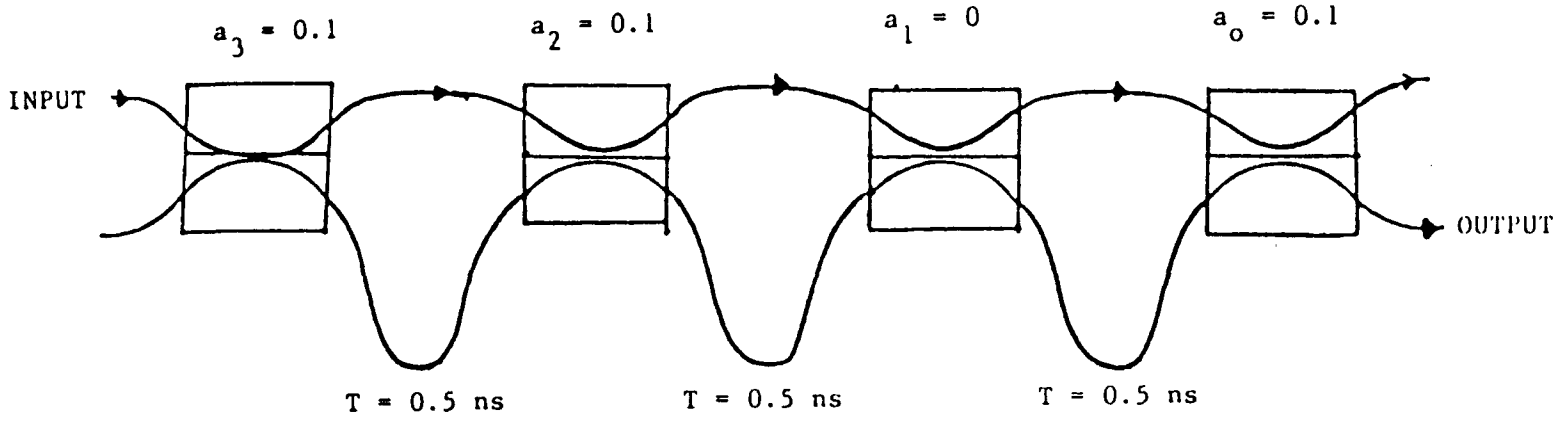

Figure 2.7 The Four-Bit Code Sequence Generator (1101)

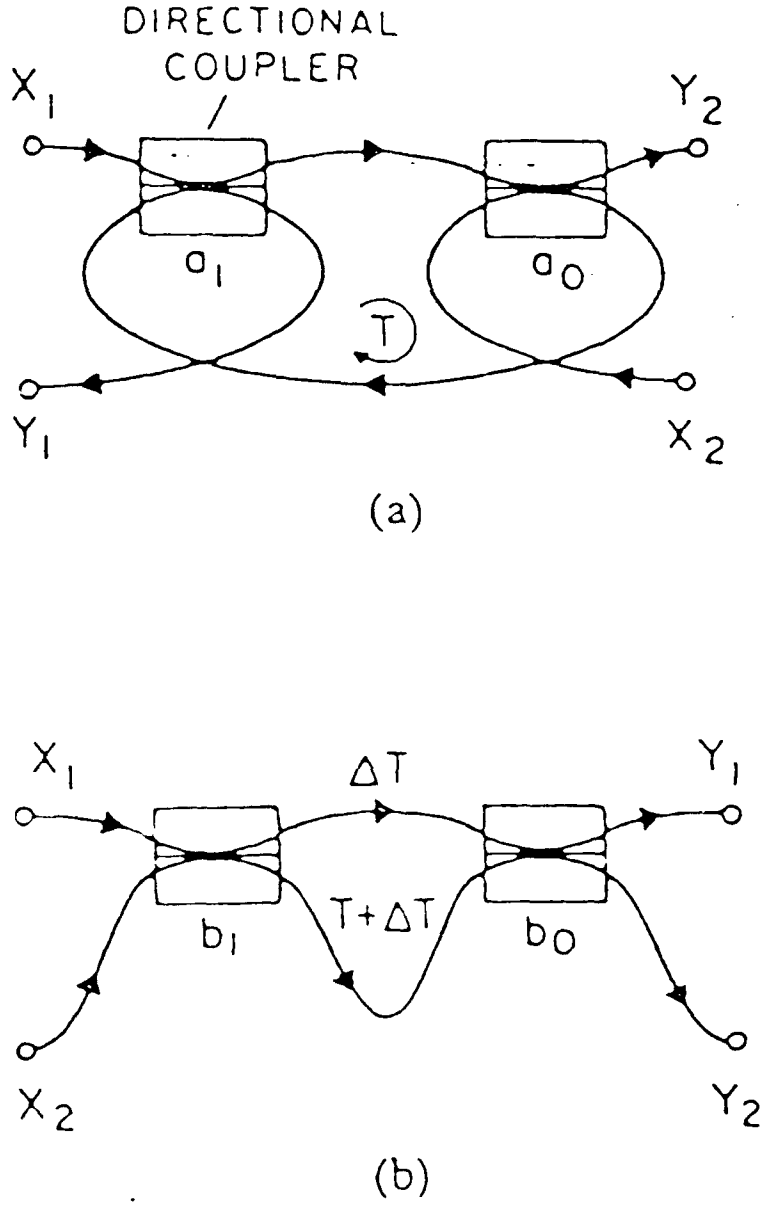

Figure 2.8 Basic Recursive and Non-Recursive Fiber Optic Structures:
(a) Recursive Element and (b) Non-Recursive Element.

certain temporal coincidences occur, readily determined by inspection, limiting the output to just N impulses, the relative intensities of which depend on the individual coupling coefficients in a systematic, but generally nonlinear, fashion. In the limit of weak coupling coefficients, the sequence and ratio of output intensities are approximately equal to the sequence and ratio of the coupling coefficients.

2.2.1.3 RECIRCULATING LATTICE

Although essentially an IIR (infinite impulse response) structure, as shown in Fig. 2.8 (a), a recirculating lattice functions as a coded sequence generator in the limit of weak coupling. The recirculating structure implies that the coded sequence emerges in reverse order to that of the coupling coefficients.

2.2.2 MATCHED FILTER

Techniques for matched filtering are essentially those for coded sequence generation, as discussed in Section 2.2.1. An example of such architecture is shown in Fig. 2.7.

2.3 NUMERICAL FUNCTIONS

Numerical functions are best considered in the time domain. Basis of operation is the systolic propagation of equally spaced pulses, representing one component of the multiplication, through a sequence of delay lines of equal time delay, coupled via 4-port couplers with coupling strengths representing the numerical values of the other component of the multiplication. The output appears as a further pulse train containing the product, generally with other discarded pulses. A system which can perform coded sequence generation can also perform matrix multiplication. Thus, tapped transversal filters, recirculating lattices and non-recirculating delay lines can all be employed to implement matrix processing functions.

Matrix-vector and matrix-matrix multipliers form a class of related operations, the principal difference being system complexity. The matrix-vector multiplier was chosen as one of the three processors to be developed under this program because of its relative simplicity. However, the processor can be expanded to demonstrate matrix-matrix multiplier functions.

2.3.1 MATRIX-VECTOR MULTIPLIER

The basic architecture for performing rank n matrix-vector multiplication is an n-stage coupled fiber lattice comprising (n+1) 4-port couplers. One example of the matrix-vector multiplier is shown in Fig. 2.9. In time domain representation, n input pulses represent the n components of the vector while the system coupling parameters represent the matrix elements. The output pulse train represents the product vector. As described, such a system is restricted to operation with Toeplitz matrices, i.e., all elements on a diagonal are equal; this has been a limiting feature of all previous experimental demonstrations of this function. Extension to general matrix operation necessitates introduction of switchable coupling elements, discussed further below.

2.3.1.1 RECIRCULATING LATTICE

Earlier demonstrations of matrix-vector multiplication in open literatures utilized a recirculating lattice structure, as shown in Fig. 2.8 (a). This suffers from certain limitations, notably the existence of second-pass pulses, necessitating introduction of "dead-time" between individual calculations. As a result, reported implementations were limited to Toeplitz

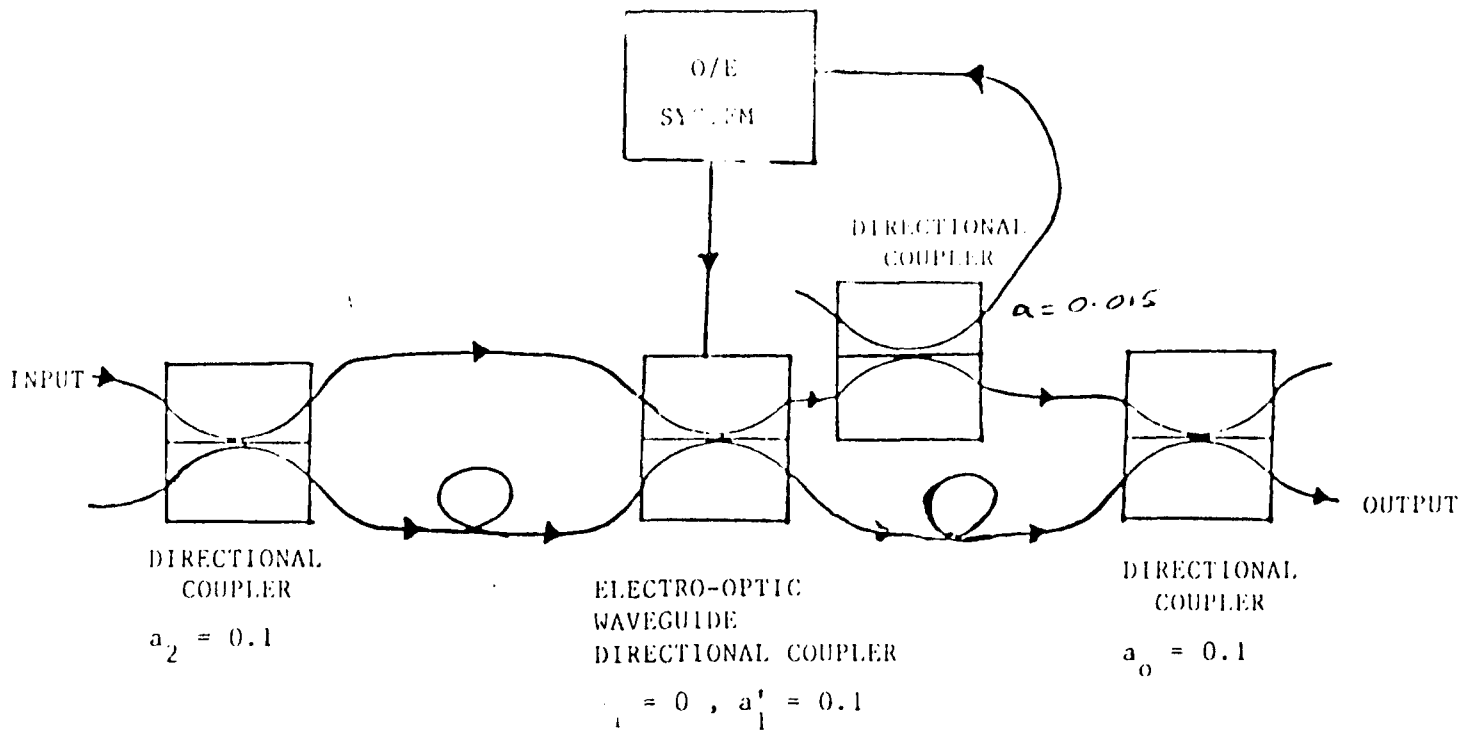

Figure 2.9 Matrix-Vector Multiplier

implementation.

2.3.1.2 NON-RECIRCULATING LATTICE

Matrix-vector multiplication can likewise be implemented in a non-recirculating lattice structure, as shown in Fig. 2.9, with the added advantage of freedom from dead time requirements. As in the previous case, implementation is restricted to Toeplitz matrices, unless switchable coupling coefficients are incorporated.

2.3.1.3 RECOMMENDED STRUCTURE

Preferred structure for implementation of a matrix-vector multiplier of rank n is the (2n-1)-stage non-recirculating lattice. Fig. 2.9 shows an example of matrix-vector multiplier of rank 2. This arrangement provides output on a single fiber and is intrinsically free from spurious second-pass effects. In order to extend the principle to operation with general matrices, it is proposed to implement a structure incorporating a switched directional coupler.

2.3.2 MATRIX-MATRIX MULTIPLICATION

Extension of matrix-vector techniques to the more general matrix-matrix multiplication is simple in concept, generally

necessitating more extensive systems and component arrays. A generic architecture of matrix-vector multiplication is shown in Fig. 2.10.

2.3.2.1 RECIRCULATING LATTICE

A relatively simple extension of the recirculating lattice to matrix-matrix multiplication is based on the observation that the operation can be resolved into separate matrix-vector operations, performed sequentially, as one would expect from the basic principle of matrix-matrix multiplication.

2.3.2.2 NON-RECIRCULATING LATTICE

Matrix resolution concepts, similar to those outlined in the previous section, can be applied to implement matrix-matrix multiplication in the non-recirculating lattice.

2.3.2.3 2-DIMENSIONAL LATTICE

The 2-D fiber lattice is configured as a spatial representation of an n x m matrix, with coupling coefficients corresponding to its elements, as shown in Fig. 2.10. Input is parallel, in row-ordered format, giving a column-ordered parallel output. The characteristic delay period is defined by the length difference of two fibers between two adjacent

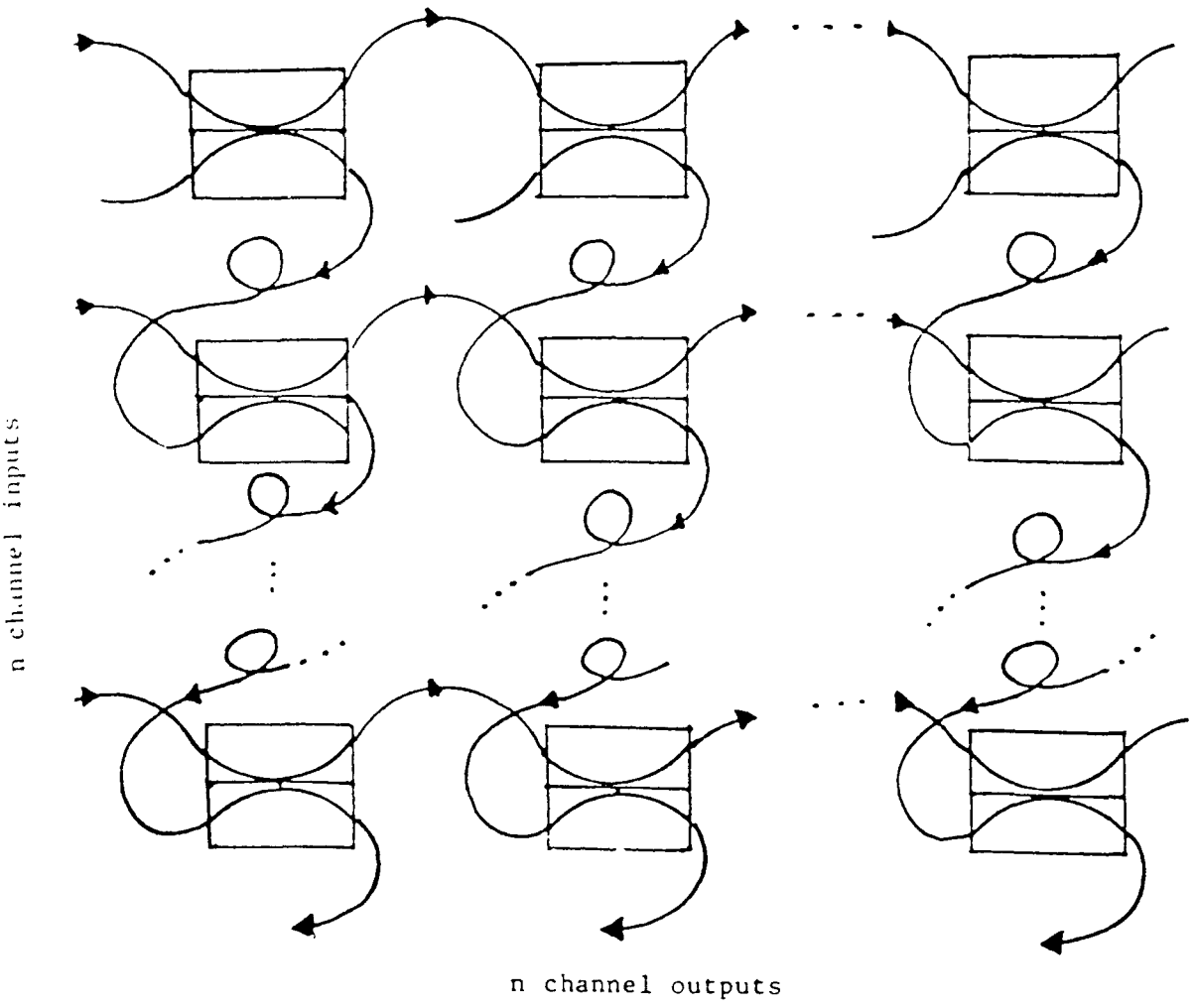

Figure 2.10 The Matrix-Matrix Multiplier.

couplers, with potential high-speed operation.

2.3.2.4 WDM TECHNIQUES

An alternative systolic approach utilizes the principal of superposition to perform simultaneous operations at different optical wavelengths, as shown in Fig. 2.11. In 2 x 2 case, two-element vectors are input at two wavelengths simultaneously. Since the matrix operates on both vectors identically, no wavelength dependent coupling is required. The output comprises the two vector terms, presented between discarded cross-product terms, simultaneously at two wavelengths. System requirements are wavelength MUX/DEMUX components, dispersion free fiber at the wavelengths concerned and wavelength independent couplers.

2.4 SUMMARY OF THEORETICAL PERFORMANCE ASSESSMENT

As a result of the literature survey of more than 250 papers, fiber optic based signal processors in the six categories (band-pass, notch and matched filters, coded sequencing generator, matrix-vector, and matrix-matrix multiplier) were reviewed. Based on components available, the system performance was characterized by key parameters, including frequency response, center frequency, pass-band width, quality

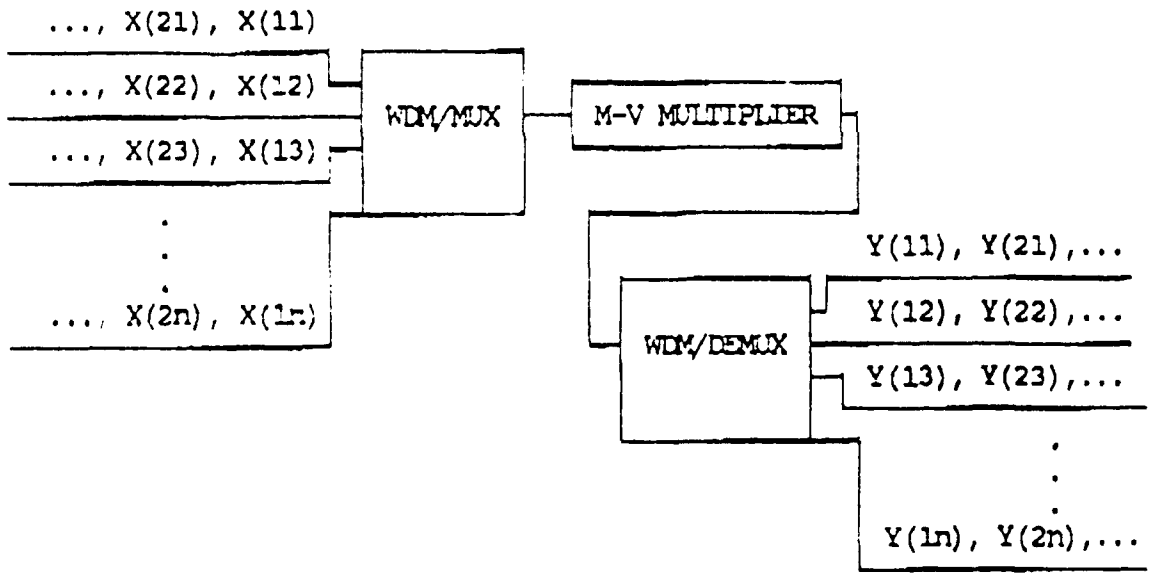

Figure 2.11 WDM Techniques as an Alternative Systolic Approach

factor, dynamic range, power budget, noise performance, and programmability. The results of performance assessment are reported in Section 3 of this report.

Optimum band-pass filter performance is achieved by the use of an infinite impulse response (IIR) structure, with multiple transit effects enhancing the effective tap number of the system. Time domain and numerical processors are best implemented in non-recursive, finite impulse response (FIR) structures. These structures have minimum spurious, second transit interference. Coupler-based lattices are generally preferable, because of their single fiber output.

3.0 REALIZABLE PERFORMANCE ASSESSMENT

The objective of Task 2(SOW 4.1.2) is to delineate the realizable performance for each of the six processing functions based on the theoretical performance relationship developed under Task 1 and on the available optical componentry. For most of the applications considered in this program, the following parameters appear appropriate to characterize the system performance:

Frequency Response

Center Frequency

Pass-Band Width

Quality Factor

Dynamic Range

Power Budget

Noise Performance

Programmability

Sections 3.1 to 3.8 are devoted to the discussion of these parameters. A rigorous mathematic treatment for ideal and exponentially attenuated transverse filters is included in Appendix B.

3.1 FREQUENCY RESPONSE

Most analytical expressions for frequency response of fiber optical delay line elements exist in open literature. Based on Z-transform theory and time-index expressions for impulse response, we have derived schematic models for most of the fiber configurations identified. In many circumstances, direct analytical solutions can be obtained. In situations where this is not the case, recourse must be made to numerical techniques.

For an ideal tapped delay line transversal filter, as shown in Fig. 2.1, with N taps of equal weight and with equal temporal separation t, the well-known frequency expression for the frequency response is

$$H(f) = \sin(N\pi ft)/\sin(\pi ft)$$

where t represents:

(a) the physical incremental distance between taps for an ideal tapped delay line transversal filter, or

(b) the length increment between neighboring fibers for a fiber bundle transversal filter, or a star coupler transversal filter with a star coupler be the power division element.

If the fiber propagation attenuation, a, is included in the calculation, the frequency response becomes

$$H(f) = (1 + a^{**}2N - \cos(2.\pi.N.f.t)) / (1 + a^{**}2 - \cos(\pi.f.t))$$

For a single feed-forward loop element constructed from two directional coupler, as a dual coupler, non-recirculating delay line, as shown in Fig. 2.2, the frequency response can be shown to be

$$H(f) = (C1^{**}2 + C2^{**}2 + 2.C1.C2.\cos(2.\pi.f.dt))^{**}0.5 / (C1 + C2)$$

where:

$$C1 = (1 - k1).(1 - k2).a1.a2$$

$$C2 = k1.k2.a1.a2.a$$

a1, a2, and a are the attenuations of the two couplers and the excess attenuation of the fiber loop, respectively; and k1 and k2 are the two coupling coefficients.

For a dual-coupler recirculating delay line, as shown in Fig. 2.3:

$$H(f) = (1 - C2) / (1 + C2^{**}2 - 2.C2.\cos(2.\pi.f.t))^{**}0.5$$

with notation as above.

For a single-coupler recirculating delay line, as shown in Fig. 2.6:

$$H(f) = (1 - C5).((C4-C3.C5)^{**}2 + C3^{**}2 + 2.C3.(C4-C3.C5).\cos(2.\pi.f.t))^{**}0.5 / ((C3 + C4 - C3.C5).(1 + C5^{**}2 - 2.C5.\cos(2.\pi.f.t))^{**}0.5)$$

where C3 = (1 - k), C4 = k**2.a, and C5 = k.a; where k is the coupling coefficient and a is the loop attenuation.

3.2 CENTER FREQUENCY

The equations in Section 3.1 are formulated in terms of the temporal delay characterizing either the inter-tap separation in linear transversal filters or the differential delay in recursive or non-recursive loop structure. The center frequency of the band-pass filter structure is normally defined by the reciprocal of the characteristic delay element, t. Because of the material dispersion of glass fiber, the propagation delay is a function of the operating wavelength.

For most optical materials, the index of refraction can be expressed by a semi-empirical representation,

$$(n^{**}2 - 1) = \sum_i (A(i).\lambda^{**}2/(\lambda^{**}2 - B(i)^{**}2))$$

where the constants A(i) and B(i) represent the strength and wavelength of the principle electronic oscillators. For synthetic fused silica, a third order approximation gives:

$$A(1) = 696.1663, \quad B(1) = 68.4043$$

$$A(2) = -407.9426, \quad B(2) = 116.2414$$

$$A(3) = 897.4794, \quad B(3) = 9896.161$$

where wavelength is specified in nm.

Based on the assumption of U.V. grade fused silica for fiber core material, the following results are obtained:

WAVELENGTH DEPENDENCE OF DELAY CHARACTERISTICS

λ (nm)	n	t (ns/m)	f(o) (GHz.m)
632.8	1.4570	4.8601	.20576
786.0	1.4536	4.8489	.20623
830.0	1.4528	4.8461	.20635
904.0	1.4517	4.8424	.20651
1064.0	1.4496	4.8355	.20681
1300.0	1.4469	4.8264	.20719
1500.0	1.4446	4.8187	.20752

indicating systematic variations of the order of 0.86% across the wavelength range of potential interest.

3.3 PASS-BAND WIDTH

Although the frequency responses of the majority of structures

under consideration are capable of expression analytically, similar representation of fundamental pass-band width is not so readily achieved. It has been shown that for the transversal filter, the full pass-band width to the -4 dB points is equal to the reciprocal of the delay increment:

$$df(4dB) = 1/Nt$$

In many cases, however, 3 dB bandwidth is a more conventional representation, in which case numerical solution for the roots of the equation:

$$H(f) = 0.5$$

is generally required in order to provide band-width characterization.

For the ideal equal-tap, equal-delay transversal filter, solution of:

$$\sin(N.x)/\sin(x) = 0.5$$

where $x = \pi.f.t$, provides numerical representation of the pass-band width as a function of tap number, N. Values of x and corresponding -3 dB widths (in units of 1/t) for systems of up to 10 taps are tabulated, together with -4 dB values derived as mentioned above.

DEPENDENCE OF FILTER BANDWIDTH ON TAP NUMBER

N	df(3dB) (1/t)	df(4dB) (1/t)
2	0.248	0.500
3	0.156	0.333
4	0.116	0.250
5	0.092	0.200
6	0.076	0.167
7	0.064	0.143
8	0.056	0.125
9	0.050	0.111
10	0.045	0.100

Empirically, the -3 dB bandwidth is approximately 0.5 of the -4 dB figure, i.e., df(3dB) = 1/(2N).

Similar analysis enables the filter bandwidth in the exponentially attenuated transversal filter and the various recirculating and non-recirculating loop structures to be characterized as a function of power coupling factor and tap number. A rigorous mathematic treatment of filter characteristics is included in Appendix B.

3.4 QUALITY FACTOR

The quality factor Q, of a filtering structure, is defined as the ratio of the center frequency of the first order (m = 1) principal lobe, f(1) to the bandwidth, df, i.e.,

$$Q = f(1)/df.$$

For the ideal transversal filter, Q = 2N.

3.5 DYNAMIC RANGE

The characteristic equations for frequency response indicate the presence of notches between pass-bands and side-lobes; in cases such as the ideal transversal filter, these representatives are cast in terms of trigonometric functions indicating theoretically infinite notch depth. In the majority of configurations, however, this is not the case, and the theoretical expressions indicate a limiting notch depth, generally dependent on the coupling coefficients and attenuations present in the system. By considering the maximum and minimum values taken by these expressions, and defining dynamic range, R, as the ratio of maximum to minimum transmission, the following analytical relationships can be obtained:

A. Ideal Tapped Delay Line Transversal Filter:

   Theoretically infinitely deep notches.

   $R = \infty$

B. Attenuating Transversal Filter:

   $R = (a^{**}2N.(a^{**}2N + 2))/(a^{**}2.(a^{**}2 + 2))$

   where $a = -\ln(1 - k)$, k is the tap coupling factor and the system has N taps.

C. Dual-Coupler Non-Recirculating Delay Line and Non-Recirculating Lattice:

R = ((C1**2 + C2**2 + 2C1.C2)

/(C1**2 + C2**2 - 2C1.C2))**.5

where:

C1 = (1 - k1).(1 - k2).a1.a2

C2 = k1.k2.a1.a2.a

a1, a2, and a are the attenuations of the two couplers and the excess attenuation of the fiber loop respectively, and k1 and k2 are the two coupling coefficients.

D. Dual-Coupler Recirculating Delay Line and Recirculating Lattice Section:

R = ((C2**2 + 3)/(C2**2 - 1))**.5

with notation as above.

E. Single-Coupler Recirculating Delay Line:

R = (((1 - C5).(C4 - C3.C5)**2 + C3**2 + 2.C3.(C4-C3.C5)).

(C3 + C4 - C3.C5)(1 + C5**2 + 2.C5))**.5

/ (((1 - C5).(C4-C3.C5)**2 + C3**2 - 2.C3.(C4-C3.C5)).

(C3 + C4 - C3.C5)(1 + C5**2 - 2.C5))**.5

where C3 = (1 - k), C4 = k**2.a, and C5 = k.a; k is the coupling coefficient and a is the loop

attenuation.

3.6 POWER BUDGET

Optical fiber signal processing configurations can be conveniently classified as those in which optical power is conserved and those which intrinsically discard significant fractions of the available incident power. Note, however, that even in configurations which are theoretically power-conserving, temporal redistribution of the energy of an input single pulse into output pulse train and vice versa may result in differences between input and output pulse amplitudes. Furthermore, absorption losses in fibers, together with absorption and scattering losses in couplers, may serve to introduce additional attenuation factors into hypothetically loss-less configurations.

3.6.1 POWER CONSERVING CONFIGURATIONS

The class of power-conserving fiber processor configurations comprises essentially the set of two-port configurations and includes fiber-bundle and star-coupler transversal filters, together with single-coupler recirculating loop structures. These exhibit the common architectural feature of the absence of free, unused output ports; all optical power entering the

single input port, other than that dissipated by intrinsic attenuation or scattering, ultimately emerges from a single output port.

3.6.2 POWER DISCARDING CONFIGURATIONS

The power discarding configurations are characterized by the presence of unused exit ports, the optical outputs from these unused ports are discarded and not recirculated or otherwise utilized in the processing function. This class of architectures includes the tapped delay line transversal filter, together with the two-coupler recirculating and non-recirculating structures, i.e., the 3-port and 4-port configurations. The discarded power may, in some cases, be directly complementary to the signal power and, therefore, potentially utilizable, but this is not generally so, and each architecture must be treated individually in this respect.

Optical power efficiency, i.e., the ratio of output to input powers, can be determined in terms of the system transfer function $H(z)$, utilizing the fact that the optical power is proportional to the d.c. frequency component in the baseband optical intensity signal, i.e., $z = 1$ in the transfer function. The following expressions for power transmission,

T, in two-coupler recirculating and non-recirculating lattice elements have been identified.

A. Two coupler recirculating element, as shown in Fig. 2.7 (a):

$$T(11) = (k1 + (1 - 2.k1)k2.a1)/(1 - k1.k2.a1)$$

$$T(12) = ((1 - k1)(1 - k2).a2)/(1 - k1.k2.a1)$$

where T(11) represents the situation in which input and output are associated with different fibers at the same directional coupler and T(12) describes the converse situation, k1 and k2 are the coupling coefficients of the two couplers and a1 and a2 are attenuation of the loop and the forward fiber line respectively.

B. Two-coupler non-recirculating element:

$$T(11) = (1 - k1)(1 - k2)a2 + k1.k2.a1$$

$$T(12) = k1.a2.(1 - k2) + k2.a1.(1 - k1)$$

where similar notation is used.

C. Tapped delay line (N taps):

$$T = h(0) + h(1) + h(2) + \ldots + h(N-1)$$

3.7 NOISE PERFORMANCE

Noise in fiber structures has been investigated both theoretically and experimentally. Essentially, the power

spectrum of the autocovariance spectrum has the form:

$$c(t1,t2) = \text{SIGMA}(G(M).d(t2-t1-Mt))$$

where d is the Dirac delta function and the impulse intensities, G(M) are relatively complex mathematical expressions. To the extent that it is currently developed, the theory predicts the following, all observed experimentally:

(A) The periodic form of the spectrum, with a characteristic notch at d.c.

(B) The shape of the basic period as a function of coupling coefficient.

(C) The dependence of the spectrum on state of polarization.

(D) Insensitivity to environmental conditions.

3.8 PROGRAMMABILITY

Principal processor parameters for programmability are tap separation, tap strength, and tap number.

3.8.1 TAP SEPARATION

The influence of tap separation on processor characteristics reflects the direct proportionality linking spatial separation and temporal delay between adjacent sampling points. Thus,

tap separation defines analog filter center frequencies, matched filter and code generator pulse separations, and pulse rates in matrix multiplier configurations.

The extent to which programmable tap separation is feasible obviously depends on the tap technology under consideration. It is important to note that truly continuously variable programmable tap separation schemes are virtually non-existent at present, the sole identified example being the acousto-optic diffraction scheme; positional programmability is achieved by physically moving an acousto-optic transducer along the fiber.

The alternative approach is based on selection of a limited number of taps from an extended array fabricated on a single fiber, giving a variable, but quantized, tap separation with inter-tap increment equal to the tap separation of the fundamental array. This approach requires the availability of at least a binary tap strength programming capability.

Applicable techniques include fused coupler, macrobend, and evanescent coupler taps.

3.8.2 TAP STRENGTH

Tap strength influences filter pass-band response shape, pulse amplitudes in matched fiber and code generators and analog values in matrix multipliers.

Techniques for tap strength programming can be divided into those in which the actual tap coupling factor may be controlled and those in which the power extracted by a fixed coupling tap is subsequently modulated by an external modulation agency.

Applicable technologies for internally controllable taps include both integral and non-integral acousto-optic taps, tunable evanescent wave couplers, and, possibly, Bragg reflector taps with electro-optic control of reflectivity.

3.8.3 TAP NUMBER

Tap number defines filter pass-band width, matched filter and code generator pulse train length, and the ultimate size of matrix capable of handling in matrix multiplier configurations. Tap number considerations are probably more effectively resolved by considering sparsely utilized programmable tap arrays with specific taps set to zero.

Alternatively, a variable number of effective taps may be implemented in single-coupler and dual-coupler recirculating delay-line structures, by simply varying the coupling coefficient, although tapped power uniformity is obviously compromised by this process. As an example, consider single and dual coupler recirculating delay lines with variable coupling coefficient (assumed equal in the dual coupler case) and assume a threshold for tap viability of 10%, i.e., emergent pulses of intensity less than this figure are ignored. Numerical simulation of the output pulse train intensities indicates the number of effective taps strongly dependent on coupling strength, k, as follows:

k	Single	Dual
0.1	3	1
0.2	4	1
0.3	4	1
0.4	4	2
0.5	4	2
0.6	4	3
0.7	2	4
0.8	1	6
0.9	1	12
0.95	-	23

Similar calculations can be readily performed for other threshold levels and for two coupler situations with unequal coupling coefficients.

Note that notch filter configurations are effectively defined by just two taps, and number programmability considerations may not be relevant in this situation.

3.9 SUMMARY OF REALIZABLE PERFORMANCE ASSESSMENT

Using the models and performance relationship derived, real component parameters were considered for all processing functions. In each case, the major limiting factor in extending processor performance is the upper frequency limit imposed by bend loss considerations in small diameter fiber loops, and the issue of tap programmability is the key to processor reconfigurability.

Using typical data for silica fiber, together with established relationships for fiber bending loss as a function of bend radius, figures for bend loss as a function of mandrel radius have been generated. Although generally quoted in terms of loss per unit length, it is relevant in the present case to consider also loss per turn, since this may define ultimate utility. Results are tabulated for fibers of core radius 2, 3, and 5 microns, at bending radii from 1 meter to 1 mm, with approximate equivalent fundamental pass-band center frequencies and are quoted in terms of dB/turn.

Bending Radius (Meter)	Equivalent Fundamental Passband (GHz)	2 micron Radius Fiber (dB/turn)	3 micron Radius Fiber (dB/turn)	5 micron Radius Fiber (dB/turn)
1.0	.032	0	0	0
0.5	.064	0	0	0
0.2	.16	0	0	0
0.1	.32	0	4.1 E-32	7.1 E-18
0.05	.64	3.3 E-23	2.5 E-14	2.9 E-7
0.02	1.6	2.9 E-7	9.3 E-4	5.4 E-1
0.01	3.2	5.0 E-2	2.6 E 0	5.4 E 1
0.005	6.4	1.7 E 1	1.1 E 2	4.5 E 2
0.002	16	4.5 E 2	8.5 E 2	1.3 E 3
0.001	32	1.1 E 3	1.4 E 3	1.5 E 3

From the calculated loss/turn figures, it is apparent that mandrel radii of less than 10 - 20 mm are unacceptable; this technology is probably thus limited to frequencies below 3 - 5 GHz.

The study under this task has resulted in advances overcoming these limitations, as discussed in Section 6, System Design/Plan of this final report. One such advance lead to an invention followed by an award of U.S. patent number 4,934,777, entitled "Cascaded Recirculating Transmission Line Without Bending Loss Limitations." A copy of this patent is included in Appendix C.

4.0 KEY COMPONENT CHARACTERIZATION

Guided by requirements resulting from the processor architecture assessment, candidate components were identified and characterized; preferred technologies were specified. Classes of components studies comprised of the following:

- Fibers
- Coupler/taps (fixed and switchable)
- Polarization control components
- Wavelength selective components
- External modulators
- Spatial light modulators

As stated in the Contract, optical transmitters and receivers required for characterization and demonstration of processors may be available from RADC during the course of the program. We were directed to focus program funds on processor development rather than transmitter and receiver development.

The results of this Task were reported in various monthly activity reports and Components Design Plans (CDRL-A002) and are summarized here.

4.1 FIBERS

A number of characteristics of optical fibers determine their suitability for application on delay line signal processing, the most demanding processor function on fiber optics properties. These characteristics include glass composition, attenuation, dispersion, propagation velocity, linearity, and polarization control. Detailed discussion of these characteristics and a summary of all commercially available fibers is included in Appendix D.

4.2 COUPLERS AND TAPS

Existing techniques for fiber tap implementation can be broadly classified as radiated light taps, guided wave couplers and taps, and integrated optic waveguide couplers, and include:

(A) Radiated Light Taps:

- Macrobend tap
- Fiber grating tap
- Acousto-optic diffraction tap

(B) Guided Wave Couplers and Taps:

- Fused fiber coupler
- Planar waveguide coupler
- Evanescent-Field coupler

Reflective tap

Non-reciprocal coupler

(C) Integrated Optic Waveguide Couplers

where the term "coupler" has been used somewhat arbitrarily to describe devices in which the extracted optical power is confined to a further fiber or planar waveguide. Of these, the fused coupler and reflective tap are intrinsically fixed in position and tap strength, allowing no external control of coupling parameters once fabricated. The evanescent-field coupler and macrobend tap are mechanical in operation and fixed in location. The external control of coupling parameters can be accomplished at rates consistent with mechanical movement. In order to achieve high-speed tap reconfiguration in any processor system, it is apparent that devices with optical or electrical control are ultimately required.

To implement the processors designed under this contract requires both static and switchable 4-port couplers with precisely defined coupling efficiency. The couplers under consideration must be reciprocal, a requirement which effectively excludes radiated light taps, non-reciprocal couplers and reflective devices from further consideration.

The remaining candidate technologies are:

- Fused fiber coupler
- Evanescent wave coupler
- Planar waveguide coupler

Of these, only the planar waveguide coupler, in suitable active material system, fulfills the switching capability requirement of the matrix-vector multiplier application.

4.2.1 STATIC COUPLER

Fused fiber couplers, while in principle capable of manufacture to specified splitting ratios with moderate precision and repeatability, do not lend themselves to post-fabrication adjustment and, thus, do not provide the opportunity for system reconfiguration and optimization implicit in the use of tunable devices. Primarily for this reason, the polished fiber evanescent wave directional coupler, with its capability for precise tuning of coupling coefficient, is the recommended technology for implementation of static coupler requirements.

4.2.2 SWITCHED COUPLER

Two technologies for implementation of the switched coupler function are available, Ti:lithium niobate and III-IV

semiconductor. Of these, the former is currently preferred, on grounds of superior insertion loss and fiber-interfacing characteristics.

4.3 POLARIZATION CONTROL COMPONENTS

The use of periodic coupling principle to achieve power transfer between two waveguides is well known in the fields of microwaves, integrated optics, and bulk optics; similar techniques can be applied in optical fibers to transfer power between similar or dissimilar guided modes. Basic device configurations considered here are birefringent fiber polarization coupler and two-mode transverse mode coupler, both of which can be configured as Mach-Zehnder interferometer modulators.

Additional birefringence can be imparted to a birefringent fiber by application of external pressure. Specifically, it can be shown that when a birefringent fiber is squeezed along an axis at 45 degrees to the intrinsic birefringent axes, the magnitude of the total birefringence is approximately equal to the intrinsic birefringence; the effect can be regarded as a rotation of the internal birefringence, approximately proportional to the applied pressure.

The birefringent fiber polarization converter comprises a single length of intrinsically birefringent polarization maintaining fiber. Applied to the fiber is a series of compression regions, each of length equal to half a characteristic beat length for the fiber in question and separated by a half beat length. Light, initially polarized along one fiber axis, encountering a region of pressure deformation, is partially converted to the orthogonal mode. The effect of a periodic sequence of pressure regions is ultimate complete power coupling, the assumption of multiple coupling regions being necessary to keep the force/unit length sufficiently small so the small angle approximation remains valid.

The two-mode transverse fiber coupler operates in a similar mechanical fashion; in this case, the coupling taking place between the two lowest-order sets of transverse modes of a fiber used at a wavelength below cut-off.

The two devices described above can be incorporated into in-line Mach-Zehnder interferometer modulators. Both couplers are symmetrical, in that they transfer power in both

directions between the modes being coupled. As in a normal interferometer, amplitude modulation is achieved by following the interferometer with a mode selective filter (polarizer for the birefringent fiber case and mode filter in the two-mode case). Extinctions of >30 dB and >40 dB have been observed in polarization and two-mode conversion modulators respectively.

Two experimental demonstrations have been made of this principle. The first featured coupler excitation via a piezo-electrically driven pressure element, capable of operation at frequencies in excess of 80 KHz. An alternative implementation used surface acoustic wave excitation, derived from an array of transducers half a beat length wide and spaced by a similar distance, achieving a modulation depth of 70% at a frequency of 4.35 MHz.

4.4 WAVELENGTH SELECTIVE COMPONENTS

The recent development of techniques for the fabrication of robust, low-loss distributed Bragg reflectors on exposed polished fiber cores offers an alternative technique for achieving optical modulation in the all-fiber format. Essentially, such gratings act as reflective elements, with

well defined spectral response. In particular, the characteristic reflection spectrum of an etched structure with a pitch optimized for an optical wavelength of 1092 nm comprises a single peak, with a maximum reflectivity of 98% and a near-theoretical width (FWHM) of less the 0.8 nm. Since the peak reflection wavelength is defined completely by the grating pitch, application of any technique to tune that pitch results in a spectral shift of the reflection characteristic. Utilizing a piezo-electric element to provide longitudinal grating extension, tuning of the reflection peak over a spectral range substantially in excess of the linewidth has been demonstrated in our laboratories. Similar behavior, although with much slower response time, has been demonstrated by thermal tuning. In conjunction with a source of suitably narrow emission linewidth, this approach offers an efficient amplitude modulation, experimental results indicating an extinction of 20 dB or better.

4.5 EXTERNAL MODULATORS

Within this component category, we studied external modulators based on electro-optic, acousto-optic, and piezo-electric effects. Device configuration includes both free space design and optical waveguide design.

4.6 SPATIAL LIGHT MODULATORS (SLM)

A full survey and analysis of all available SLM technologies is beyond the scope of the present program. However, the alterable tap weighting function is of central importance to optical fiber processor operation and future development of the technology, and it must be carefully considered. On this basis, we have identified a number of technology options which are most compatible with optical fiber processor architectures, and consideration of which will enable the most complete determination of processor capabilities to be made.

A number of candidate SLM devices, including electro-optic modulator arrays, integrated optic devices, liquid crystal modulators, magnetic-optic modulators, and organic photochromic devices were included in the study. When an SLM device is incorporated in a fiber optic based signal processor, it is desirable to implement tap weighting and summing configurations using compatible tap, modulator, and propagating technologies. The taps can be realized in either guided-wave or free-space configurations. In the case of guided-wave taps, one must consider the technology compatibility, modal compatibility, and spatial

dimensionality. Free-space taps provide additional system design flexibility where a two dimensional SLM device can be integrated with a linear fiber array.

5.0 COMPONENT BREADBOARDING

From requirements indicated by system studies, Component Design Plan was submitted to RADC as part of the contract requirement of CDRL A002. The document addresses the design and development of two major components required for the development of advanced optical processors:

(1) Polished evanescent wave directional couplers, designed to coupling strengths not generally available in this or alternative technologies. Four different types of couplers were designed and developed: 0.1 and 0.9 couplers with single mode fibers, and 0.1 and 0.025 couplers with polarization-maintaining fibers.

(2) Switched directional coupler in lithium niobate channel waveguide, with 0.1 coupling efficiency.

These components are required to demonstrate the operation of the following signal processors:

- Band-pass filtering at 4.75 GHz center frequency with simultaneous high quality factor and low sidelobe level.
- Adjustable 4 bit coded sequence generation at 2 Gbit/s pulse rate.
- Matrix-vector multiplication with a general 2 x 2

matrix at 0.5 Gbit/s rate.

5.1 COMPONENT DESIGN AND SPECIFICATIONS

As we discussed in Section 4, both static and switchable 4-port couplers with precisely defined coupling coefficient are required to perform the signal processing functions. Static couplers will be fabricated based on evanescent coupling of polished single mode fibers or polarization-maintaining fibers. The switchable coupler will be fabricated based on Ti : diffused $LiNbO_3$ waveguide technology.

5.1.1 POLISHED EVANESCENT DIRECTIONAL COUPLER

The 4-port couplers are fabricated from polished half-couplers. The basic design approach is as follows:

(1) Select a suitable fiber for the application in hand.

(2) Assume zero lateral translation, calculate the dependence of coupling on core-to-core separation.

(3) From (2), identify the core separation corresponding to 100% coupling.

(4) From (3), select a core-to-core separation slightly (e.g., 5-10%) less than that indicated for 100% coupling, ensuring an over-coupled device.

(5) Calculate the corresponding lateral translation tuning

characteristics, and check for design conformity. These procedures were adopted to produce the design specification outlined in Section 5.1.3.

5.1.2 LITHIUM NIOBATE SWITCHED DIRECTIONAL COUPLER

5.1.2.1 CHANNEL WAVEGUIDE

The following key waveguide fabrication parameters have been established:

Titanium thickness:	75 nm
Titanium stripe width:	7 μm
Diffusion temperature:	1050°C
Diffusion time:	10 hours

5.1.2.2 COUPLER PARAMETERS

Disposable parameters in switched directional coupler design include:

- Guide separation in the interaction region
- Choice of zero-coupling state
- Electrode configuration
- Optical mode (TE or TM)

Existing designs are targeted toward switch-based 100%

coupling; implementation of lower coupling; i.e., the 0-10% considered here, introduces alternative constraints. The need for an acceptable dynamic range within the 0-10% range implies a corresponding requirement for good extinction in the nominal 0% coupling state; this is seen as the key design consideration in the present case. To maximize intrinsic extinction, use of the "bar-state," i.e., optical output and input on a common physical waveguide, is recommended.

Operation of TE or TM optical mode is feasible, use of TE being preferred for a number of reasons. First, increased drive requirement enhances voltage resolution, giving improved control over coupling ratio. Secondly, incorporation of integrated polarizers resulting in enhanced attenuation of TM modes becomes possible. The presence of TM modes degrades extinction. A further design subtlety is selection of coupler parameter to achieve coincident nulls for TE and TM modes.

The basic configuration comprises two electrodes, deposited in register with the two arms of the coupler; this provides the added bonus of providing TM attenuation automatically. In current technology, this configuration is capable of achieving extinction of the order of 20 to 25 dB.

To achieve maximum extinction in the zero-coupled state, it is necessary not only to specify but also to maintain the optical wavelength. Extinction in the ideal modulator can be calculated as a function of wavelength deviation. A ± 5 nm deviation in wavelength will result in an extinction ratio of 30 dB for an ideal directional coupler. In a practical coupler, these figures are further degraded by the intrinsic extinction level of the device.

5.1.2.3 ELECTRICAL DESIGN

For a directional coupler electrically controllable over a coupling range of 0-10%, the voltage-length product for TM and TE propagation is in excess of 4 V.mm and 12 V.mm, respectively. To achieve the intrinsic minimum coupling associated with the nominal zero-coupling state, an additional dc bias of the order of 10 to 50 V is required. Projected electrical drive requirements for a coupler appropriate to the present application are:

- 10% coupling 40 V
- 0.1% coupling 41 V

5.1.2.4 FIBER INTERFACE

Optimum coupler performance implies operation in TE mode with

control of input polarization, using polarization-maintaining fiber for at least the input; this demands careful design of the fiber-$LiNbO_3$ interface. Techniques for interfacing high-birefringence fiber are well-developed; present technology permits simultaneous interfacing of 8 fibers with 0.4 dB loss per interface.

5.1.3 COMPONENT DESIGN SPECIFICATIONS

The design specifications of a total of five (5) classes of optical couplers are summarized here.

A. 0.90 Coupler, Single-Mode Fiber

Operating wavelength:	1.3μm
Fiber type:	Corning SM-06S-P
Core index:	1.4514
Cladding index:	1.4469
Fiber bend radius:	600 mm
Core separation:	10.2μm
Fluid R.I.:	1.450
Coupling ratio:	0.9
Excess loss:	0.1 dB

B. 0.10 Coupler, Single-Mode Fiber

Operating wavelength:	1.3μm
Fiber type:	Corning SM-06S-P
Core index:	1.4514
Cladding index:	1.4469
Fiber bend radius:	600 mm
Core separation:	13.3μm
Fluid R.I.:	1.450
Coupling ratio:	0.1
Excess loss:	0.1 dB

C. 0.10 Coupler, Polarization-Maintaining Fiber

Operating wavelength:	1.3μm
Fiber type:	York HB1250
Core index:	1.4514
Cladding index:	1.4469
Fiber bend radius:	600 mm
Core separation:	13.2μm
Fluid R.I.:	1.450
Coupling ratio:	0.1
Excess loss:	0.1 dB

D. 0.025 Coupler, Polarization-Maintaining Fiber

Operating wavelength:	1.3μm
Fiber type:	York HB1250
Core index:	1.4514
Cladding index:	1.4469
Fiber bend radius:	600 mm
Core separation:	14.8μm
Fluid R.I.:	1.450
Coupling ratio:	0.025
Excess loss:	0.1 dB

E. 0.10 Switched Coupler, Lithium Niobate

Operating wavelength:	1.3μm
Material:	Crystal Technology, X-cut, Y-propagating
Bias voltage:	< 40 V
Switching voltage:	< 5 V
Coupling ratio:	0.1
Extinction:	> = 25 dB
Excess loss:	2.1 dB
Transition time:	2 ns
Dynamic range:	15 dB

5.2 COMPONENT TEST PLAN

Component Test Plan was generated to describe tests and test methods for the five classes of couplers fabricated under the Component Breadboard Task. The test plan was provided to satisfy the CDRL-A0003 requirement.

5.3 COMPONENT TEST VERIFICATION

Detailed measurements of component parameters, both during fabrication and on completion, verify the analytical design approach, confirming that high-precision polished coupler components can indeed be fabricated to demanding specifications, both as single elements and in multi-element arrays. Components for delivery have been shown to conform to projected performance targets, as outlined in Section 5.1.3, and have been prepared for delivery adjusted to the levels of optical power coupling specified for the various applications described in the System Design Plan.

A complete copy of the component test report is attached in Appendix E. The document describes the results of tests and test procedures used to characterize the 4-port optical coupler signal-processing components fabricated.

6.0 PROCESSOR DESIGN/PLAN

Based on work accomplished in Tasks 1, 2, 3, and 4, a System Design Plan was prepared. This design provides a concise summary of previous work on fiber optic based signal processing designs, including descriptions and critiques of the various architectures and a discussion of processor design latitude available for each architecture. Performance improvements for key components are also described. Utilizing an optimum architecture and improved components, three processors are designed that will perform the following functions:

- Band-pass filtering at 4.75 GHz center frequency with simultaneous high quality factor and low sidelobe level.
- Adjustable 4 bit coded sequence generation at 2 Gbit/s pulse rate.
- Matrix-vector multiplication with a general 2 x 2 matrix at 0.5 Gbit/s rate.

Theoretical system performance predictions are outlined for each processor.

6.1 BAND-PASS FILTER

Table 2.2 on page 2.15 summarizes qualitatively the pertinent characteristics of the classes of filters considered during the system design phase. The evidence indicates that the cascaded recirculating delay line should be selected as one of the three processors to be breadboarded, not only because of its potentially higher center frequency, a characteristic arising from its intrinsic loop length difference dependence, but also because of its enhanced sidelobe rejection and high quality factor attainable by employing only a few couplers.

6.1.1 ARCHITECTURE

The very low excess coupler loss and the integrated technique proved in Task 4, Component Breadboarding, show that the cascaded recirculating delay line architecture can be used for band-pass filtering. With only a few couplers, it can provide a low sidelobe level, a high quality factor, and a high center frequency while avoiding fiber bending loss, making it the architecture of choice for the band-pass filter. An order 3 delay line with single mode fiber and adjustable couplers was designed. The configuration is show in Fig. 6.1. The parameters of the single mode fiber are.

Fiber type: Corning SM-06S-P

Core index n = 1.4514 at wavelength = 1.3μm

Cladding index = 1.4469

The proposed 4.75 GHz center frequency requires a fundamental delay time of t = 1/4.75 = 0.21 ns. To avoid bending loss, the loop lengths should be 21.70 cm for the first loop, 26.04 cm for the second loop, 30.38 cm for the third loop, a 5 : 6 : 7 time fundamental delay length (i.e., light propagating path length in fundamental delay time). In order to avoid loss, four couplers are built in a monolithic silicon with a single fiber without splice.

$$a_0 = a_1 = a_2 = a_3 = 0.9$$

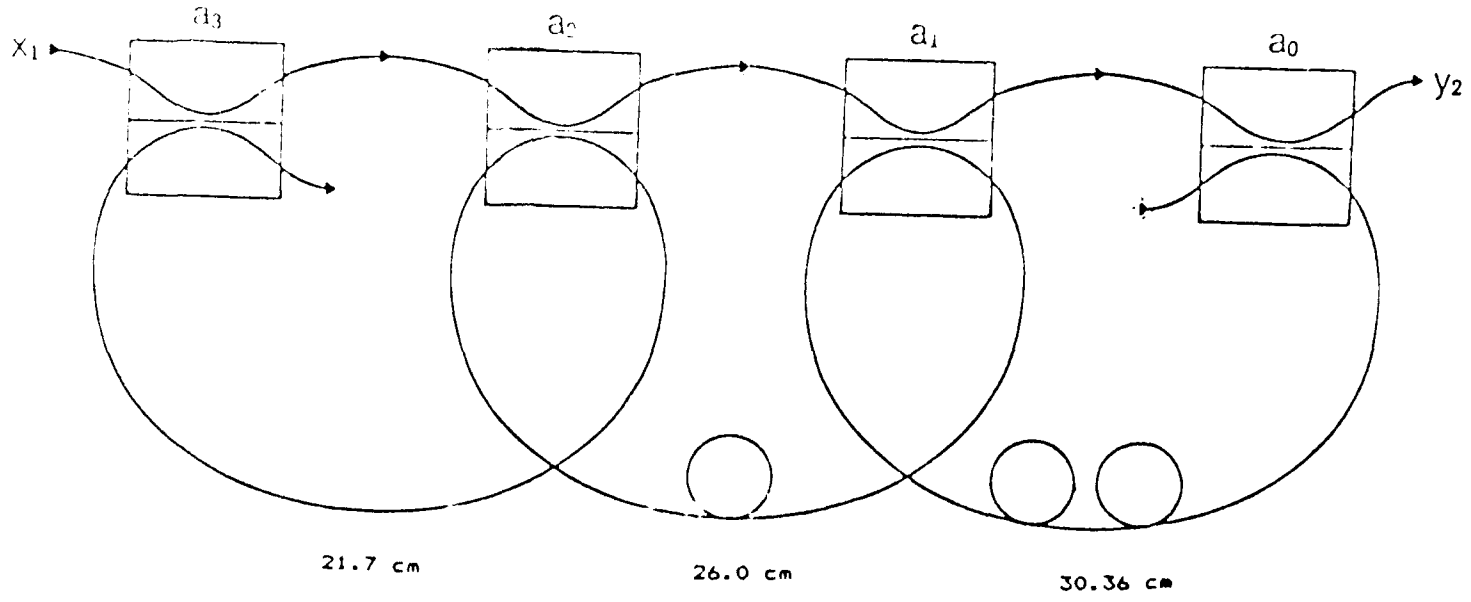

τ = 1/4.75 GHz = 0.21 NS (1 CM = 4.8 PS)

Figure 6.1 Theoretical scheme of an Order 3 cascaded recirculating delay line for Band-pass filter

Therefore, the system was being made at the same time the couplers were fabricated. The practical figure is shown in Fig. 6.2.

Since the coupling coefficients of the couplers are adjustable, they will be pre-set at 90%, which is the most probable value for the final setting. Higher coefficients give better performance but decrease the power efficiency. Therefore, high power lasers and high sensitivity receivers are required. The coefficients can be adjusted for optimum performance before and during the operation.

6.1.2 PREDICTED PERFORMANCE

The performance of a band-pass filter can be determined from its frequency response. As discussed above, performance depends strongly on the coupling coefficients and the capability of the source/receiver system. Based on the source/receiver system available, suitable coefficients may be derived. The frequency responses are calculated and predicted for three different sets of coefficients: $a_1=a_2=a_3=a_4=0.7$; 0.8; 0.9 and are shown in Figs. 6.3, 6.4, and 6.5 respectively.

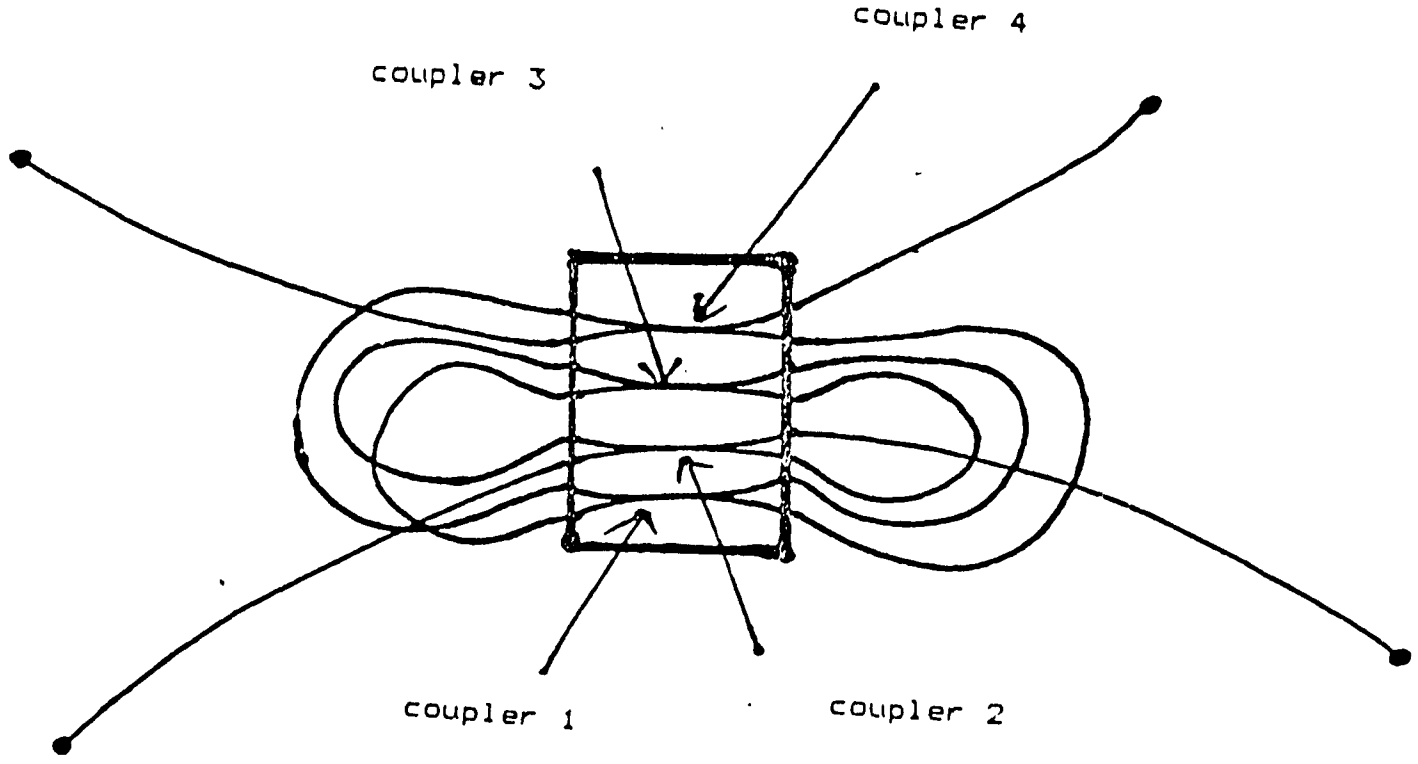

Figure 6.2 Designed integrated Band-pass filter

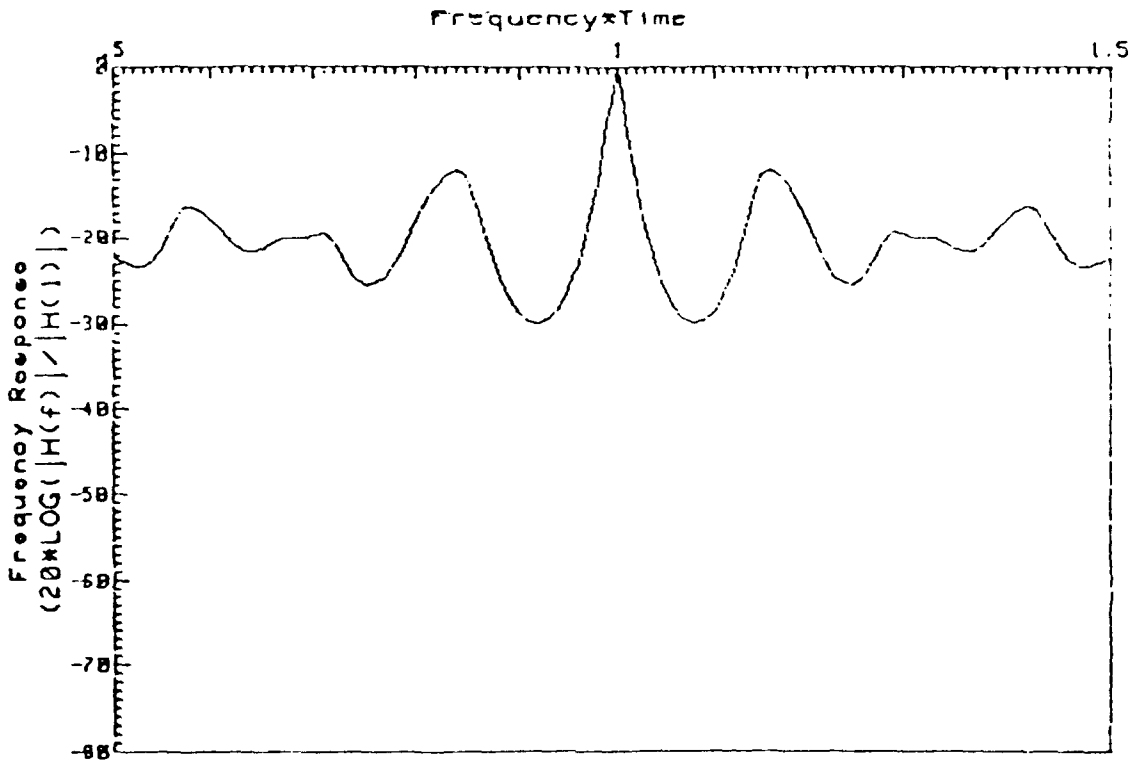

Figure 6.3. Normalized frequency response of the cascade recirculating delay line of order 3.

The insertion loss per coupler -.0436480540245 dB.

The coupling coefficients are $a_1=a_2=a_3=a_4=0.7$.

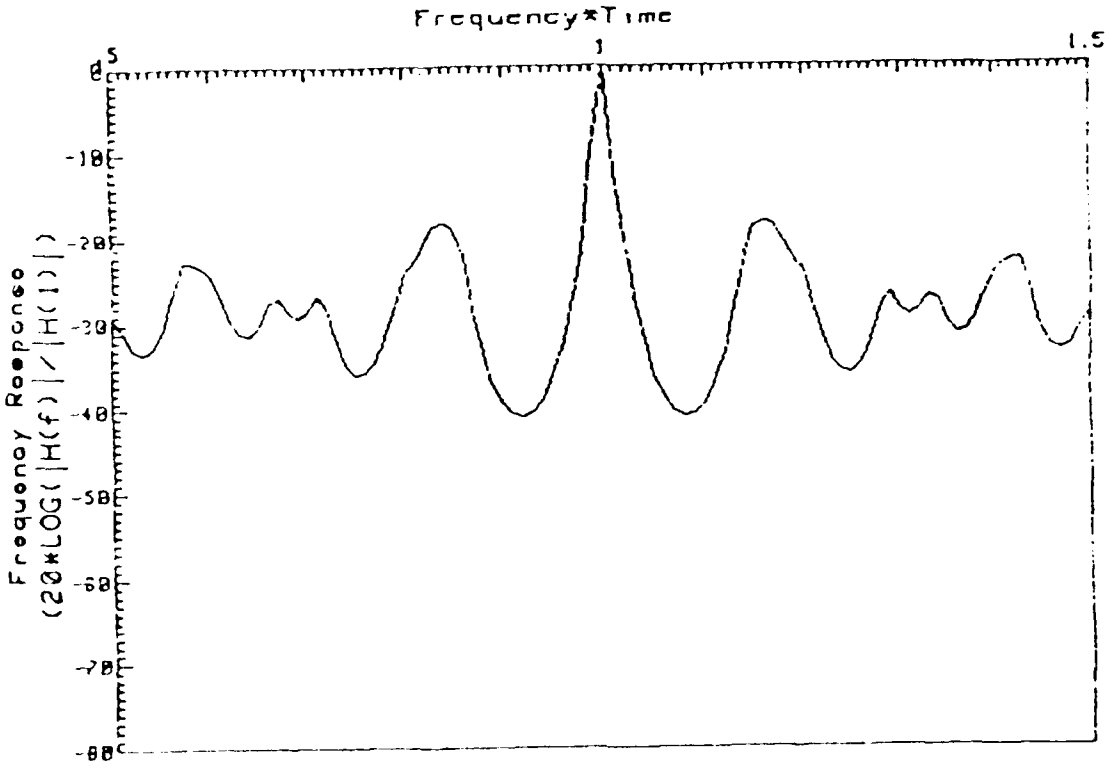

Figure 6.4. Normalized frequency response of the cascade recirculating delay line of order 3.

The insertion loss per coupler -.0436480540245 dB.

The coupling coefficients are $a_1=a_2=a_3=a_4=0.8$.

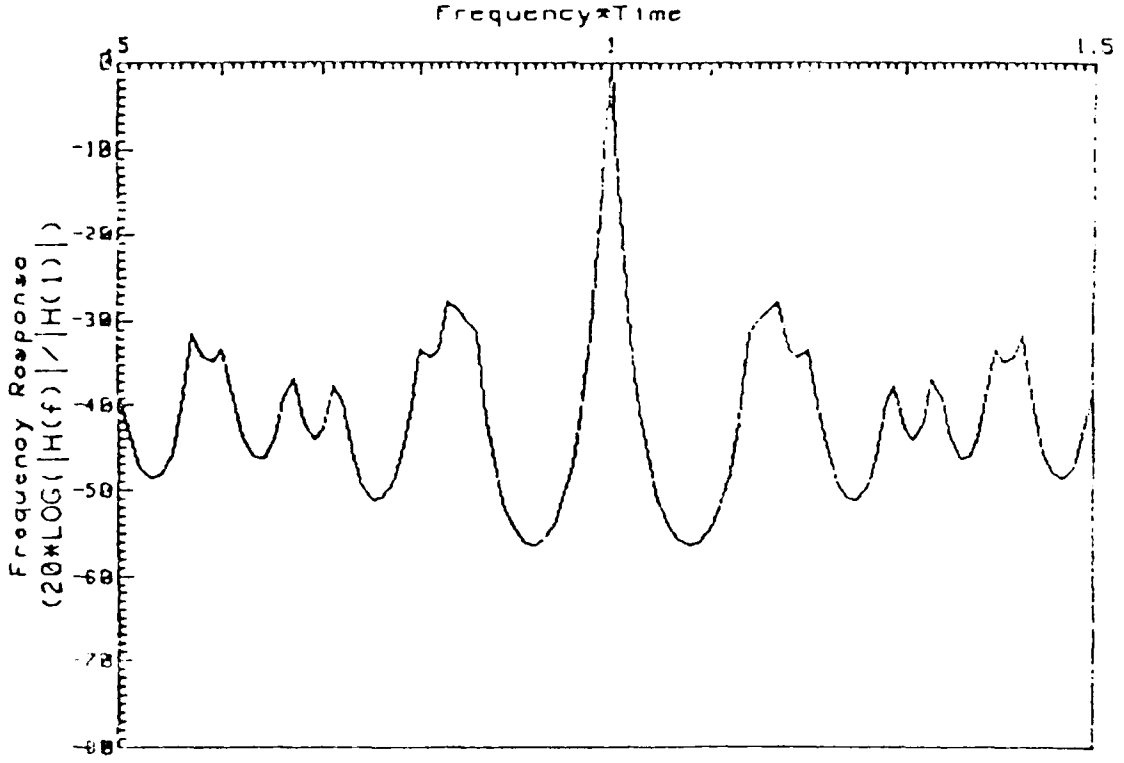

Figure 6.5. Normalized frequency response of the cascade recirculating delay line of order 3.

The insertion loss per coupler -.0436480540245 dB.

The coupling coefficients are $a_1=a_2=a_3=a_4=0.9$.

The peak-to-sidelobe ratios and quality factors in each case are summarized in Table 6.1.

COUPLING COEFFICIENCY	Q	PEAK-TO-SIDELOBE RATIO (dB)	POWER EFFICIENCY (%)
All .7	69	-12	8.2
All .8	102	-18	4.33
All .9	146	-28	1.18

TABLE 6.1. PREDICTED PERFORMANCES IN TERMS OF COUPLING COEFFICIENTS.
THE CASCADED RECIRCULATING DELAY LINE OF ORDER 3.
THE INSERTION LOSS PER COUPLER IS -0.44 dB.

6.2 CODED SEQUENCE GENERATOR

The preferred structure for a coded sequence generator is the non-recirculating lattice delay line. In this configuration, optical output emerges from a single fiber, with no second-pass interference. It is also easy to extend the length of the sequence by adding couplers. In comparison, the recirculating lattice suffers from multiple-pass interference

and bending loss, while the tapped delay line structures require signal summation external to the fiber and, perhaps, weighting modulators.

6.2.1 ARCHITECTURE

As recommended in the design studies, the non-recirculating lattice delay line is applicable to coded sequence generation. An order 3 non-recirculating lattice delay line with a delay time of 0.5 ns was designed. Single mode fiber and four couplers with parameters specified in the previous sections are employed. The configuration of the delay line is shown in Fig. 6.6. The length difference of the upper and lower fibers linking two adjacent couplers in this figure are 10.34 cm. Optical signal of 1.3μm wavelength propagating in a 10.34 cm long glass fiber (Corning SM-06S-P) of refraction index 1.4514 gives the desired delay time of 0.5 ns.

6.2.2 PREDICTED PERFORMANCES

The proposed coded sequence generator is capable of generating 4-bit coded sequences with a speed of 2 Gbit/s. Four sequences, 1111, 1101, 1011, 1001, can be performed by adjusting the coupling coefficients. Sequence 1111 is achieved by letting all coupling coefficients be equal to some

non-zero value a; sequence 1101 by $a_2=0$ and $a_0=a_1=a_3=a$; sequence 1011 by $a_1=0$ and $a_0=a_2=a_3=a$; and sequence 1001 by letting $a_1=a_2=0$ and $a_0=a_3=a$. Their uniformities and extinctions depend on the constant a and are summarized in Tables 6.2 and 6.3. Sequences 1101 and 1011 have the same uniformity and extinction when using the same a. Sequence 1001 will give exactly uniform coded 1 pulses and absolute extinction in coded 0. In addition, coded sequences less than 4-bit may also be generated by selecting suitable coupling coefficients. For example, 3-bit coded sequence may be generated with $a_0=0$.

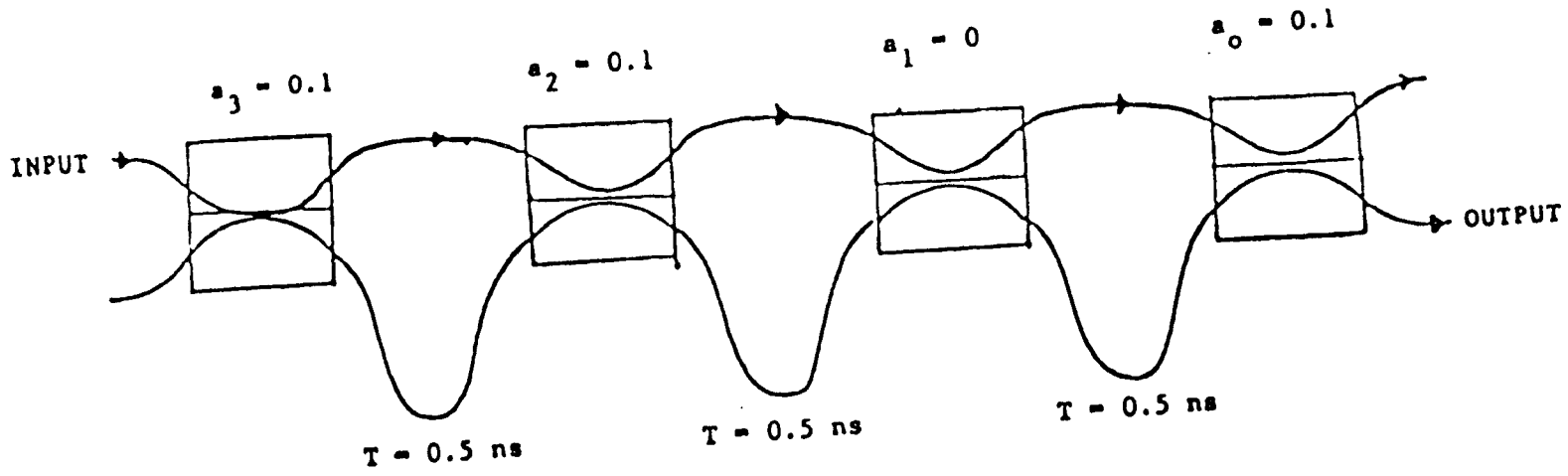

$A1 = A2 = A3 = A4 = 0.1$ CODE 1111

$A1 = A2 = 0,\ A3 = A_O = 0.1$ CODE 1001

DATA RATE: 2 GBIT/S

Figure 6.6 Four-bit coded sequence generator

a	uniformity (dB)
.05	.012
.07	.024
.10	.053
.20	.248
.30	.626

TABLE 6.2. UNIFORMITY OF SEQUENCE 1111

a	Extinction (dB)
.05	-24.7
.07	-22.4
.10	-19.0
.20	-12.0
.30	- 7.0

TABLE 6.3. UNIFORMITY AND EXTINCTION OF SEQUENCES 1101 AND 1011

Both sequences have the same characteristics.

Coded 1 pulses are exactly uniform.

6.3 MATRIX-VECTOR MULTIPLIER

6.3.1 ARCHITECTURE

A 2 x 2 general matrix-vector multiplier utilizing an order 2 non-recirculating lattice delay line is selected, requiring three couplers. Its configuration is shown in Fig. 6.7. An electrically tunable (switched) coupler, a_1, has been fabricated and put between a_2 and a_3. Because the switched coupler operates with polarized light only, polarization maintaining fiber for the waveguide and delay material is needed. In addition, the other couplers are also fabricated using polarization maintaining fibers. Between the light source and the processor, an extra coupler is utilized to couple input light to the opto-electronic subsystem for switching a_1. The opto-electronic subsystem is an electrical circuit designed to drive the switched coupler. In its free state it supports a bias voltage to the switched coupler so that the coupling coefficient of the switched coupler is a_1=0 (unswitched state). When the first pulse coupled from coupler a_3 reaches the opto-electronic subsystem, its bias voltage changes, and the coupling coefficient becomes a_1=0.1 (switched state).

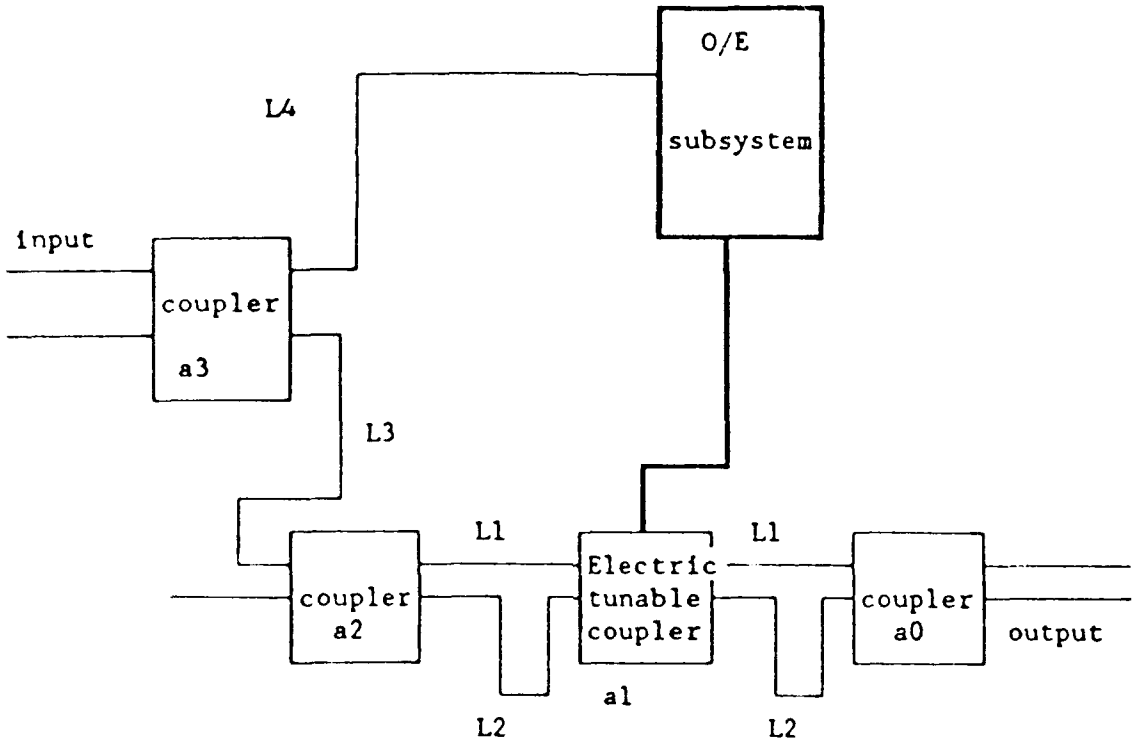

—— : polarization maintaining fiber

—— : electrical wire

L_1 = 20 cm
L_2 = 61.36 cm
L_3 = 50 cm
L_4 = 50 cm

Figure 6.7. Matrix-vector multiplier.

In order to implement a non-recirculating lattice delay line with a delay time of 2 ns, fiber lengths used in each stage are calculated and indicated in Fig. 6.7. The coupling coefficients of the couplers are set:

$a_0=0.1$

$a_1=0$ at unswitched state

$a_1=0.1$ at switched state

$a_2=0.1$

and

$a_3=0.025$

6.3.2 PREDICTED PERFORMANCE

Time domain application of this processor can yield matrix-vector multiplication. When two pulses with amplitudes 1:0.5 (representing a vector with elements 1 and .5) are fed into the processor the resultant y_1 and y_2 of the matrix-vector multiplication is obtained from the output pulses:

$$\begin{pmatrix} y_1 \\ y_2 \end{pmatrix} = \begin{pmatrix} 1 & 0 \\ 1 & 1 \end{pmatrix} \cdot \begin{pmatrix} 2 \\ 1 \end{pmatrix} = \begin{pmatrix} 2 \\ 3 \end{pmatrix}$$

The ratio of the two pulses that depends on the coupling coefficients of the coupler is compared with the ideal value $y_2/y_1=1.5$ in Table 6.4.

a	y_2/y_1
0.06	1.54
0.10	1.57
0.14	1.61
0.18	1.66
0.22	1.72
0.26	1.8

TABLE 6.4. PREDICTED PERFORMANCES OF THE MATRIX-VECTOR MULTIPLIER DESIGNED WITH RESPECT TO COUPLING COEFFICIENCIES.

In ideal case $y_2/y_1=1.5$

7.0 SYSTEM BREADBOARD EXPERIMENT

The program proceeded into the breadboard stage as required in SOW 4.1.5. The construction and characterization of coded sequence generator was subcontracted to Plessey Research Caswell Limited, and the work required for the other two processors, band-pass filter and matrix-vector multiplier, was conducted at PCO. The breadboard of coded sequence generator was completed successfully. However, the work at PCO has suffered from a number of setbacks and was not completed. First, the 4.75 GHz transmitter and receiver pair required for the breadboard experiment were not available to PCO from the government. The technical progress was further jeopardized by the departure of a key technical staff member, who was the only qualified person at PCO to complete the experiment. At that time, PCO had already incurred costs of more engineering/technician hours than the contract provided.

7.1 TEST RESULTS -- CODED SEQUENCE GENERATOR

In Appendix F, we describe the design, construction, and testing of a quasi-monolithic, splice-free 4-stage optical fiber coded sequence generator. The breadboard system permits generation of reconfigurable 4-bit pulse sequences, with pulse repetition rate of 2 GHz, i.e., 500 ps interval within the

pulses in the output train. The program has confirmed the feasibility of the manufacture of monolithic arrays of evanescent wave coupler elements in a single length of fiber with uniform coupling characteristics and repeatable coupler separation, suitable for the assembly of splice-free multi-stage optical signal processing systems.

Detailed measurement of coupler parameters, both during fabrication and on completion, verifies the analytical design approach, confirming that high precision couplers can be fabricated to demanding specifications in multi-element arrays configured on a single fiber length. The breadboard system has been shown to conform to projected performance targets and has been prepared for delivery adjusted to the specified level of optical power coupling detailed in the System Design Plan.

The quasi-monolithic construction approach adopted in this case represents a new departure for multiple coupler assemblies, permitting manufacture of multiple individual coupler elements on a single fiber length at separations considerably less than the mechanical dimensions of an individual mechanical assembly. An output pulse repetition rate of 2 GHz has been demonstrated here, based on an

incremental fiber delay length of 103 mm. This dimension is obviously capable of significant further reduction; given current technology, it appears perfectly feasible to reduce the incremental delay by a factor of 10 , to order 10 mm, giving an output pulse repetition rate of 20 GHz.

The operating instructions and user's notes for the coded sequence generator are included in Appendix G.

APPENDIX A

BIBLIOGRAPHY OF FIBER OPTIC BASED SIGNAL PROCESSING

FIBRE-OPTIC BASED SIGNALLING PROCESSING BIBLIOGRAPHY

[1] Fiber optic delay lines for microwave signal processing,
K.Wilner and A.P.van den Heuvel,
Proc. IEEE, **64**, 805-807 (1976)

[2] Fiber and integrated optics techniques for radar and communications signal processing,
G.M.Dillard, H.F.Taylor and B.R.Hunt,
Proc. Nat. Telecoms. Conf., 1976, p37.5/1-5

[3] Optical fiber delay line signal processing,
K.P.Jackson, S.A.Newton, B.Moslehi, M.Tur, J.W.Goodman and H.J.Shaw,
IEEE Trans., **MTT-33**, 193-210

[4] Fiber optic lattice signal processing,
B.Moslehi, J.Goodman, M.Tur and H.J.Shaw,
Proc. IEEE, **72**, 909-930 (1985)

[5] Optical fibre signal processing,
B.Culshaw,
Proc. SPIE, **468**, 167-173 (1984)

[6] Optical fibre systems for signal processing,
B.Culshaw, in Advanced Signal Processing, ed. D.J.Creasey

[7] Fiber optic delay line devices for R.F. signal processing,
C.T.Chang, J.A.Cassaboom and H.F.Taylor,
Elect .Letts., **13**, 678-680 (1980)

[8] Novel narrowband fibre-optic microwave filter,
M.F.Lewis and C.L.West,
Elect. Letts., **22**, 1016-1017 (1986)

[9] Cascaded fibre-optic microwave filters,
M.F.Lewis, I.R.Mason and C.L.Wood,
IEE Colloq. on Optical Techniques for Information Processing, London, 1987

[10] High frequency narrowband single mode fiber optic transversal filter,
C.C.Wang,
J .Lightwave Tech., **LT-5**, 77-81 (1986)

[11] Microbend optical fiber tapped delay line for GHz signal processing,
J.E.Bowers, S.A.Newton and C.C.Cutler,
App. Phys. Letts .,**41**, 139-141 (1982)

[12] Optical fiber V-groove transversal filter,
S.A.Newton, K.P .Jackson and H.J.Shaw,
App. Phys. Letts., **43**, 149-151 (1983)

[13] Switched optical delay line signal processors,
R.I.MacDonald,
J. Lightwave Tech ., **LT-5**, 856-861 (1987)

[14] Filter response of single mode fiber recirculating delay lines,
J.E.Bowers, S.A.Newton, W.V.Sorin and H.J.Shaw,
Elect. Letts., **18**, 110-111 (1982)

[15] Single mode fiber recirculating delay lines,
S.A.Newton, J.E.Bowers and H.J.Shaw,
Proc. SPIE, **326**, 108-115 (1982)

[16] Frequency filters using fibre optic delay lines,
Y.Sano and K.Nakamura,
Proc ECOC 1982, Cannes.

[17] Programmable time-delay devices,
R.A.Soref,
Appl .Opt ., **21**, 3736-3737 (1984)[18]

[18] Fiber optic signal processor with applications to matrix-vector multiplication and lattice filtering,
M.Tur, J.W.Goodman, B.Moslehi, J.E.Bowers and H.J.Shaw,
Opt. Letts., **7**, 463-465 (1982)

[19] Optical guided wave signal processor for matrix vector multiplication and filtering,
M.Tur, J.W.Goodman, H.J.Shaw, B.Moslehi and J.E.Bowers,
U.S.Patent 4,588,255

[20] All-fibre signal processing components and applications,
T.Bricheno and D.P.M.Chown,
Proc. ECOC 1986, p.421-424 (1986)

[21] Integrated fibre optical signal processing systems,
D.P.M Chown and T.Bricheno,
IEE Colloq. on Advanced Fibre Waveguide Devices, London 1986

[22] Fibre optic tapped delay line filter employing coherent optical processing,
D.E.N Davies and G.W.James,
Elect .Letts., **20**, 95-97 (1984)

[23] Coherent optical fiber transversal filter,
D.E.N.Davies,
CLEO 1984 Technical Digest, Paper ThN5

[24] Reflectively tapped optical fiber transversal filters,
C.E.Lee, R.A.Atkins and H.F.Taylor,
Elect. Letts., **23**, 596-598 (1987)

[25] Let's design algorithms for VLSI systems,
H.T.Kung,
Proc. Conf. on VLSI Architecture, Design, Fabrication, CalTech 1979, p.65-90 (1979)

[26] Low dispersion notch filter for multi-GHz frequencies using fiber optic delays,
J.D .impson and R.Konecny,
IEEE Trans. Nucl. Sci., **NS-32**, 2129-2131 (1985)

[27] Fiber optic variable delay lines,
J.E.Bowers, S.A.Newton and H.J.Shaw,
Elect. Letts., **18**, 999-1001 (1982)

[28] Microwave frequency response of an optical fiber delay line,
S.A.Newton and P.S.Cross,
Elect .Letts., **19**, 480-482 (1983)

[29] Optoelectronic switch matrices: recent developments,
R.I. MacDonald and D.K.W.Lam,
Opt. Eng., **24**, 220224 (1985)

[30] All-fiber components using periodic coupling,
R.C.Youngquist, J.L.Brooks,W.P.Risk, G.S.Kino and H.J.Shaw,
IEE Proc. Pt. J, **132**, 277-286 (1985)

[31] Fiber optical delay lines for pulse coding,
R.L.Ohlhaber and K.Wilner,
Electro-Opt Syst. Des., **9** (2), 33-35 (1977)

[32] Encoding decoding optical fiber network,
E.Marom and O.G.Ramer,
Elect. Letts., **14**, 48-49 (1978)

[33] 1 Gbit/s code generator and matched filter using an optical fiber tapped delay line,
K.P.Jackson, S.A.Newton and H.J.Shaw,
App. Phys. Letts., **42**, 556-558 (1983)

[34] High speed pulse train generation using single mode fiber recirculating delay lines,
S.A.Newton, R.S.Howland. K.P.Jackson and H.J.Shaw,
Elect. Letts., **19**, 756-758 (1983)

[35] Reflex optoelectronic switching matrix,
D.K.W.Lam and R.I.MacDonald,
J .Lightwave Tech ., **LT-2**, 88-90 (1984)

[36] DMA fiber-optic network with optical processing,
P.R.Prucnal, M.A.Santoro, S.K.Setigal and I.P.Kaminow,
Elect .Letts ., **22**, 1218-1219 (1986)

[37] Ultrafast all-optical synchronous multiple access fiber networks.
P.R.Prucnal, M.A.Santoro and S.K.Setigal,
IEEE J .Select Area Comm ., **SAC-4**, 1484-1493 (1986)

[38] Optical delay line matched filters,
E.Marom,
IEEE Trans., **CAS-25**, 360-364 (1978)

[39] Noncoherent radar moving target indicator using fiber optic delay lines,
C.T.Chang, D.E.Altman, D.R.Wehner and D.J.Albares,
IEEE Trans. Circ. and Syst ., **CAS-26**, 1132-1134 (1979)

[40] Fiber optics matched delay filter for RF direction finding,
S.A.Pappert, M.N.McLandrich and C.T.Chang,
J. Lightwave Tech., **LT-3**, 273-276(1985)

[41] Coherent optical fiber delay line processor,
K.P.Jackson, G.Xiao and H.J.Shaw,
Elect. Letts., **22**, 1335-1337 (1986)

[42] Analog matrix multiplication by directional coupling between optical fibers,
J.P.Palmer and P.B.Ward,
Proc. SPIE, **232**, 157-159 (1978)

[43] Why systolic architectures,
H.T.Kung,
Computer ,**15**, 37-46 (1982)

[44] Systolic arrays for VLSI,
H.T.Kung and C.E.Leiserson,
in Sparse Matrix Proceedings 1978 eds. I.S.Duff and G.W .Stewart p. 262-282

[45] Alorithms for VLSI arrays
H.T.Kung and C.S.Leiserson,
in Introduction to VLSI systems, eds. C.Mead and L.Conway, Addison-Wesley (1980)

[46] Scattering arrays for matrix computations,
J-M.Delosme and M.Morf,
Proc. SPIE, **298**, 74-83 (1981)

[47] Fiber optic signal processor with applications to matrix-vector multiplication and lattice filtering,
M.Tur, J.W.Goodman, B.Moslehi, J.E.Bowers and H.J.Shaw,
Opt. Letts.,**7**, 463-465 (1982)

[48] Fibre optic multichannel correlation/convolution,
M.Shabeer, I.Andonovic and B.Culshaw,
Elect. Letts ., **23**, 310-311 (1987)

[49] Fiber optic matrix multiplier using a 2-dimensional systolic array architecture,
M.Shabeer, I.Andonovic and B.Culshaw,
Opt . Letts., **12**, 959-961 (1987)

[50] Laser phase noise effects in fiber optic signal processors with recirculating loops,
M.Tur and B.Moslehi,
Opt Letts **8**, 229-231 (1983)

[51] Spectral structure of phase-induced intensity noise in recirculating delay lines,
M.Tur, B.Moslehi, J.E.Bowers, S.A.Newton, K.P.Jackson, J.W.Goodman, C.C.Cutler and H.J.Shaw,
Proc. SPIE, **412**, 2227 (1983)

[52] Theory of laser phase noise in recirculating fiber optic delay lines,
M.Tur, B.Moslehi and J.W.Goodman,
J .Lightwave Tech., **LT-3**, 20-21 (1985)

[53] Analysis of optical phase noise in fiber optic systems employing a laser source with arbitrary coherence time,
B.Moslehi,
J .Lightwave Tech., **LT-4**, 1334-1351 (1986)

[54] Rayleigh backscattering in optical fiber recirculating delay lines,
M.Nazarathy and S.A.Newton,
Appl .Opt ., **25**, 1051-1055 (1986)

[55] Phase-induced intensity noise in concatenated fiber-optic delay lines,
M.Tur and A .rie,
J. Lightwave Tech., **LT-6**, 1200-130 (1988)

APPENDIX B

CALCULATIONS OF FILTER CHARACTERISTICS

FILTER CHARACTERISTIC CALCULATIONS

The following notes collect together in a coherent format material originally presented in the Monthly Reports for May, June and July 1987.

1 FREQUENCY RESPONSE - ATTENUATING FILTER

The standard analytical expression for the frequency response of the idealised equal-weight, equal-delay transversal filter can be derived by considering the output response to an input frequency f. as being represented by the summation of the appropriate set of delayed versions of the input. In the case of the ideal transversal filter, the standard representation is:

$$I_{out} = I_{in}/j \,.\, Re \sum_{n=0}^{n=N-1} \exp(2.\pi.j.f(t + kT))\} \qquad (1.1)$$

where N is the number of taps, k is the tap coupling coefficient and T is the inter-tap delay period.

From Born & Wolf (Principles of Optics), the key mathematical step is the use of the identity:

$$\sum_{n=0}^{n=N-1} \exp(-jnx) = \{1-\exp(-jNx)\}/\{1-\exp(-jx)\}$$

$$= \{2 - 2.\cos(Nx)\}/\{1 - 2.\cos(x)\}$$

$$= \{\sin(N.x/2)\}/\{\sin(x/2)\} \qquad (1.2)$$

which with the substitution:

$$x = 2.\pi.f.t$$

reduces to the standard form for the AMPLITUDE response :

$$H(f) = \sin(N.\pi.f.dt)/\sin(\pi.f.dt). \qquad (1.3)$$

This derivation can be extended to incorporate the effects of power extraction along the length of the fibre, the situation that obtains in the tapped optical fibre transversal filter. Defining an attenuation constant, a, in terms of the tap coupling factor, k, (assumed constant) as:

$$\exp(-a) = (1 - k) \qquad (1.4)$$

the output amplitude series becomes:

$$I_{out} = I_{in}/j \,.\, Re \sum_{n=0}^{n=N-1} a^n.\exp(2.\pi.j.f(t + kT))\} \qquad (1.5)$$

giving by analogy:

$$\sum_{n=0}^{n=N-1} a^n.\exp(-jnx) = \sum_{n=0}^{n=N-1} \{a.\exp(-jx)\}^n$$

$$= \{1 - a^n.\exp(-jNx)\}/\{1 - a.\exp(-jx)\} \qquad (1.6)$$

giving:

$$H(f) = \{(1 + a^{2N} - \cos(2.\pi.N.f.dt))\}/\{(1 + a^2 - \cos(\pi.f.dt))\} \quad (1.7)$$

where N is the number of tap points and dt is the incremental delay period. For the idealised configuration in which negligible power extraction occurs, i.e. a = 0, this expression reduces to the well-known sin(Nx)/sin(x) form.

2 FREQUENCY RESPONSE

Analytical expressions for frequency response of fibre delay line elements based on the major technology options are collected here, using consistent notation.

2.1 Ideal Tapped Delay Line Transversal Filter

$$H(f) = \sin(N.\pi.f.dt)/\sin(\pi.f.dt) \quad (2.1)$$

2.2 Attenuating Transversal Filter

$$H(f) = \{(1 + a^{2N} - \cos(2.\pi.N.f.dt))\}/\{(1 + a^2 - \cos(\pi.f.dt))\} \quad (2.2)$$

2.3 Dual-Coupler Non-recirculating Delay Line

$$H(f) = \sqrt{(C_1^2 + C_2^2 + 2.C_1.C_2.\cos(2.\pi.f.dt))}/(C_1 + C_2) \quad (2.3)$$

where:

$$C_1 = (1 - k_1).(1 - k_2).a_1.a_2 \quad (2.4)$$

$$C_2 = k_1 k_2 a_1.a_2 \quad (2.5)$$

a_1, a_2 and a are the attenuations of the two couplers and the excess attenuation of the fibre loop respectively and k_1 and k_2 are the two coupling coefficients.

2.4 Dual-coupler Recirculating Delay Line

$$H(f) = (1 - C_2) / \sqrt{(1 + C_2^2 - 2.C_2.\cos(2.\pi.f.dt))} \quad (2.6)$$

with notation as above.

2.5 Single-coupler Recirculating Delay Line

$$H(f) = (1 - C_5).((C_4 - C_3.C_5)^2 + C_3^2 + 2.C_3.\sqrt{(C_4 - C_3.C_5).\cos(2.\pi.f.dt)}) /((C_3 + C_4 - C_3.C_5).\sqrt{(1 + C_5^2 - 2.C_5.\cos(2.\pi.f.dt))}**0.5) \quad (2.7)$$

where $C_3 = (1 - k)$, $C_4 = k^2.a$ and $C_5 = k.a$, where k is the coupling coefficient and a is the loop attenuation.

3 CENTRE FREQUENCY

The foregoing equations were formulated in terms of the temporal delay characterising either the inter-tap separation in linear transversal filters or the differential delay in recursive or non-recursive loop structures; as noted previously, pass-band centres in filter structures are generally located at frequencies defined by the reciprocal of the characteristic delay increment, dt. Dispersion of the refractive index, n, with optical wavelength implies that the propagation velocity (v = c/n), and hence the delay

(dt = 1/v = n/c) associated with a given fixed fibre path length, are similarly wavelength dependent.

In the majority of optical materials, including virtually all known glasses, the refractive index is a well behaved function of wavelength over the entire ultra-violet, visible and near infra-red region, a convenient semi-empirical representation being the Sellmeier oscillator [2], having the form:

$$(n^2 - 1) = \sum(A(i).lambda^2/(lambda^2 - B(i)^2)) \qquad (3.1)$$

where the constants A(i) and B(i) represent the strength and wavelength of the principle electronic oscillators. For synthetic fused silica, a third order approximation gives:

A(1) = 696.1663, B(1) = 68.4043
A(2) = -407.9426, B(2) = 116.2414
A(3) = 897.4794, B(3) = 9896.161,

where wavelength is specified in nm. Based on the assumption of U.V. grade fused silica for fibre core material, the following results are obtained:

WAVELENGTH DEPENDENCE OF DELAY CHARACTERISTICS

lambda (nm)	R.I.	dt (ns/m)	f(o) (GHz.m)
632.8	1.4570	4.8601	.20576
786.0	1.4536	4.8489	.20623
830.0	1.4528	4.8461	.20635
904.0	1.4517	4.8424	.20651
1064.0	1.4496	4.8355	.20681
1300.0	1.4469	4.8264	.20719
1500.0	1.4446	4.8187	.20752

indicating systematic variations of the order of 0.86% across the wavelength range of potential interest.

4 PASS-BAND WIDTH

Although the frequency responses of the majority of structures under consideration are capable of expression analytically, similar representation of fundamental pass-band width is not so readily achieved. For the transversal filter, a standard result is that the full pass-band width to the -4 db points is equal to the reciprocal of the delay increment:

$$df(4db) = 1/dt \qquad (4.1)I$$

n many cases, however, 3 dB bandwidth is a more conventional representation, in which case numerical solution for the roots of the equation:

$$H(f) = 0.5 \qquad (4.2)$$

s generally required in order to provide band-width characterisation.

For the ideal equal-tap, equal-delay transversal filter, solution of:

$$(SIN(N.x)/SIN(x))^2 = 0.5 \qquad (4.3)$$

where $x = \pi.f.dt$, provides numerical representation of the pass-band width as a function of tap number, N. Values of x and corresponding -3 dB widths (in units of 1/dt) for systems of up to 10 taps are tabulated, together with -4 dB values derived as mentioned above.

DEPENDENCE OF FILTER BANDWIDTH ON TAP NUMBER

N	df(3dB) (1/dt)	df(4dB) (1/dt)
2	0.248	0.500
3	0.156	0.333
4	0.116	0.250
5	0.092	0.200
6	0.076	0.167
7	0.064	0.143
8	0.056	0.125
9	0.050	0.111
10	0.045	0.100

Empirically, the -3 dB bandwidth is approximately 0.5 of the -4 dB figure, i.e. df(3dB) = 1/(2N) Similar analysis enables the filter band-width in the exponentially attenuated transversal filter and the various recirculating and non-recirculating loop structures to be characterised as a function of power coupling factor and tap number; calculations of this type are currently in progress.

5 QUALITY FACTOR

The quality factor, Q, of a filtering structure, is defined as the ratio of the centre frequency of the first order (m = 1) principal lobe, f(1) to the bandwidth, df, i.e.:

$$Q = f(1)/df \tag{5.1}$$

For the ideal transversal filter, Q = 2N, following the arguments above.

6 DYNAMIC RANGE

The characteristic equations for frequency response, summarised above, indicate the presence of notches between pass-bands and side-lobes; in cases such as the ideal transversal filter, these representations are cast in terms of trignometric functions indicating theoretically infinite notch depth. In the majority of configurations, however, this is not the case and the theoretical expressions indicate a limiting notch depth, generally dependent on the coupling coefficients and attenuations present in the system . By considering the maximum and minimum values taken by these expressions, and defining dynamic range, R, as the ratio of maximum to minimum transmission, the following analytical relationships can be obtained:

6.1 Ideal Tapped Delay Line Transversal Filter

Theoretically infinitely deep notches.

6.2 Attenuating Transversal Filter

$$R = (a^{2N}.(a^{2n} + 2))/(a^2.(a^2 + 2)) \tag{6.1}$$

where $a = -\ln(1 - k)$, k is the tap coupling factor and the system has N taps.

6.3 Dual-coupler Non-recirculating Delay Line

$$R = \sqrt{((C_1^2 + C_2^2 + 2C_1.C_2)/(C_1^2 + C_2^2 - 2C_1.C_2))} \qquad (6.2)$$

where:

$C_1 = (1 - k_1).(1 - k_2).a_1.a_2$

$C_2 = k_1.k_2.a_1.a_2.a$

a_1, a_2 and a are the attenuations of the two couplers and the excess attenuation of the fibre loop respectively and k_1 and k_2 are the two coupling coefficients.

6.4 Dual-coupler Recirculating Delay Line

$$R = \sqrt{(C_2^{**2} + 3)/(C_2^{**2} - 1))} \qquad (6.3)$$

with notation as above

6.5 Single-coupler Recirculating Delay Line

$$R = (((1 - C_5).(C_4 - C_3.C_5)^2 + C_3^2 + 2.C_3.(C_4 - C_3.C_5)) \times \sqrt{(C_3 + C_4 - C_3.C_5)(1 + C_5^2 + 2.C_5))/} (((1 - C_5).(C_4 - C_3.C_5)^2 + C_3^2 - 2.C_3.(C_4 - C_3.C_5)) \times \sqrt{C_3 + C_4 - C_3.C_5)(1 + C_5^2 - 2.C_5))} \qquad (6.4)$$

where $C_3 = (1 - k)$, $C_4 = k^2.a$ and $C_5 = k.a$, where k is the coupling coefficient and a is the loop attenuation.

6.6 4-Port Lattice Sections

4-port lattice sections can be regarded as essentially dual-coupler delay line structures of the recirculating or non-recirculating type and can be analysed accordingly, appropriate note being taken of the bidirectional direction of propagation where necessary. Thus, using the expressions reported previously:

6.6.1 Non-recirculating Lattice Sections

$$R = \sqrt{((C_1^2 + C_2^2 + 2C_1.C_2)/(C_1^2 + C_2^2 - 2C_1.C_2))} \qquad (6.5)$$

where:

$C_1 = (1 - k_1).(1 - k_2).a_1.a_2$ (6.2)
$C_2 = k_1.k_2.a_1.a_2.a$ (6.3)

a_1, a_2 and a are the attenuations of the two couplers and the excess attenuation of the fibre loop respectively and k_1 and k_2 are the two coupling coefficients.

6.6.2 Recirculating Lattice Sections

$$R = \sqrt{(C_2^2 + 3)/(C_2^2 - 1))} \qquad (6.4)$$

with notation as above.

7 POWER BUDGET

It is important to note that optical fibre signal processing configurations can be classified as those in which optical power is conserved and those which intrinsically discard significant fractions of the available incident power, which is thus unavailable for subsequent utilisation. Thus, whereas the total available optical power is shared between the fibres in the fibre-bundle transversal filter, in the practical tapped delay line equivalent, where power is extracted at each tap, and power incident on successive taps decreases exponentially along the line, the total available output power is of the order of N.k, where k is the tap coupling coefficient, typically a few per cent, and N is the number of taps. Similarly, whereas total power utilisation is a feature of the single coupler recirculating and dual-coupler non-recirculating delay line structures, this is not the case in the dual-coupler recirculating loop, which features an unused output port, dumping of the order of (1 - k) of the incident power on the first pass.

Note, however, that even in configurations which are theoretically power-conserving, temporal redistribution of the energy of an input single pulse into an output pulse train, and vice versa, may result in differences between input and output pulse amplitudes. Furthermore, absorption in fibres, together with absorption and scattering losses in couplers, may serve to introduce additional attenuation factors into hypothetically loss-free configurations.

d T(12) describes the converse situation, k1 and k2 are the coupling coefficients of the two couplers and a1 and a2 are attenuation of the loop and the forward fibre line respectively.

Optical power efficiency, i.e. the ratio of output to input powers, can be determined in terms of the system transfer function H(z), utilising the fact that the optical power is proportional to the dc frequency component in the baseband optical intensity signal, i.e. $z = 1$ *in the transfer function. The following* expressions for power transmission, T, in two-coupler recirculating and non-recirculating lattice elements have been identified.

7.2.1 Two coupler Recirculating Element

$$T_{11} = (k_1 + (1-2.k_1)k_2.a_1)/(1-k_1.k_2.a_1) \quad (7.1)$$

$$T_{12} = k_1.a_2(1-k_2) + k_2.a_1(1-k_1) \quad (7.2)$$

7.2.2 Two-coupler non-recirculating element:

$$T_{11} = (1 - k_1)(1 - k_2)a_2 + k_1.k_2.a_1 \quad (7.3)$$

$$T_{12} = k_1.a_2.(1 - k_2) + k_2.a_1.(1 - k_1) \quad (7.4)$$

where similar notation is used. (

7.2.3 Tapped Delay Line (n taps):

$$T = h(0) + h(1) + h(2) + ...+h(n-1) \quad (7.5)$$

8 NOISE PERFORMANCE

Noise in fibre structures has been investigated both theoretically and experimentally. Essentially, the power spectrum of the autocovariance spectrum has the form:

$$c(t_1,t_2) = \sum(G(M).d(t_2 - t_1 - Mt)) \quad (7.6)$$

where d is the Dirac delta function and the impulse intensities, G(M) are relatively complex mathematical expressions. To the extent that it is currently developed, the theory predicts the following, all observed experimentally:

(i) The periodic form of the spectrum, with a characteristic notch at d.c.

(ii) The shape of the basic period as a function of coupling coefficient.

(iii) The dependence of the spectrum on state of polarisation.

(iv) Insensitivity to environmental conditions.

APPENDIX C

CASCADED RECIRCULATING TRANSMISSION LINE WITHOUT BENDING LOSS LIMITATIONS

PATENT NO. 4,934,777

United States Patent [19]

Jou et al.

[11] Patent Number: 4,934,777

[45] Date of Patent: Jun. 19, 1990

[54] CASCADED RECIRCULATING TRANSMISSION LINE WITHOUT BENDING LOSS LIMITATIONS

[75] Inventors: Dong-Chuang Jou, Simi Valley; Ching-Jong Lil, Monrovia; Bor-Uei Chen, Studio City, all of Calif.

[73] Assignee: PCO, Inc., Chatsworth, Calif.

[21] Appl. No.: 326,657

[22] Filed: Mar. 21, 1989

[51] Int. Cl.[5] G02B 6/26

[52] U.S. Cl. 350/96.15; 350/96.16

[58] Field of Search 350/96.15, 96.16

[56] References Cited

U.S. PATENT DOCUMENTS

4,128,759	12/1979	Hunt et al.	250/199
4,469,397	9/1984	Shaw et al.	350/96.15
4,557,552	12/1985	Newton et al.	350/96.15
4,558,920	12/1985	Newton et al.	350/96.15
4,671,605	6/1987	Soref	350/96.15
4,723,827	2/1988	Shaw et al.	350/96.15
4,753,529	6/1988	Layton	356/345
4,768,850	9/1988	Moslehi et al.	350/96.15
4,778,239	10/1988	Shaw et al.	350/96.16

OTHER PUBLICATIONS

K. P. Jackson et al., "Optical Fiber Delay-Line Signal Processing", IEEE Trans. Microwave Theory Tech., vol. MIT-33, p. 193, 1985.

M. Tur et al., "Fiber-Optic Signal Processor with Applications to Matrix-Vector Multiplication and Lattice Filtering," Opt. Lett., vol. 7, p. 463, 1982.

K. P. Jackson et al., "Microbend Optical Fiber Tapped Delay Line for Gigahertz Signal Processing," Appl. Phys. Lett., vol. 41, p. 139, 1982.

J. E. Bowers, et al., "Filter Response of Single-Mode Fiber Recirculating Delay Lines," Electron Lett., vol. 18, p. 110, 1982.

B. Moslehi et al., "Fiber-Optic Lattice Signal Processing," Proc. IEEE vol. 72, p. 909, 1984.

C. C. Wang, "Cascaded Single-Mode Fiber Optic Transversal Filters", Proc. SPIE High Frequency Optical Communication, vol. 716, p. 82, 1986.

S. A. Newton et al., "Optical Fiber V-Groove Transversal Filter," Appl. Phys. Lett., vol. 43(2), p. 149, 1983.

Primary Examiner—William L. Sikes

Assistant Examiner—John Ngo

Attorney, Agent, or Firm—Antonio M. Fernandez

[57] ABSTRACT

A single-mode optical fiber delay line for filtering at high frequencies utilizes an nth order cascaded recirculating configuration comprised of n + 1 couplers. Each coupler has two input fibers and two output fibers. One of the output fibers of each coupler except the last is connected to one of the input fibers of the next coupler in cascade to form a feed-forward path. The other output fiber of each coupler except the first is connected to the other input fiber of the preceding coupler, thus forming a feed-backward path. The feed-forward path and the feed-backward path of adjacent couplers form a delay loop. The delay time in each succeeding delay loop is increased by an incremental delay τ equal to the reciprocal of the center frequency of the filter. The delay in the first delay loop is selected to be some multiple m of τ, where m is an integer selected for a total delay T which permits the use of optical fiber of a length sufficient to avoid bending losses in the optical fiber. The incremental time delay τ can be made extremely small, thereby making the operating frequency of the filter extremely high.

5 Claims, 4 Drawing Sheets

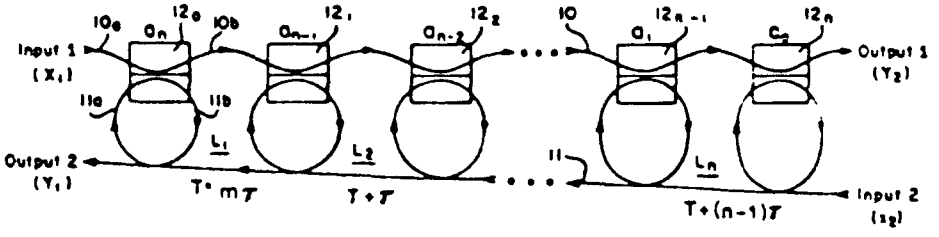

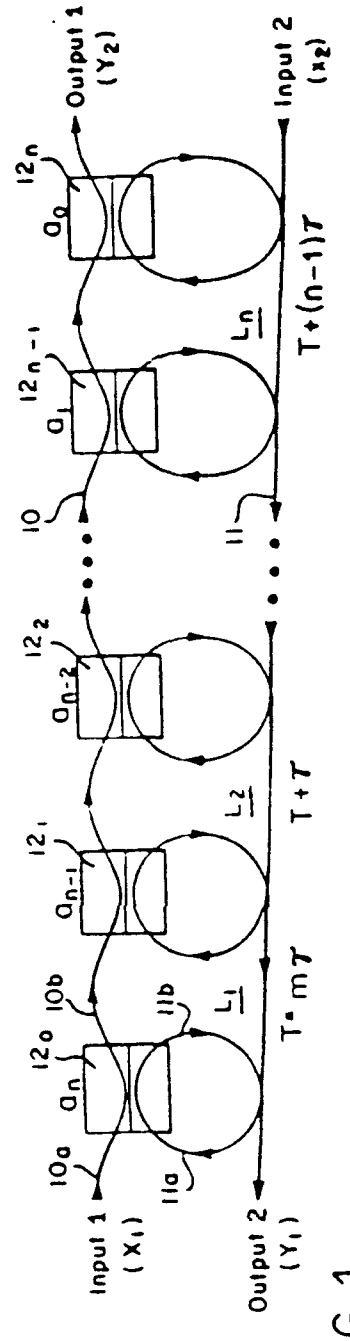
Output 1 (Y2)
Input 2 (x2)
12n
Qo
12n-1
Q1
10
11
Ln
T+(n-1)T
12₂
Qn-2
L2
T+T
12₁
Qn-1
10b
11b
12o
Qn
L1
T+mT
10a
11a
Input 1 (X1)
Output 2 (Y1)

FIG. 1

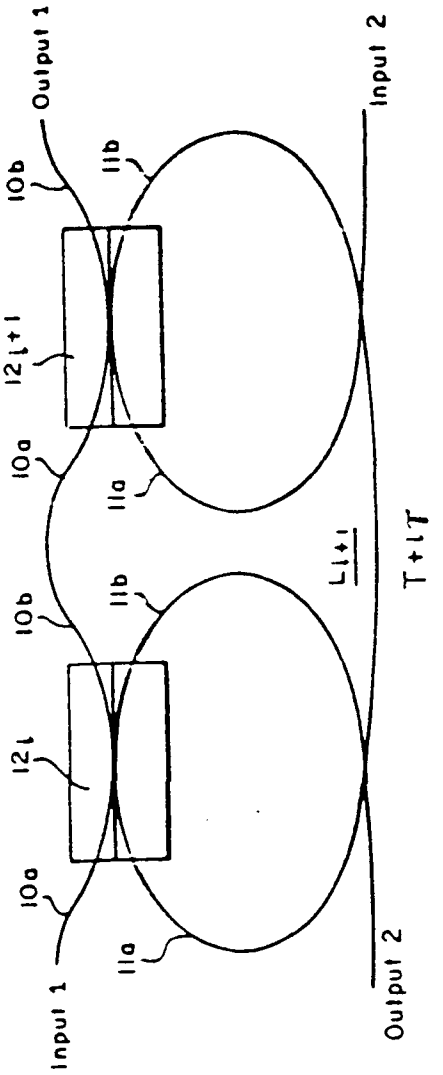
Output 1
Input 2
10b
11b
12l+1
10a
11a
Ll+1
T+lT
12l
Input 1
Output 2

FIG. 1a

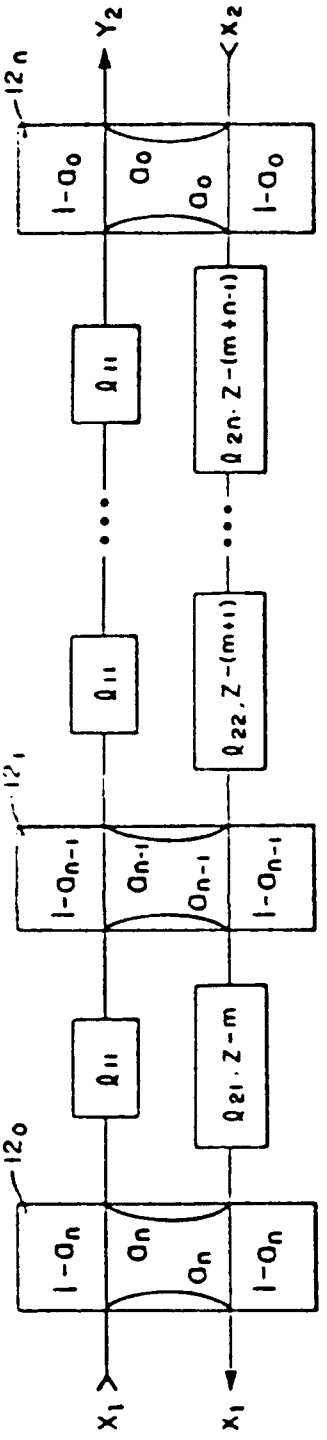
Y2
X2
12n
1-a0
a0
a0
1-a0
Q11
Q2n·Z-(m+n-1)
Q11
Q22·Z-(m+1)
12₁
1-an-1
an-1
an-1
1-an-1
Q11
Q21·Z-m
12o
1-an
an
an
1-an
X1
X1

FIG. 2

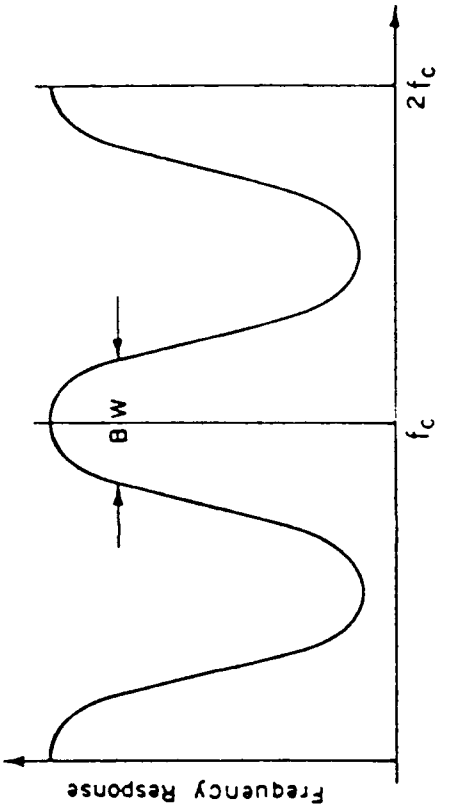
2fc
BW
fc
Frequency Response

FIG. 2a

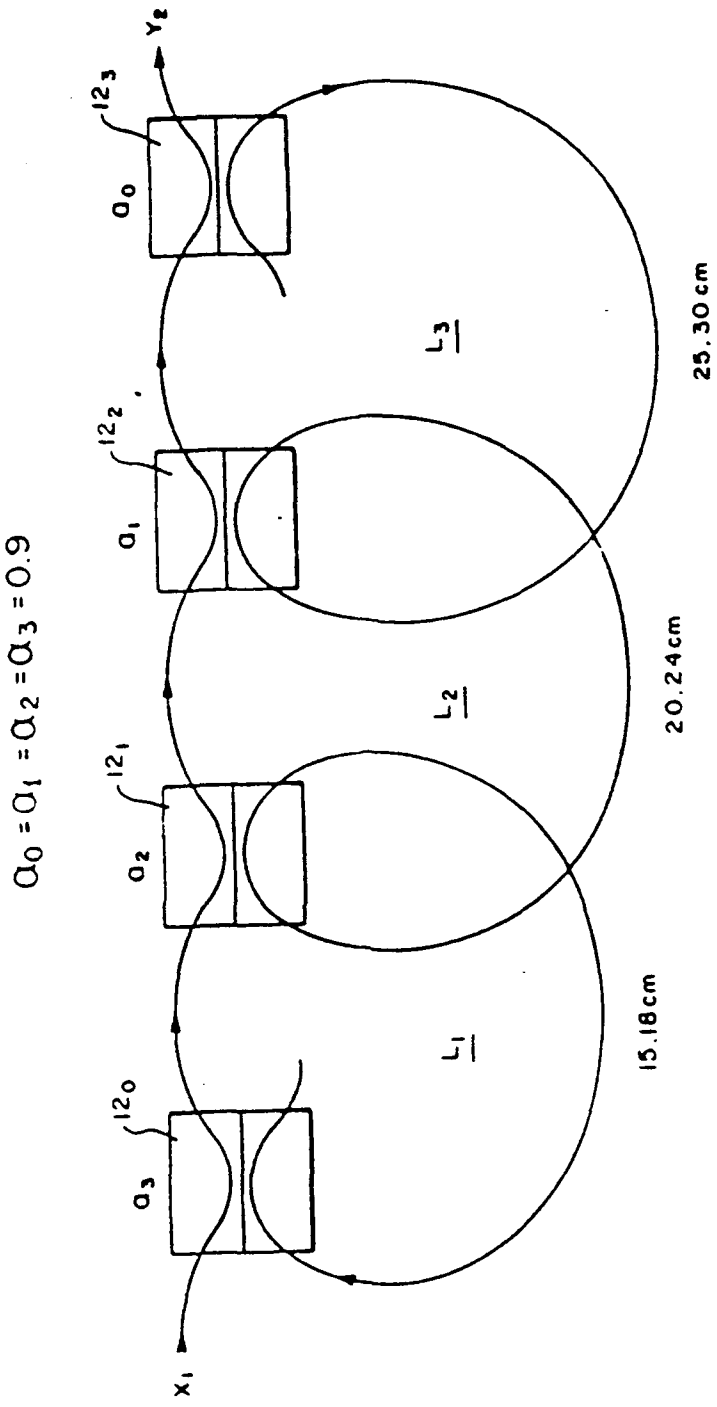
$\alpha_0 = \alpha_1 = \alpha_2 = \alpha_3 = 0.9$
Y_2
12_3
α_0
L_3
25.30cm
12_2
α_1
L_2
20.24cm
12_1
α_2
L_1
15.18cm
12_0
α_3
X_1

FIG. 3

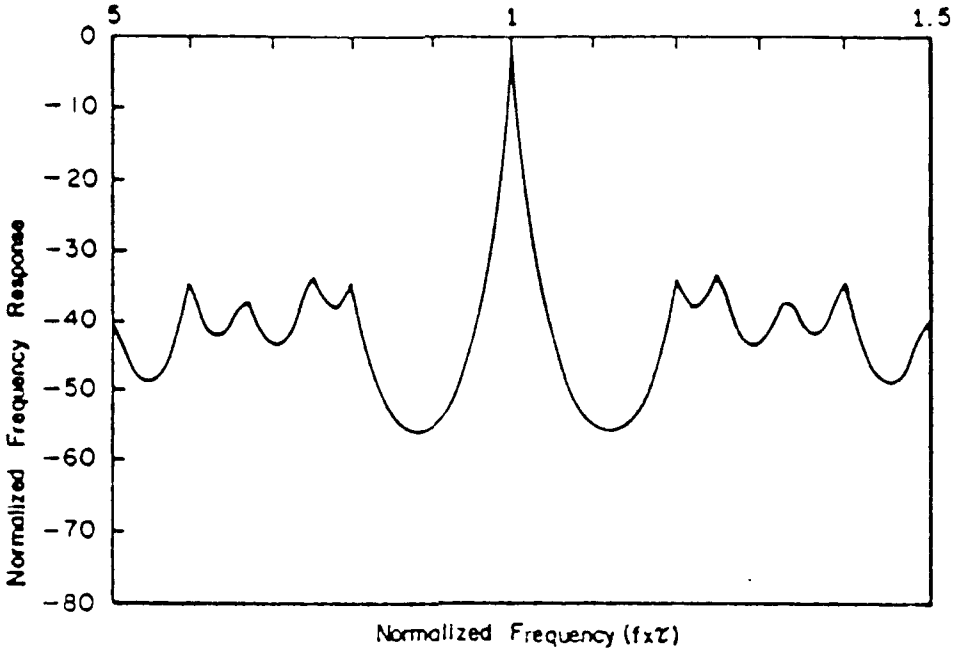
.5
1
1.5
0
-10
-20
-30
-40
-50
-60
-70
-80
Normalized Frequency Response
Normalized Frequency (fxτ)

FIG. 4

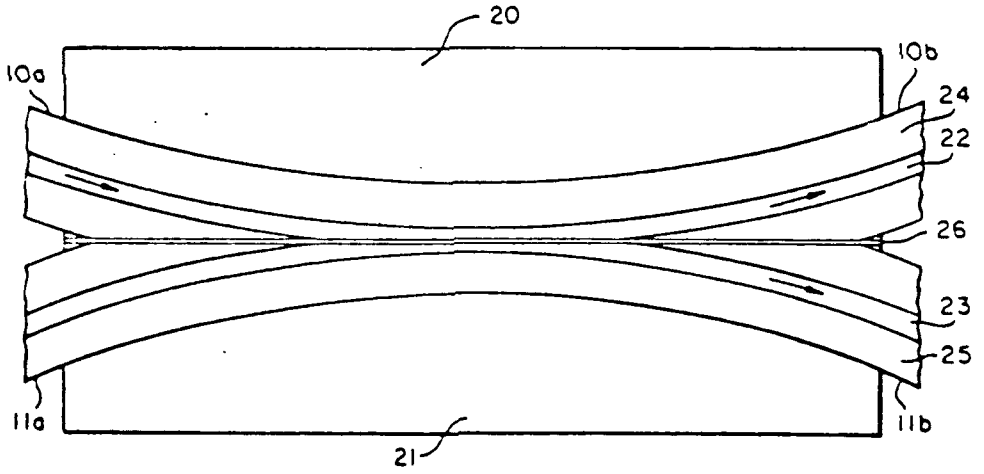
20
10a
10b
24
22
26
23
25
11a
11b
21

FIG. 5

CASCADED RECIRCULATING TRANSMISSION LINE WITHOUT BENDING LOSS LIMITATIONS

This invention was made with Government support under Contract F30602-87-C-0015 awarded by the Department of the Air Force. The Government has certain rights in this invention.

TECHNICAL FIELD

The invention relates to an nth order recirculating filter utilizing directional couplers connected in cascade along a length of transmission line to form delay loops, and more particularly to a novel architecture for such recirculating filters using optical fibers which overcomes fundamental bending loss limitations in forming delay loops.

BACKGROUND OF THE INVENTION

Although electronic signal processing techniques are effective at frequencies below 1 to 2 GHz, they are of limited applicability at higher frequencies. Single-mode optical fiber, on the other hand, is an excellent frequency-independent delay medium (0.2 km/μsec), with demonstrated modulation bandwidth >100 GHz.km and low loss (<0.2 dB/km). The low loss, large bandwidth, and the small size associated with single mode optical fiber make it an attractive choice as a delay line to implement signal processing functions at microwave frequencies. As a result, use of such a fiber can form the basis of signal processing elements offering orders of magnitude increase in bandwidth over electrical devices.

Signal processing optical fiber devices are schematically, structurally and operationally similar to their electronic counterparts. The design, architectures and analysis are also essentially equivalent. However, the fundamental bending loss limitation inherent in recirculating delay line structures has impeded the use of optical fiber for such delay applications as performing a bandpass filter function.

Many processing operations using basic tapped and recirculating delay lines together with more complex feed-forward and feed-backward lattices, have already been demonstrated. K. P. Jackson, et al., "Optical fiber delay-line signal processing," IEEE Trans. Microwave Theory Tech., Vol. MTT-33, p. 193, (1985). Simple tapped delay lines carry out basic transversal filter operations (convolution, correlation, matched filter and code generation) as well as bandpass filters and notch filter operations at frequencies above 1 GHz. See K. P. Jackson, et al., "Microbend optical fiber tapped delay line for gigahertz signal processing," Appl. Phys. Lett., Vol. 41, p. 139, (1982); J. E. Bowers, et al., "Filter response of single-mode fiber recirculating delay lines," Electron. Lett., Vol. 18, p. 110, (1982); S. A. Newton, et al., "Optical fiber V-groove transversal filter," Appl. Phys. Lett., Vol. 43(2), p. 149, (1983); C. C. Wang, "Cascaded single-mode fiber optic transversal filters," Proc. SPIE High Frequency optical communication, Vol. 716, p. 82, (1986). Recirculating delay lines are capable of temporary data storage and data rate transformation and have been demonstrated as frequency filters above 1 GHz. Fiber-lattice structures can perform matrix-vector multiplication at 100 MHz and broadband filtering at frequencies in excess of 1 GHz. B. Moslehi, et al., "Fiber-optic lattice signal processing," Proc. IEEE, Vol. 72, p. 909, (1984).

Extension to frequencies of 10 GHz, and above, is straightforward in principle. However, it requires the use of shorter fiber lengths, more compact designs and faster optoelectronic interfaces. The designs to date result in processors which operate at much lower frequencies. In addition, in a straightforward implementation, bending losses in the fiber place a lower limit on the length of the loop. For example, in a tapped fiber delay line of the type disclosed in U.S. Pat. No. 4,558,920 to Newton, et al., the tapping points are usually separated by a distance equal to the circumference of the cylinder around which the optical fiber is looped. The bending loss will limit the minimum loop length (cylinder circumference) and thus limit the high frequency of operation. For higher frequencies, it is necessary to consider alternative designs and architectures, e.g. multiple tap points per fiber loop around the cylinder, linear tap configurations, or a recirculating lattice. The present invention considers a recirculating lattice approach.

SUMMARY OF THE INVENTION

In accordance with the present invention, an nth order cascaded recirculating filter utilizes couplers spaced along a length of transmission line. Each coupler has two inputs and two outputs. One of the outputs of each coupler is connected to one of the inputs of the next coupler in cascade to form a feed-forward transmission path, and the other one of the outputs of each coupler connected to the other input of the preceding coupler to form a feed-backward transmission path. The feed-forward path and feed-backward path form a closed delay loop. Each delay loop along the cascaded couplers is made longer by an increment of delay time τ equal to the reciprocal of the desired center frequency f_c for the bandwidth of the filter. The feed-backward loop between the first pair of couplers is provided with a basic delay T equal to a multiple m of the increment τ, where m is an integer selected to be large enough to avoid incurring bending losses in the feed-backward transmission path between cascaded couplers.

BRIEF DESCRIPTION OF THE DRAWINGS

FIG. 1 illustrates schematically a nth order cascaded recirculating filter.

FIG. 1a illustrates a single closed delay loop in the cascaded recirculating filter illustrated in FIG. 1 with a delay $T=i\tau$.

FIG. 2 illustrates a block diagram in Z-transformation form for the nth order cascaded recirculating filter of FIG. 1.

FIG. 2a is a graph of filter characteristics for the nth order cascaded recirculating filter of FIG. 1 shown in the Z-transformation form in FIG. 2.

FIG. 3 illustrates schematically an examplar third order cascaded recirculating filter.

FIG. 4 is a graph showing the frequency response for the third order filter of FIG. 3.

FIG. 5 illustrates in a cross-sectional view the structure of a coupler used in the present invention.

DESCRIPTION OF PREFERRED EMBODIMENTS

Referring to FIG. 1, a cascaded recirculating filter consists of two optical transmission paths 10 and 11, and directional couplers 12_0, 12_1, 12_2 ... 12_{n-1}, 12_n, preferably implemented with single-mode optical fibers and evanescent coupling between inputs 10a and 11a, and

some coupling, e.g., 50 to 90%, between input 10a and output 11b and between input 11a and output 10b with 100% efficiency (i.e., with zero loss of power in the coupler). Each coupler 12_i has two inputs 10a and 11a, and two outputs 10b and 11b, as shown in FIG. 1a.

One of the outputs of each coupler is connected to one of the inputs of the next coupler in sequence to form a feed-forward transmission path, namely the fiber 10 connecting the upper output 10b of coupler 12_i to the upper input 10a of the next coupler 12_{i+1} in cascade. The other output fiber is connected to the input fiber of the preceding coupler to form a feed-backward transmission path, namely the transmission path 11 connecting the lower output 11b of coupler 12_{i+1} to the lower input 11a of the preceding coupler 12_n, as shown in FIG. 1a for two adjacent couplers 12_i and 12_{i+1}. The transmission paths 10 and 11 between two adjacent couplers 12_i and 12_{i+1} form a delay loop L_{i+1} by coupling the feed-forward transmission path 10 with the feed-backward transmission path 11 in the couplers. Thus, the delay loop L_{i+1} consists of the output 10b from the center of coupler 12_n which is connected directly to the input 10a of the coupler 12_{i+1}, and from there coupled to output 11b of the coupler 12_{i+1} which feeds back to the input 11a of the coupler 12_i. The total delay $T+i\tau$ is of the loop length from the center of the coupler 12_i through the coupler 12_{i+1} and back to the center of the coupler 12_i. The output 11b of the coupler 12_i feeds back to the input of the preceding coupler not shown in FIG. 1a.

Such a loop L_i is, without defining the feed-backward delay as $T+i\tau$, known in the prior art (see Moslehi, et al., cited above, FIG. 5a). The present invention concerns a novel architecture for an nth order filter utilizing cascaded couplers where the novelty is the delay in the delay loop defined as $T+i\tau$, as will now be described in more detail with reference to FIG. 1.

The coupling coefficient of the coupler 12_n on the right hand side is indicated as a_n, and the others from right to left as $a_1 \ldots a_{n-2}, a_{n-1}, a_n$, where "coupling coefficient" is defined as the fraction of power coupled from one transmission path through the coupler into the other. For example, if the coupling coefficient is 0.7, the fraction of power coupled from the input transmission path 10a to the output transmission path 11b is 7/10, i.e., 70%. Energy thus coupled into the delay loop L_i is coupled back into the transmission path 10 through the output 10b with the same coupling factor, namely 0.7 of the fraction 7/10, which is equal to 0.49. The balance of $0.3 \times 7/10 = 0.147$ recirculates in the loop. As will be noted with reference to an exemplar for a third order filter shown in FIG. 3, a high uniform coefficient of coupling is preferred for the filter function, although it is recognized that other designs may be employed such as tapering the coefficient of coupling from 0.5 to 0.9, or from 0.9 to 0.5.

In this configuration, the corresponding delay of the first loop on the left is set for a basic period T equal to some multiple τ indicated as $m\tau$ where τ is defined as an "incremental delay time" and m is an integer. A pertinent value of m will be discussed below. The incremental delay time τ is set equal to the reciprocal of the center frequency f_c of the desired passband response. This arrangement will become clear after the structure is described. The corresponding delay of the second loop L_2 is $T+\tau$ and of the succeeding loops are $T+2\tau$, $T+3\tau \ldots T+(n-1)\tau$.

From the foregoing, it is evident each loop has two ports with two terminals at each port (two inputs, two outputs). In order to more easily derive the transfer function H(f) of the filter, where H(f) is a complex function equal to the ratio of the output to the input as a function of frequency, the equivalent block diagram representation of the cascaded recirculating filter in Z-transformation form shown in FIG. 2 is used. A. V. Oppenheim, et al., "Digital Signal Processing," Englewood Cliffs, N.J., Prentice-Hall, 1975; S. K. Mitra, et al., "Digital ladder networks," IEEE Trans. Audio Electroacoust., Vol. AU-21, p. 30, (1973). The Z-transformation block diagram is a simple series of elements with each element being a two-port system, each port having an input and an output terminal. In a linear and time-invariant two-port system the two pairs of signals X_1, Y_1 and Y_2, X_2 at the two ports can be related by a chain matrix where X_1 is an input and Y_1 is an output. From the Z-transformation form, it is evident from FIG. 2 that if g represents the chain matrix of an element and G is the chain matrix of the overall system, then G is the product of the chain matrices representing all of the elements multiplied in the same order in which they are cascaded in the system:

$$G = g_1 g_2 \ldots g_{n-1} g_n \qquad (1)$$

And it is seen evident that a delay in the feedback path between adjacent couplers 12_0, 12_1, 12_2, $\ldots$ 12_{n-1}, 12_n increases from $Z^{-(\ )}$ by one unit of delay for each successive coupler to provide the required feed-backward loop delays of Z^{-m}, $Z^{-(m+1)} \ldots Z^{-(m+n-1)}$ for the cascaded recirculating filter. In accordance with the present invention, Z^{-m} corresponds to the Z-transform of delay time T, and T is some multiple of a loop incremental delay time τ which defines the center frequency of the delay line, i.e., where the center frequency f_c shown in FIG. 2a is equal to the reciprocal of the loop incremental delay time τ. This is done in order to avoid extremely tight fiber optic bending for very small loop delays required for selecting a center frequency higher than 1 GHz or 2 GHz corresponding to a high frequency of filter operation, which would otherwise result in bending losses. Thus, in accordance with this invention, T is made equal to some multiple m of the loop incremental delay time τ, where m is a positive integer, i.e., the time delay $T = m\tau$ for the first feed-backward delay loop L_1 is made large enough (by proper selection of m) to avoid tight bending of the optical fiber 11. Then for each subsequent loop $L_2, \ldots L_n$, the delay T is incremented by an additional unit of delay τ, where $\tau = 1/f_c$. This incremental delay added to each successive delay loop is readily provided by increasing the length of the loop connecting the output 11b and the input 11a of adjacent couplers 12_{i+1} and 12_n respectively, of loop L_n over the total length of the previous feed-backward delay loop L_{i-1}. The increment of delay loop length to be added can be readily calculated once τ is determined, i.e., once the center frequency of the desired filter operation is determined.

An examplar for an optimized third-order cascaded recirculating filter is shown in FIG. 3. Given a desired center frequency of 4 GHz, the design parameters, including the optical fiber length for each stage and the coupling coefficient, are as shown. The velocity of light, v, in the optical fiber having an index of refraction $n = 1.5$ is

$$v = \frac{c}{n} = \frac{2.9978 \times 10^8 m/s}{1.5} = 2.0235 \times 10^8 m/s \quad (2)$$

where c is the speed of light in space. The incremental delay τ for the given center frequency of 4 GHz is given by

$$\tau = \frac{1}{f_c} = \frac{1}{4GHz} = 0.25 ns \quad (3)$$

The incremental length L_τ of optical fiber required for a delay of 0.25 ns is then determined to be

$$L_\tau = v\tau = 2.0235 \times 10^8 m/s \times 0.25 ns = 5.06 cm \quad (4)$$

To avoid unacceptable bending losses, a preferred minimum loop length is about 15 cm. Therefore, the factor m is selected to be 3, and the delay T for the first loop corresponds with a loop length L_1 of 15.18 cm. The loop length for the remaining two cascaded filter loops L_2 and L_3 then correspond to 20.24 and 25.30 cm, as shown.

The frequency response of the filter in FIG. 3 is shown in FIG. 4. This filter exhibits a quality factor (Q) of 185, where Q is the ratio of center frequency to bandwidth of the filter and side lobe rejection ratio of greater than 33 dB. Higher operating frequencies can be achieved by calculating T and τ appropriately. In principle, τ can be made infinitesimally small since the bending loss is a function of the radius for the loop of delay T, rather than a loop for incremental delay time τ. Although there is a practical limit to how small τ can be made with accuracy, operation in the 50 GHz to 100 GHz frequency range should be achievable.

Bidirectional couplers with a coupling coefficient a can be readily fabricated. A coupling coefficient of 0.9 is typical for a coupler fabricated as illustrated in FIG. 5. Two silicon blocks 20 and 21 are first prepared to receive optical fibers 10' and 11' as shown in cross section with a bend of large radius (about 2.5 cm). After the optical fibers are cemented in their curved grooves, as with epoxy, the mating (grooved) surfaces are polished until the cores 22 and 23 of the optical fibers 10' and 11' have been ground past their cladding layers 24 and 25 to very near their center lines. A thin film of oil 26 having about the same index of refraction as the core is provided between the polished surfaces to assure the coupling desired. The two blocks are ideally aligned so that the center lines of the optical fibers are tangent at the center of the blocks. Couplers fabricated in this or similar manner are commercially available with two input fiber pigtails and two output fiber pigtails protruding from the mated blocks. One output fiber pigtail from one block may be fused directly to the input fiber pigtail of the next block in cascade to form the continuous feed-forward transmission path 10. The necessary lengths of optical fiber required to make up the delay loops are then cut and fused to the other input and output fiber pigtails.

The advantage of the present invention over conventional recirculating delay line filters that employ a constant delay loop length for each stage is significant in that it permits fabricating filters operating at much higher frequencies without limit due to bending losses; the limit is only in how small the incremental delay time τ may be made.

Although preferred embodiments have been described and illustrated with optical fiber used for the transmission paths, it will be evident to those skilled in the art that the present invention may be practiced with other forms of transmission lines, such as dielectric supported strip lines of the symmetrical or sandwich type, or of the unsymmetrical type referred to as microstrip lines, or other types of microwave transmission lines, such as coaxial cables or waveguides. Consequently, it is intended that the claims be interpreted to cover such other transmission lines used in a recirculating delay line filter of the general Z-transform characteristics illustrated in FIG. 2.

We claim:

1. An nth order recirculating filter utilizing directional couplers connected in cascade along a length of transmission line, wherein each coupler has two inputs and two outputs for receiving and transmitting energy, a first one of the outputs of each coupler being connected to a first one of the inputs of the next coupler in cascade to form a feed-forward path, and a second one of the two outputs of each coupler connected to a second one of the two inputs of a preceding coupler to form a feed-backward path, said feed-forward path and said feed-backward path between adjacent ones of said couplers forming a loop with an incremental increase in the delay in each successive feed-backward path between adjacent ones of said couplers, wherein said incremental increase is a delay time τ equal to the reciprocal of the center frequency f_c of a desired bandwidth of filter operation, and said first loop has a delay T equal to a multiple m of τ, where m is an integer greater than one.

2. An nth order recirculating filter as defined in claim 1 wherein said transmission line is comprised of single-mode optical fiber and said integer m is selected to provide a loop delay which corresponds with a loop length sufficient to avoid bending losses.

3. An nth order recirculating optical fiber bandpass filter having a center frequency f_c comprising

a plurality of directional fiber-optic couplers in cascade, each coupler having two input optical fibers and two output optical fibers, each coupler except a last one of said couplers in cascade having one output optical fiber connected to an input optical fiber of the next coupler in cascade for direct transmission of light through said couplers in a feed-forward light path,

each coupler except said last one of said couplers having a second one of said two input fibers connected to a second one of said two output fibers of the next coupler in cascade to form a delay loop for transmission of light from the next coupler in a feed-backward path with a predetermined delay,

said predetermined delay for a first loop between a first pair of couplers connected in cascade being predetermined to be $m\tau$, where τ is a delay equal to the reciprocal of said center frequency f_c and m is an integer greater than one selected to provide a first loop with delay T equal to $m\tau$ and of sufficient length to avoid losses associated with bending of optical fiber, and

the loop delay between successive pairs of couplers numbered 0, 1, 2, . . . n in sequence along said light path is incremented by a delay equal to τ, thereby to provide a total delay for the ith delay loop of $T + i\tau$, where i is the number of the input coupler of

the ith delay loop, and τ is equal to the reciprocal of said center frequency f_c.

4. An nth order recirculating fiber bandpass filter as defined in claim 3 wherein the loop delay between successive pairs of couplers is implemented by incremental increase in loop length.

5. An nth order cascaded recirculating filter comprising

a plurality of optical couplers spaced along a first single-mode optical fiber, each coupler having

a first single-mode optical fiber input and a first single-mode optical fiber output connected to form said first single-mode optical fiber,

a second single-mode optical fiber input and a second single-mode optical fiber output, said second single-mode optical fiber output of each coupler connected to said second single-mode optical fiber input of the next preceding coupler along said first single-mode optical fiber to form a feed-backward loop between adjacent couplers with a loop length in each successive feed-backward delay loop of delay time T that is increased by an incremental delay time τ from one pair of adjacent couplers to the next, where the incremental increase in delay time τ for each successive pair of adjacent couplers is the reciprocal of the center frequency of a desired bandwidth of filter operation, and said incremental increase in delay time τ is implemented by an incremental increase in loop length, and said feed-backward delay loop time T is equal to some multiple m of τ, where m is an integer greater than one selected to provide a feed-backward delay time T for the first loop of a length sufficient to avoid bending losses at the desired bandwidth of filter operation.

* * * * *

APPENDIX D

CHARACTERIZATION STUDY OF OPTICAL FIBERS

2.3.1.1 Glass Composition

Although a wide range of glass systems has been investigated, few have found applicability in optical fiber fabrication. For propagation, in the visible/near I.R., silica-based fibers (phosphorous or germanium doped SiO2 core with pure SiO2 cladding) are currently preferred types (1), exhibiting near-theoretical losses, although lead silicate and soda-lime glasses have been investigated. Motivated by the possibility of further reduction in Rayleigh scattering losses available at longer wavelengths, new fluoride glass systems are under investigation, emphasis being placed on the system ZrF4-BaF2 and its derivatives (2).

2.3.1.2 ATTENUATION

Attenuation in optical fibers results from a number of wavelength dependent mechanisms, including scattering, absorption, and externally-induced losses, such as those due to bending. Although each of these losses can be small over a particular range of optical wavelengths, their combined effect restricts operation of a fiber system to a relatively narrow spectral band. The attenuation of a fiber limits the length and number of taps that a delay line processor can accommodate, indicating a requirement for minimum loss consistent with other requirements. Since the S.O.W. calls for consideration of operation in the wavelength range 0.8 - 1.6 um, discussion is conveniently constrained to silica based fibers, although alternative types are noted in what follows for completeness.

2.3.1.2.1 Intrinsic Attenuation

This heading covers the fundamental loss mechanisms existing within an ideal glass matrix.

2.3.1.2.1.1 Short Wavelength Absorption Edge

Short-wavelength absorption is due to inter-band electronic transitions within the glass, exhibiting an approximate exponential wavelength dependence:

$$a(sw) = A.\exp(k/L),$$

the so-called Urbach edge. The constant A has the value 0.81 for pure silica (3), increasing to 1.36 and 1.51 for germanium phosphosilicate and germanium borosilicate fibers respectively (4).

For Ge, P, B and F-doped silica glasses, the electronic absorption bands occur in the U.V. at energies around 10 eV (5); this figure shifts towards the visible for long wavelength glasses.

2.3.1.2.1.2 Long Wavelength Absorption Edge

The long wavelength absorption edge represents a multi-phonon absorption tail arising from overtones and combination bands of fundamental material vibrations at longer wavelengths (typically in the range 7 - 11 μm (5)). the position of the fundamental absorption is defined empirically by (6):

$$w = ((k/u)^{**}.5)/2.pi.c$$

where w is in wavenumbers, k is an inter-atomic interaction force constant and u is the reduced atomic mass. Analytically, the long wavelength edge has the form (5):

$$a(lw) = C.\exp(-j/L).$$

2.3.1.2.1.3 Rayleigh Scattering

Rayleigh scattering arises from random composition and density fluctuations on a microscopic scale, causing refractive index changes in the glass. The spatial separation of these fluctuations is small compared to the wavelength of light, inducing a scattering loss decreasing as the fourth power of the optical wavelength (7):

$$a(sc) = B/(L^{**}4)$$

All transparent matter scatters light due to thermal fluctuations which, in turn, generate fluctuations in refractive index. In glass, these fluctuations are frozen in on cooling through the annealing temperature. Similar, more important, fluctuations arise from dopant concentration fluctuations; these tend to dominate overall scattering.

2.3.1.2.1.4 Discussion

Below a wavelength of 1.6 μm, the dominant loss mechanism in silica-based fiber is Rayleigh scattering, caused by perturbation of the propagating electromagnetic wave by microscopic-scale material inhomogeneities, and exhibiting an inverse quadratic wavelength dependence. At longer wavelengths, structural absorption processes resulting from interatomic bond absorption predominate, limiting silicate glasses to operation below about 1.6 μm. The two loss processes combine to yield an optical transmission maximum around 1.5 μm.

2.3.1.2.2. Extrinsic Attenuation

This heading includes loss process external to the fiber.

2.3.1.2.2.1 Impurity Absorption

All materials contain at least some impurities which absorb light at different wavelengths. For glasses, characteristic absorption species include:

Hydroxyl groups:

The first overtone of the fundamental O-H stretch vibration is responsible for the absorption peak occurring around 1.4 μm in silica glass; higher overtones occur at 950 and 725 nm (8). Similar absorptions occur in the relatively more hygroscopic fluoride fibers (9).

Transition metal ions:

The absorption spectra of the first row transition metal ions are broad, with strengths varying from glass to glass. The most common sources are copper, iron, cobalt, vanadium and chromium (10,11).

Lanthanide ions:

Lanthanide ions exhibit absorptions which are considerably narrower, and of lower intensity, than those of the transition metals (12).

Miscellaneous absorbers:

Other absorbers identified in glasses include ammonium, phosphate and sulphate ions, together with dissolved carbon monoxide and dioxide, although these are generally very sharp or at relatively long wavelengths.

2.3.1.2.2.2 Scattering

Two classes of extrinsic scattering have been identified in glasses.

Mie Scatter:

Mie scatter varies as L**-2, and has been correlated with impurity particles with dimensions of the order of the wavelength of light. The identity of the particles is unknown, but they are believed to arise as starting material

impurities or as processing contaminants. This type of scattering is significantly reduced in current processing technology.

Wavelength Independent Scatter

This type of scatter is a major cause of loss in fluoride fibers in particular, being due to imperfections with dimensions greater than the light wavelength; bubbles and crystalline precipitates are typical sources. This scattering process is eliminated in silica fibers.

2.3.1.3 DISPERSION

The bandwidth of an optical delay line will be limited by the dispersion of the fiber, which, in turn, depends on the wavelength and bandwidth of the source, as well as the type of fiber. Several different classes of dispersion can contribute to limit the bandwidth of an optical fiber, the dominant mechanism depending on the waveguide properties and the spectrum of the optical source.

For a typical low loss monomode fiber, dispersion is dominated by the material dispersion of fused silica, slightly modified by the influence of core dopants. Such fibers typically exhibit dispersion of around 110ps/km.nm at 1.06 μm, with zero dispersion at around 1.3 μm.

2.3.1.3.1 Modal Dispersion

Modal dispersion applies solely to multimode fibers, and is included here chiefly for completeness. Multimode fiber can guide a number of transverse

modes that do not, in general, propagate at the same group velocity. Modulation bandwidths of multimode fiber are typically in the range of a few MHz-km to several hundred MHz-km. Bandwidths of just over 1 GHz-km can be obtained using a specially designed graded index multimode fiber.

2.3.1.3.2 Waveguide Dispersion.

Waveguide dispersion results from the fact that the propagating optical energy in a monomode fiber is shared between the core and the cladding materials, which have differing characteristics. Waveguide dispersion in a step index fiber has the form:

$$W = (-D.dn/c.L).(V.d2(Vb)/dV2)$$

where V is the normalized frequency, defined by:

$$V = 2.pi.a\ (2n.dn)**0.5/L$$

D is the fiber length, b a normalized propagation constant, n is the core refractive index, dn is the index difference and a the core radius. Numerically (13):

$$V.d2(Vb)/dV2 = 4.501 - 3.106V + 0.547V**2$$

giving good agreement with experiment in the range 1.3 to 2.4 μm for silica based fibers.

2.3.1.3.3 Wavelength Dispersion (Material dispersion)

The refractive indices of most glasses exhibit significant dispersion with wavelength, generally capable of representation by means of a suitable power series in reciprocal wavelength. Modulation bandwidth of a monomode fiber is then typically limited by the dependence of the fiber refractive index on the optical carrier wavelength; this is due to the different group delays suffered by different spectral components of the source. Analytically, wavelength dispersion is a function of the second derivative of index with wavelength:

$$M = (-L/c).(d2n/dL2)$$

where c is the velocity of light.

For near I.R. wavelengths, a convenient empirical relationship is (14):

$$f(3dB) = 187.3/(S.T\ dt(g)/dL\ )$$

where f(3dB) is the modulation bandwidth of the fiber in GHz, T is its length, (dt/dL) is the differential dispersion (ps/nm-kn) and S is the half-width of the optical source, including modulation sidebands.

2.3.1.3.4 Polarization Dispersion

In some delay line implementations, polarization of guided light in the fiber may need to be preserved. This has resulted in the development of polarization maintaining fibers, possessing either highly elliptical cores or cladding

stress lobes, resulting in high levels of uniform birefringence along the fiber. Such fibers exhibit significant polarization dispersion between the two orthogonal modes, with magnitude 50 - 1000 ps/km.nm.

2.3.1.3.5 Discussion

A significant characteristic of silica fiber is the fact that whereas waveguide dispersion is negative at all wavelengths, material dispersion is positive at wavelengths longer than a critical value L(mo) . A fiber design can thus be tuned to exhibit zero dispersion at some wavelength less than this critical value (in the region of 1.3 μm for silica fiber); in current "Dispersion Shifted" fibers this is generally arranged to coincide with the silica fiber attenuation minimum around 1.5 μm. Alternatively it is possible to implement relatively low (5 ps/km.nm), but nearly constant, dispersion over a particular wavelength range. Such "Dispersion Flattened" fibers typically possess two dispersion minima, nominally at wavelengths of 1.3 and 1.55 μm. Similar fiber designs can be generated for fluoride-based infra-red fibers.

2.3.1.4 PROPAGATION VELOCITY

Closely allied with the subject of dispersion is the absolute propagation velocity along a fiber, a key parameter since it defines the space-time relationships underlying the operation of most processor architectures. Far from cut-off, the characteristic group delay of a monomode fiber is defined essentially by the refractive index of the core; nearer cut-off, this is not the case, and intrinsic delay may thus be a relatively strongly varying function of optical wavelength.

2.3.1.5 LINEARITY

The fundamental linear dynamic range of a fiber is limited by quantum noise in the low signal limit and constrained by nonlinear loss processes at high signal levels. The minimum detectable power transmitted by a low loss fiber is limited by quantum noise, defined by the noise-equivalent power (NEP) (15), is:

$$N.E.P. = 2h.u.B$$

where h is Planck's constant, u is the optical frequency and B is the sampling bandwidth.

The upper limit to responsivity is defined by stimulated Raman (16) and stimulated Brillouin scattering, the primary effect of which is the transfer of energy from the propagating wave to a forward or backward wave at lower frequency. The critical power at which stimulated Raman back-scattering becomes important is given approximately (16) by

$$P(crit) = 231.Aa/LY(o)$$

where A is the fiber core cross-sectional area, L is the fiber length, a is the linear attenuation constant, Y(o) is the Raman gain coefficient, with a value of the order of 5 E-10 cm/W (17).

Based on the foregoing equations, the inherent dynamic range of a fiber can be estimated. While Raman scattering is essentially independent of signal

(modulation) bandwidth, quantum noise is linearly proportional to signal bandwidth. The fundamental optical dynamic range of a fiber thus decreases linearly with increasing signal bandwidth, being typically 80 dB for a 10 GHz signal along a 200 m delay path.

2.3.1.6 FIBER ASSESSMENT

Optical fibers are conveniently classified in terms of their wavelength range of operation, attenuation characteristics, zero-dispersion wavelength, maximum dispersion and the wavelength band over which it is applicable. Table 1 summarizes data on currently available monomode fibers, applicable in the present case. Fluoride-glass infra-red fibers are not considered here.

Manufacturer	W'length	Attn.	Z.D.	Disp	Band
AT&T	1310-1550	0.35	1310	3.2	1285-1300
BICC	1330-1550	0.2	1300	3.5	1285-1330
BIW Cable Systems	1300-1550	0.7	1310	3.5	1285-1300
Cableoptic S A	1275-1325	0.5	1315	4	
Celwave systems	1285-1330	0.4	1300	3.5	1285-1330
Corning Glass Works	1300	0.4	1300	3.5	1285-1330
Corning Glass Works	1550	0.22	1550	2.5	1525-1575
Diagnide Inc	850	5	1300		
EOTec Corp	820	3			
EOTec Corp	850	3.5			
Fibronics Ltd	1300-1550	0.5	1315	3.5	1285-1330
Furakawa Electric	1285-1233	0.4	1310	3.5	1285-1330
GEC Optical Fibers Ltd	1300	0.4	1305	6	1275-1325
ISPRA Fiberoptics	1300	0.45	1300	3.5	1290-1330
ITT E-O Products	1300	0.5	1310	3.5	1285-1330
Northern Telecom	1300-1550	0.4	1310	3	1285-1330
Olex Cables	800-1600	0.6	1300	18	
Optical Cable	1130-1270	0.5		3.5	
Pirelli cable corp	1300	0.4		3.5	1285-1330
Remee Products	1300	0.5		3.5	1285-1330
Siecor Corp	1300	0.4	1310	3.5	1295-1325

SpecTran Corp	1300-1550	0.3	1310	3.5	1300
Standard Wire & Cable	1300-1550	0.5	1300		1285-1330
Sumitomo electric	1310-1550	0.4	1310	3.5	1285-1330
York V.S.O.P.	800-	5			
York V.S.O.P.	1250	2			

2.3.1.7 REFERENCES

(1) Lightguide technology review and status

M A Saifi

Mat Res Soc Symp Proc 24, 413-431(1984)

(2) Progress in fluoride fibers for optical communication

P W France, S F Carter, M W Moore and C R Day

Brit Telecom Tech J 5, 28-44 (1987)

(3) T C Rich and D A Pinnow

App Phys Letts 20, 264-265 (1972)

(4) F P Partus and M A Saifi

Western Elect Eng 24, 39-47 (1980)

(5) H Osani, T Shioda, T Moriyama, S Araki, M Hariguchi, T Izawa and

H Takata

Elect Letts 12, 549-550 (1976)

(6) Compressibility and absorption frequency of ionic materials

B Szigeti

Proc Roy Soc A204, 51 (1950)

(7) R D Maurer

Proc IEEE 61, 452-263 (1973)

(8) D B Keck, R D Maurer and P C Schultz

App Phys Letts 22, 307-309 (1973)

(9) OH absorption in fluoride glass infrared fibers

P W France, S F Carter, J R Williams, K J Beales and J M Parker

Elect Letts 20, 607 (1984)

(10)P C Schultz

J Am Ceram Soc 57

(11)Oxidation states at 3d transition metals in ZrF4 based glasses

P W France, S F Carter and J M Parker

Phys Chem glasses 27, 32-41 (1986)

(12)Impurity absorption loss due to rare earth elements in a fluoride glass

Y Onishi, S Mitachi, S Shibata and T Manate

Jap J Appl Phys 20, L191 (1981)

(13)Transmission characteristics of a single mode fiber in the 1.3 μm wavelength region

Y Ishida, M Ohashi, N Uesigi and N Shibate

J Lightwave Tech LT-2, 322-327 (1984)

(14)Considerations for single mode fiber systems

K Ogawa

Bell Syst Tech J 61, 1919(1982)

(15)Principles of Quantum Electronics

D Marcuse

Academic press, New York (1980)

(16)Optical power handling capacity of low-loss optical fibers as determined by stimulated Raman and Brillouin scattering

R G Smith

Appl Opt 11, 2489-2494 (1972)

(17)Stimulated Raman gain coefficients for lithium niobate, barium sodium niobate and other materials

W D Johnson, I P Kaminow and J D Bergman App Phys Letts 13,190-192 (1968)

APPENDIX E

FIBER OPTIC BASED SIGNAL PROCESSING COMPONENT TEST RESULTS

FIBER OPTIC BASED SIGNAL PROCESSING

CONTRACT NO. F30602-87-C-0015

COMPONENT TEST RESULTS

(CLIN A003)

Prepared by:

P J Duthie
D C J Reid
C J Groves-Kirkby

Approved by:

I Bennion
R Davis
M J Cardwell

Plessey Research Caswell Limited
Allen Clark Research Centre
Caswell, Towcester,
Northants., NN12 8EQ

SUMMARY

A range of novel optical fibre and related waveguide directional coupler components has been developed, suitable for incorporation in a variety of optical tapped delay line signal processing system configurations. Components developed include polished polarisation-maintaining couplers fabricated in high-birefringence fibre and exhibiting polarisation extinction comparable with or superior to that available from state-of-the-art components, and high-speed switched couplers suitable for processor applications involving high-speed reconfiguration of coupling parameters. The programme has confirmed the feasibility of manufacture of monolithic arrays of evanescent wave coupler elements with uniform characteristics, suitable for the assembly of multi-stage processor systems, and has resulted in the derivation of a novel fabricational topology for recursive lattice structures, permitting assembly of superficially asymmetric structures from two identical elements.

Detailed measurements of component parameters, both during fabrication and on completion, verify the analytical design approach, confirming that high-precision polished coupler components can indeed be fabricated to demanding specifications, both as single elements and in multi-element arrays. Components for delivery have been shown to conform to projected performance targets and have been prepared for delivery adjusted to the levels of optical power coupling specified for the various applications described in the System Design Plan.

1. INTRODUCTION

This document describes the results of tests and test procedures used to characterise the 4-port optical coupler signal-processing components fabricated as part of Contract No. F30602-87-C-0015 Fibre Optic Based Signal Processing, and carried out during the course of Task 4.1.3.1, Component Breadboard. The tests were specified in the Component Test Plan, submitted as ELIN A003.

2. GENERAL

2.1 COMPONENT SPECIFICATIONS

The Component Design Plan, previously submitted as ELIN A002, October 1988, outlines target design parameters for 5 classes of optical fibre coupler, appropriate for the assembly of prototype signal procesors, and forming the basis of the Component Breadboard Phase, Task 4.1.3.1 of the S.O.W, now completed. Pertinent details of these follow here.

2.1.1 0.90 Coupler, Monomode Fibre

Operating Wavelength :	1.3 μm
Fibre type :	Corning SM-06S-P
Core index :	1.4514
Cladding Index :	1.4469
Fibre bend radius :	600 mm
Core separation :	10.2 μm
Fluid R.I. :	1.446
Coupling Ratio :	0.9
Insertion Loss :	<0.1 dB

2.1.2 0.10 Coupler, Monomode Fibre

Operating Wavelength :	1.3 μm
Fibre type :	Corning SM-06S-P
Core index :	1.4514
Cladding Index :	1.4469
Fibre bend radius :	600 mm
Core separation :	13.3 μm
Fluid R.I. :	1.450
Coupling Ratio :	0.1
Insertion Loss :	<0.1 dB

2.1.3 0.10 Coupler, Polarization-Maintaining Fibre

Operating Wavelength :	1.3 μm
Fibre type :	York HB1250
Core index :	1.4514
Cladding Index :	1.4469
Fibre bend radius :	600 mm
Core separation :	13.2 μm
Fluid R.I. :	1.450
Coupling Ratio :	0.1
Insertion Loss :	<0.1 dB

2.1.4 0.025 Coupler, Polarization-Maintaining Fibre

Operating Wavelength :	1.3 μm
Fibre type :	York HB1250
Core index :	1.4514
Cladding Index :	1.4469
Fibre bend radius :	600 mm
Core separation :	14.8 μm
Fluid R.I. :	1.450
Coupling Ratio :	0.025
Insertion Loss :	<0.1 dB

2.1.5 0.10 Switched Coupler, Lithium Niobate

Operating Wavelength :	1.3 μm
Material :	Crystal Technology, X-cut, Y-propagating
Bias voltage :	< 40 V
Switching voltage :	< 10 V
Coupling Ratio :	0.10
Extinction :	20 - 25 dB
Insertion loss :	2.1 dB (predicted chip loss)
Transition time :	2 ns
Dynamic range :	10 - 15 dB

2.2 FABRICATION TESTS

Certain testing procedures are intrinsic to, and were consequently carried out during, the actual fabrication process, since the nature of a number of the coupler structures to be fabricated demanded in-process definition of characteristics. This applied particularly to the polished half-coupler elements, where the depth of polishing determined the ultimate coupling range.

2.3 COMPONENT TESTS

Following component assembly, tests were performed to determine the characteristics, optical and electro-optic as appropriate, of the

assembled components. During this phase of testing, the parameters of variable components were adjusted to the specified values for delivery, to the extent that this was possible in isolation from the particular system configuration.

3. TEST PROCEDURES

3.1 DEFINITIONS

The figure illustrates schematically a 4-port coupler, representing all of the components considered here.

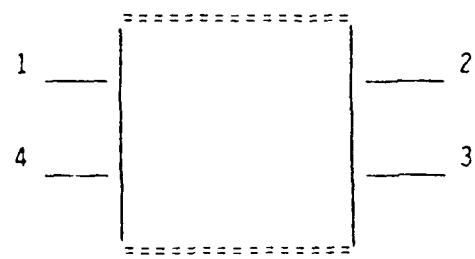

The following definitions are adopted:

Coupling Ratio : P[3]/(P[2]+P[3])
Splitting Ratio: P[3]/P[2]
Excess Loss : 10.log{(P[2]+P[3])/P[1]}
Directivity : 10.log{P[4]/P[1]}
Insertion Loss : 10.log{P[n]/P[1]}

where P[n] is any output port.

3.2 EQUIPMENT

Key items of equipment specific to the proposed tests were itemised in the Component Test Plan Report ELIN A003 submitted previously and will not be described further here. No significant deviations from this previously specified equipment were necessary.

3.3 TEST PROCEDURES

Test procedures adopted were described in the Component Test Plan Report ELIN A003 submitted previously and will not be described

further here. References to specific Procedures here relate directly to the indicated Sections of that Report.

4. TEST SCHEDULE

4.1 NOMENCLATURE

During the component breadboard phase, a multiplicity of component elements was fabricated. For convenience these are identified as follows:

(a) Half-coupler elements fabricated in polarization-maintaining fibre for assembly of components for Matrix Multiplier : MM01 - MM15.

(b) Half-coupler arrays (4 fibres per array) fabricated in monomode fibre for assembly of components for Coded Sequence Generator : CSG01 - CSG02.

NB: These were each subsequently separated by sawing into sets of 4 discrete half-coupler elements linked by single fibre lengths.

(c) Half-coupler arrays (4 active fibres plus 2 test fibres per array) fabricated in monomode fibre for assembly of components for Band Pass Filter : BPF01 - BPF02.

From these elements, a number of deliverable Components were assembled, the full inventory comprising:

Polarization-Maintaining Fibre Couplers:

K = 0.025	PMFC-2.5	# 0104
K = 0.10	PMFC-10.0	# 0912
	PMFC-10.0	# 1415

Lithium Niobate Switched Coupler:

K = 0.1 LNSC-1C.J # 1398A

Monomode Fibre Coupler Array:

K = 0.9 FBPF-4.75 # 0102

These identifiers will be used in what follows.

4.2 FABRICATION TESTS

4.2.1 Si V-Groove Geometry

V-groove structures manufactured by selective etching of (100) silicon were examined for dimensional accuracy and defects affecting, particularly, the critical central polishing region. As discussed extensively in the Monthly Reports on the programme, considerable difficulty was experienced in obtaining adequate precision of etched features in the very deep structures implicit in the component design, necessitating the introduction of certain modifications to the previously estabished process.

4.2.2 Fibre Azimuthal Alignment (Polarization-Maintaining only)

Using a far-field diffraction technique developed in-house specifically for this application, the orientation of the birefringence axes of polarization-maintaining fibre can be set precisely by lateral observation. This test was applied to each half-coupler unit during assembly, prior to polishing. Although qualitative in nature, this test was found to be extremely sensitive in use, permitting reliable, highly-accurate alignment leading to the fabrication of couplers of high polarization extinction.

4.2.3 Half-Coupler Lapping Stop-Point

For each element fabricated, the stop-point of the half-coupler lapping process was determined using measurements of the core ellipse (in the case of polarization-maintaining half-couplers) or the etched feature observation techniques outlined in Section 3.3.2 of ELIN A003. Again, while largely a routine process step, this approach provides the basis for the fabrication of quality components. However, since the object of the lapping process is speedy removal of extraneous material and minimising of the overall polishing time, the actual depth of lapping is relatively unimportant provided sufficient material remains to permit polishing to the required distance from the core and removal of surface damage.

4.2.4 Half-Coupler Polishing Stop-Point

For each component fabricated, the Stop-Point of the half-coupler polishing process was determined using the "oil-drop" technique outlined in Section 3.3.3 of ELIN A003. Based on knowledge of the relative indices of core and cladding, mineral oil was selected as the test medium in preference to the more commonly used liquid paraffin, on the grounds of its more constant composition and characteristics. Results of this test, presented as target and achieved core-to-polished face separation with a statistical breakdown of the latter, are presented in Table 1. Multiple figures for achieved polishing depth in the BPF and CSG elements represent data from the 4 active fibres in the respective arrays.

TABLE 1: POLISHING STOP POINT

Element	Coupler Type	Distance from Axis Target μm	Achieved μm
MM01	PMFC-2.5	7.4	7.0
MM04	PMFC-2.5	7.4	7.2
MM09	PMFC-10.0	6.6	6.6
MM12	PMFC-10.0	6.6	6.5
MM14	PMFC-10.0	6.6	6.6
MM15	PMFC-10.0	6.6	6.6

PMFC-2.5 : Target = 7.4 μm, Mean = 7.1 μm
PMFC-10.0 : Target = 6.6 μm, Mean = 6.6 μm

Element	Coupler Type	Distance from Axis Target μm	Achieved μm
BPF01	FBPF-4.75	5.1	5.0, 5.6, 5.9, 5.1
BPF02	FBPF-4.75	5.1	5.1, 5.1, 5.5, 5.1

Mean = 5.3 μm, Standard Deviation = 0.30 μm

Element	Coupler Type	Distance from Axis Target μm	Achieved μm
CSG04	FCSG-2.00	6.6	5.0, 6.4, 6.9, 5.3
CSG05	FCSG-2.00	6.6	5.4, 5.6, 6.7, 5.4

Mean = 5.8 μm, Standard Deviation = 0.42 μm

4.2.5 Polished Hi-Bi Half-Coupler Extinction

4.2.5.1 Prior to Polishing

The extinction of selected half-coupler elements fabricated in polarization-maintaining fibre was determined prior to polishing, using the technique outlined in Section 3.3.5 of ELIN A003. Results of this test, determined for polarization parallel and perpendicular to the fibre birefringence axis respectively, are presented in Table 2.

TABLE 2: HALF-COUPLER EXTINCTION RATIO (Prior to polishing)

Element	Coupler Type	Extinction dB Parallel	Perpendicular
MM04	PMFC-2.5	31	28
MM08	PMFC-10.0	34	30
MM12	PMFC-10.0	26	28

4.2.5.2 Post-Polishing

The extinction of selected half-coupler elements fabricated in polarization maintaining fibre was determined subsequent to polishing, using the technique outlined in Section 3.3.5 of ELIN A003. Results are tabulated in Table 3, together with the result of a comparable determination on a single fibre length.

Table 3: HALF-COUPLER EXTINCTION RATIO (Post polishing)

Element	Coupler Type	Extinction dB Parallel	Perpendicular
MM01	PMFC-2.5	25	30
MM04	PMFC-10.0	28	30
Fibre		31	28

4.2.6 Lithium Niobate Coupling Ratio (Chip Stage)

As part of the initial chip selection process, the static coupling ratio of all device chips was determined in accordance with the procedure outlined in section 3.3.6 of ELIN A003. Evaluation of the static coupling ratio as a function of coupler gap showed that devices with gaps between 5 um and 8 um had coupling in the required range of between one and three coupling lengths. Devices with coupler gaps around 6 um had optimum coupling for switch operation. These results were confirmed by electro-optic operation of a number of chips, the best of which were selected for further processing.

4.2.7 Lithium Niobate Insertion Loss (Chip Stage)

The insertion loss associated with individual switch elements was assessed at the chip-level prior to committing devices to further processing, as detailed in Section 3.3.4.2.1 of ELIN A003. Insertion losses for the intended TE mode and the suppressed TM mode observed in two chips selected for further processing to finished devices are listed in Table 4.

TABLE 4: LITHIUM NIOBATE INSERTION LOSS (Chip Stage)

All values +/-0.5 dB

Device	TE Mode dB	TM Mode dB
=1398A	3.7	22.3
=1398B	3.7	22.4

The losses of the suppressed TM mode indicate a polarization extinction ratio attributable to the integral metal film polarizers of 18.6+/-1 dB.

4.3 COMPONENT TESTS

4.3.1 Coupling Ratio (Polished Couplers)

The lateral tuning characteristics of mated half-coupler assemblies were examined for conformity with design predictions. In the particular case of the couplers destined for the Band-Pass Filter and Coded-Sequence Generator applications, the monolithic and, in the latter case, recursive nature of the assembly prevented direct characterisation of each individual coupler except under pulse excitation at a frequency sufficiently high to permit resolution of the impulse response of the fully integrated assembly. Additional test coupler elements, fibred non-recursively and independently of the integrated structure, are therefore provided in the Si V-groove units, specifically for this purpose.

Using the designated laser diode and detector system, completed polished coupler assemblies were assessed for Coupling Ratio in accordance with the procedure outlined in Section 3.3.6 of ELIN A003. Characterised components have been prepared for delivery pre-adjusted to the specified level of coupling. In addition, for each assembly, core-polished face data have been derived from the results of the "oil-drop test", for comparison with target figures.

4.3.1.1 Monomode Fibre Couplers

In order to obtain sufficient mechanical tuning latitude, the nominal 10% couplers were designed as 20% maximum coupling devices while the 90% couplers were designed as overtuned devices with maximum coupling ratios of 100%. Table 5 summarises the results of this assessment.

TABLE 5: COUPLING RATIO - MONOMODE FIBRE COUPLERS

(a) Band Pass Filter (assessed on assembled integrated array via "test fibres")

Coupler Type	Serial No.	Max Coupled Power Chann 2	Chann 3	K Design	Measured
FBPF-4.75	0102	.28	3.09	0.9	0.92

(b) Coded Sequence Generator (quantitative assessment awaiting system integration)

4.3.1.2 Polarization-Maintaining Couplers

In order to obtain sufficient mechanical tuning latitude, the nominal 2.5% and 10% couplers were designed with maximum coupling ratios of twice these figures, i.e. 5% and 20% respectively. Tunable couplers were assembled from the following combinations of half-coupler elements, the core-to-core separation being the sum of the experimentally determined core-to-polished surface distances for the two components, as indicated in Table 6.

TABLE 6: FABRICATION PARAMETERS - POLARIZATION-MAINTAINING COUPLERS

Coupler Type	Serial No.	K Design	Core-Core Sepn. μm Design	Actual
PMFC-2.5	MM0104	.025	14.8	14.2
PMFC-10.0	MM0912	.10	13.2	13.1
PMFC-10.0	MM1415	.10	13.2	13.2

4.3.2 Coupling Ratio (Lithium Niobate)

Using the designated laser diode and detector system, the coupling behaviour of the completed lithium niobate switched coupler was assessed as defined in Paragraph 3.3.7 of ELIN A003.

Figure 1 plots the response of device 1398 to dc drive, showing optical power emerging from the two output ports as a function of applied volts. Table 7 summarises output power levels, for constant arbitrary input power, at a limited set of critical conditions, namely maxima and minima of the response plots, defining key drive parameters.

TABLE 7: LITHIUM NIOBATE COUPLER DRIVE PARAMETERS

Drive V	Channel 2 dBm	Dyn Range dB	Channel 3 dBm	Dyn Range dB
-20.5	-17.9		-49.0	31
-9.4	-35.9	18	-17.9	
0	-17.8		-35.5	
-9.4	-45.0	27	-18.4	
-20.5	-17.8		-36.2	18

dBm +/- 0.5, dB +/- 1.0

From this plot and table, the optimum operating point for achieving the required 0 - 10% coupling switching is identified as a bias of -9.4 V, providing a dynamic range of 27 dB for full switching range, with a superimposed switching drive of +/-2 V. For 10% switching, available dynamic range is reduced by 10 dB, to 17 dB.

4.3.3 Insertion Loss (All Components)

4.3.3.1 Polished Coupler Insertion Loss

The insertion loss of assembled polished coupler assemblies of both monomode and polarization-maintaining types was determined using the technique outlined in Section 3.3.4.1 of ELIN A003.

4.3.3.1.1 Monomode Fibre Couplers

Insertion loss of monomode fibre couplers was found to be below the limit of characterisation and is therefore estimated to be better than -30 dB.

4.3.3.1.2 Polarization-Maintaining Couplers

Insertion loss of polarization-maintaining fibre couplers was found to be below the limit of characterisation and is therefore estimated to be better than -30 dB.

4.3.3.2 Lithium Niobate Switched Coupler Insertion Loss

The insertion loss of assembled lithium niobate switch 1398A was determined using the technique outlined in Section 3.3.4.2.2 of ELIN A003. The following figures were obtained (input on Channel 1):

Channel 2 : -11.5 +/- 1.0 dB
Channel 3 : -10.0 +/- 1.0 dB

4.3.4 Extinction Ratio (Polarization-Maintaining Components Only)

4.3.4.1 Polished Couplers

Extinction ratio of the assembled polished polarization-maintaining coupler assemblies was determined using the techniques outlined in Section 3.3.5 of ELIN A003. Results are summarised in Table 8.

TABLE 8: EXTINCTION RATIO - POLARIZATION-MAINTAINING COUPLERS

Coupler Type	Serial No.	Extinction dB Channel 2	Channel 3
PMFC-2.5	MM0104	25.82	22.24
PMFC-10.0	MM0912	21.33	22.04
PMFC-10.0	MM1415	25.91	24.37

4.3.4.2 Lithium Niobate Switched Coupler

The extinction ratio of the assembled lithium niobate switched coupler was determined using the techniques outlined in Section 3.3.5 of ELIN A003. Results are tabulated in Table 9, which shows extinction ratio for the two output ports as a function of three levels of drive voltage.

TABLE 9: POLARIZATION EXTINCTION OF LITHIUM NIOBATE SWITCHED COUPLER

Output Port 2

Drive V	Transmission dB	Extinction Ratio dB
0.00	0	23.0
7.11	-9.1	22.3
9.08	-18.8	15.3

Output Port 3

Drive V	Transmission dB	Extinction Ratio dB
9.08	0	15.4
1.87	-9.1	15.4
0.00	-17.7	15.5

4.3.5 Switching Response Time (Lithium Niobate only)

The electro-optic rise-time of assembled lithium niobate switched coupler 1398A was investigated using the technique outlined in Section 3.3.8 of ELIN A003.

Figure 2 shows the mean coupled optical power emerging from the output port of the coupler when driven with a levelled 28 dBm RF signal (Vrms = 5.6 V), plotted as a function of frequency over the range 0.3 - 2.1 GHz. Insertion of a reference level is difficult, due to the ripple observed in the response. Averaging by eye a low frequency reference level of the order of -28 dBm, and ignoring the pronounced resonance at around 0.8 GHz, the output power is seen to have fallen

by a further 3 dB at a frequency of around 1.2 GHz, indicating a response time of 0.29 ns.

6. CONCLUSIONS

The foregoing results show that the fabricated components are in general conformity with original design predictions, particularly with respect to the somewhat demanding mechanical tolerances involved in polishing half-coupler assemblies to specified depths. The major discrepancy between design and fabrication parameters arises in the case of the monolithic assemblies for the Coded Sequence Generator and Band Pass Filter. Due to limitations in the substrate polishing process, large-radius convex curvature of the polished face was experienced, a difficulty anticipated in the design phase of both components.

In the Band Pass Filter, the four active fibres were positioned in closely spaced pairs disposed symmetrically about the substrate major axis in order to equalise the effects of this on polishing depth as far as possible. However, the two additional fibres, provided to permit simple monitoring of the complex recirculating structure and utilised extensively as polishing monitors via the oil-drop assessment, were consequently situated closer to the substrate axis, at locations experiencing different polishing conditions. Polishing was stopped at the design depth as indicated by these fibres, thereby ensuring that the outer pairs of active fibres were polished slightly closer to the core, maintaining the over-coupling situation necessary to ensure the accessibility of the complete mechanical tuning range.

In the Coded Sequence Generator, however, this option was not available, due to the need to saw the substrate into its constituent chips after the polishing process, resulting in the significantly higher standard deviation exhibited by the polishing depth data for this component. In operation, this disadvantage will be adequately offset by the ability to tune each component individually.

The only other significant discrepancy between component design and fabrication parameters occurs in the lithium niobate chip insertion loss, with best-case predicted and experimentally observed figures of 2.1 and 3.7 dB respectively. This is attributed, at least in part, to the presence of metallic polarizers over the waveguides, a feature not included in the original theoretical estimate.

P J Duthie
D C J Reid
C J Groves-Kirkby
I Bennion

Plessey Research Caswell Limited,
Allen Clark Research Centre,
Caswell, Towcester, Northants, NN12 8EQ, UK

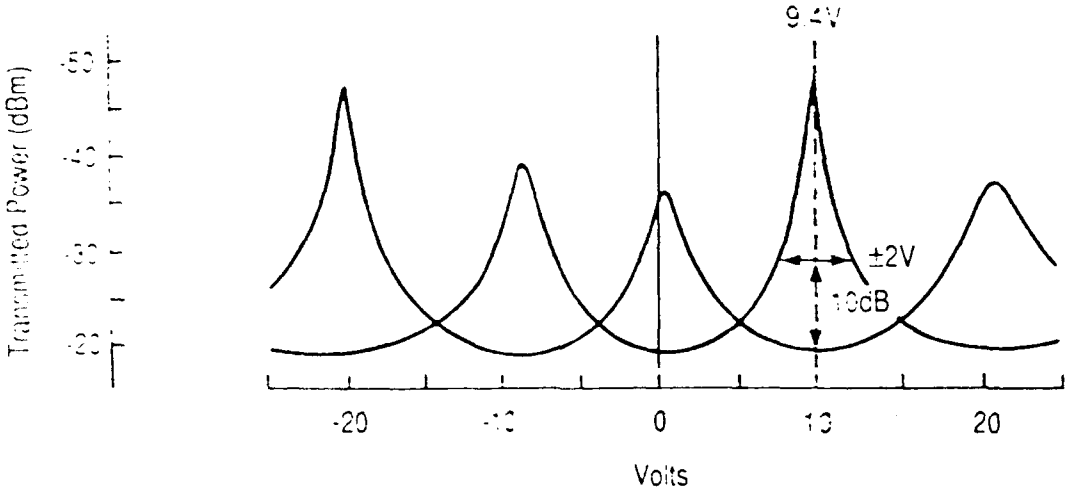

Figure 1 Lithium Niobate Switched Coupler No. 1398A
DC Response and Operating Point

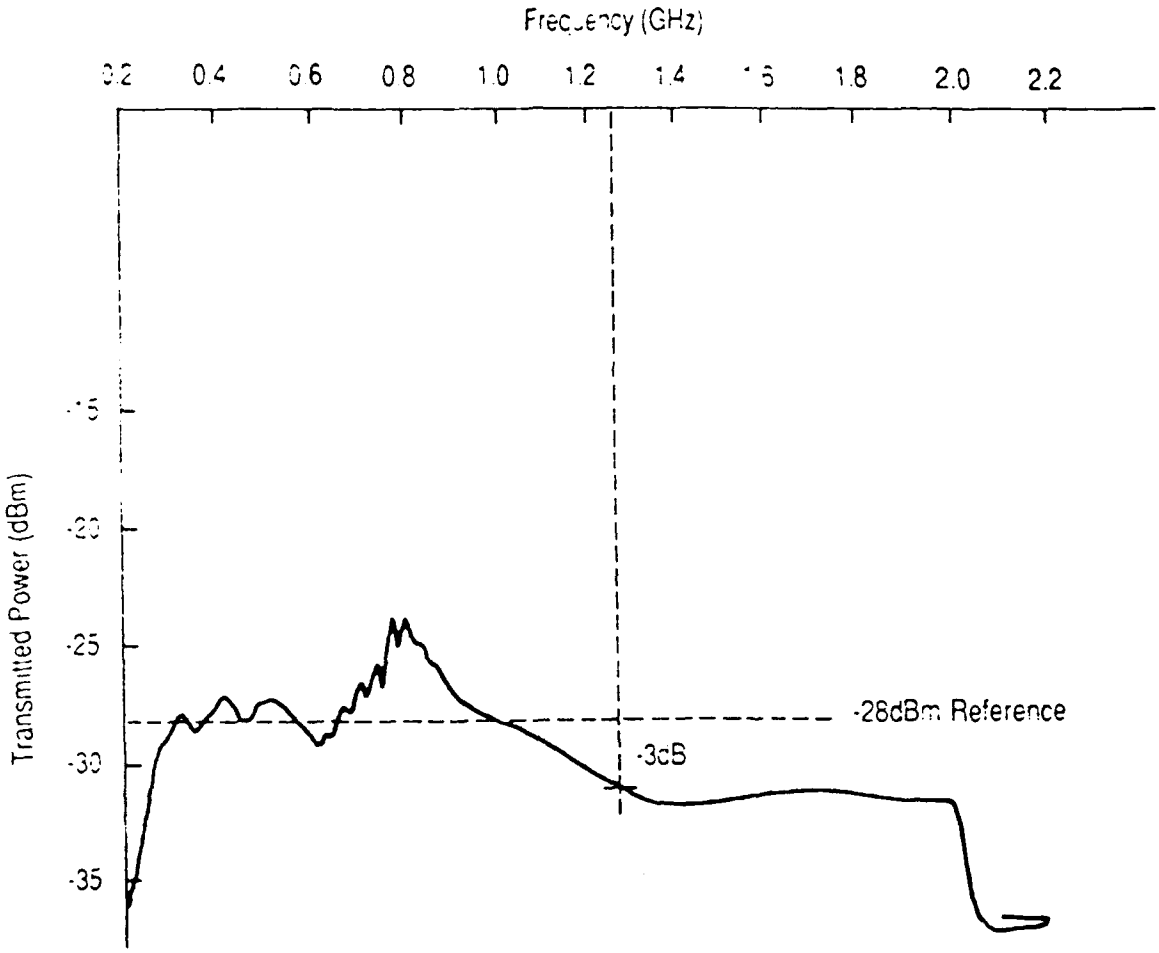

Figure 2 Lithium Niobate Switched Coupler No. 1398A Frequency Response (0.2 - 2.2GHz)

APPENDIX F

FIBER OPTIC BASED SIGNAL PROCESSING SYSTEM TEST REPORT CODED SEQUENCE GENERATOR

FIBRE OPTIC BASED SIGNAL PROCESSING

CONTRACT NO. F30602-87-C-0015

SYSTEM TEST REPORT

(CLIN A005)

CODED SEQUENCE GENERATOR

Prepared by:

C J Groves-Kirkby
D C J Reid

Approved by:

M J Goodwin
I Bennion
R Davis
M J Cardwell

Plessey Research Caswell Limited
Caswell, Towcester, Northants
England, NN12 8EQ

SUMMARY

A quasi-monolithic, splice-free 4-stage optical fibre coded sequence generator has been designed, constructed and tested. The breadboard system permits generation of reconfigurable 4-bit pulse sequences, with pulse repetition rate of 2 GHz, i.e. 500 ps interval within the pulses in the output train. The programme has confirmed the feasibility of the manufacture of monolithic arrays of evanescent wave coupler elements in a single length of fibre with uniform coupling characteristics and repeatable coupler separation, suitable for the assembly of splice-free multi-stage optical signal processing systems.

Detailed measurement of coupler parameters, both during fabrication and on completion, verifies the analytical design approach, confirming that high precision couplers can be fabricated to demanding specifications in multi-element arrays configured on a single fibre length. The breadboard system has been shown to conform to projected performance targets, and has been prepared for delivery adjusted to the specified level of optical power coupling detailed in the System Design Plan (submitted as CLIN A004 in October 1988).

1. INTRODUCTION

This document describes the results of tests used to characterise the breadboard Coded Sequence Generator, fabricated as part of Contract No. F30602-87-C-0015, Fibre Optic Based Signal Processing, and carried out during the course of Tasks 4.1.3 and 4.1.5, Component Breadboard and Processor Breadboard, respectively. The evaluation process is outlined in the System Design Plan, Section 3.2.3, submitted as CLIN A0004. This document comprises part of CLIN Item A0005

2. GENERAL

This System Test Plan Report describes the results of tests carried out on the breadboard Coded Sequence Generator assembled during the course of the System Breadboard phase, Task 4.1.5, together with results of certain component tests which, by virtue of the nature of the selected mode of construction of the System, could not be performed until this phase but which are formally associated with the Component Breadboard activity of Task 4.1.3.1.

Application of fibre optic delay line technology to coded sequence generation was studied in Tasks 4.1.1 Theoretical Performance Assessment, 4.1.2 Realisable Performance Assessment and 4.1.4 Processor Design, conclusions from these studies being collated in the System Design Plan, CLIN A004 of October 1988. To summarise, use of fibre optic delay lines for coded sequence generation is simple in principle, any weighted tapped configuration being generally applicable. Following a comparative assessment of three candidate architectures, namely the simple tapped delay line, the recirculating lattice and the non-recirculating lattice, the latter option was

identified as the preferred structure since in this arrangement the optical output appears on a single fibre with no second-pass interference.

In order to eliminate lossy splices within the multi-stage system, quasi-monolithic fabrication of appropriately spaced sets of four half coupler elements on single fibre lengths was undertaken and the feasibility of this mode of fabrication was demonstrated successfully.

2.1 SYSTEM SPECIFICATIONS

As a result of the initial theroetical assessments, the following specification for a breadboard Coded Sequence Generator was defined:

4-bit code
Complete programmability
2 Gbit/sec pulse rate

This specification defines a requirement for a third order non-recirculating lattice, with the individual couplers having a maximum permissible coupling coefficient of 0.1 (10%) to give a pulse uniformity of +/- 10 dB. The configuration proposed, and discussed in the System Design Plan, employs four mechanically tunable evanescent wave couplers, permitting implementation of the required programmability. At 1.3 μm wavelength and assuming the use of standard silica fibre, the required loop length difference between adjacent couplers is 103.6 mm, equivalent to a pulse code rate of 2 Gbit/sec.

The Component Design Plan, previously submitted as CLIN A001, October 1988, outlines design parameters for suitable optical fibre couplers, details of which are summarised here.

0.10 Coupler, Monomode Fibre

Operating Wavelength :	1.3 μm
Fibre type :	Corning SM-06S-P
Core index :	1.4522
Cladding Index :	1.4469
Fibre bend radius :	600 mm
Core separation :	13.3 μm
Fluid R.I. :	1.450
Coupling Ratio :	0.1
Insertion Loss :	<0.1 dB

2.2 COMPONENT TESTS

As noted above, results of certain component tests are reported here since the quasi-monolithic nature of the adopted structure precluded direct measurement of certain characteristics of individual couplers.

2.3 SYSTEM TESTS

A series of tests was carried out to determine the characteristics of the completed assembled system. During this phase of testing, the parameters of variable components were adjusted to the specified values for delivery.

3. TEST PROCEDURES

3.1 DEFINITIONS

Figure 3.1 illustrates schematically a 4-port coupler, representing the components of the system considered here.

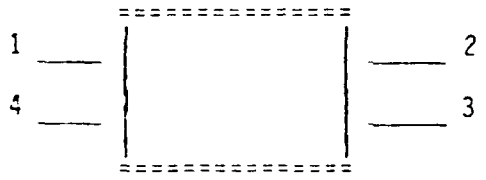

The following definitions are adopted:

Coupling Ratio : P[3]/(P[2]+P[3])
Splitting Ratio: P[3]/P[2]
Excess Loss : 10.log{P[2]+P[3]/P[1]}
Directivity : 10.log{P[4]/P[1]}
Insertion Loss : 10.log{P[n]/P[1]}

where P[n] is the optical power appearing at output port n.

3.2 EQUIPMENT

Key items of equipment specific to the tests are itemised here. In addition, a number of more general laboratory instruments, for example d.c. power supplies, oscilloscopes, graphical recorders etc. were employed as the nature of the tests dictated.

3.2.1 Laser Diode Sources (1.3 μm)

Both CW and pulsed laser sources employed were Plessey Fabry-Perot cavity devices, equipped with monomode fibre pigtail, with a nominal emission wavelength of 1.3 μm and 0 dBm output.

3.2.2 Optical Detector (CW)

Assessment of insertion loss (essentially CW measurement) was performed using a Plessey III-V semiconductor detector equipped with a monomode fibre pigtail.

3.2.3 Optical Detector (High Speed)

Optical detector for high speed measurements was a Plessey PIN photodiode, coupled directly to the detection oscilloscope system.

3.2.4 Pulse Signal Source

Pulse signals for system testing were provided by a Signal Generator, Rohde and Schwartz Type 302.4012, in conjunction with a Pattern Generator, Anritsu Type MG624A, driving the laser source directly.

3.2.5 High Speed Oscilloscope

High speed measurements of system output pulse train waveforms was performed using a Tektronix Sampling Oscilloscope, Type 7854, equipped with Type 7S12 sampling unit.

3.3 TEST PROCEDURES

3.3.1 Coupling Ratio

The Coupling coefficient, defined in Section 3.1, is determined by measurement of the optical power at output ports 2 and 3 when input port 1 is excited.

3.3.2 Insertion Loss

Insertion Loss of components is quantified in accordance with the definition given in Paragraph 3.1.

In order to prevent the loss of fibre pigtail implicit in "cut-back" techniques, the excess loss of components fabricated on optical fibre was quantified by comparison of the optical propagation of the component under investigation with the propagation of an equal length of identical fibre.

System insertion loss was quantified by direct substitution within a functioning high speed link.

3.3.3 Coded Sequence Generator Characterisation

Detailed characterisation of the assembled Coded Sequence Generator was based principally on observation of output pulse train waveforms observed using the specified source and receiver. Basic data for numerical assessment was provided by photographs of oscilloscope traces of these output waveforms, subsequent quantification being via direct measurement of trace dimensions and application of equipment calibration factors.

4. TEST SCHEDULE

4.1 COMPONENT TESTS

4.1.1 Coupling Ratio

The lateral tuning characteristics of mated half-coupler assemblies was examined for conformity with design predictions. In each case, it was possible to achieve the design value of 0.1 (10%) coupling using the mechanical tuning facility.

Using the designated laser diode and detector system, completed polished coupler assemblies were assessed for Coupling Ratio in accordance with the procedure outlined in Section 3.3.1. Characterised components were prepared for system commissioning pre-adjusted to the specified 10% level of coupling.

4.1.2 Insertion Loss

The insertion loss of assembled polished coupler assemblies was determined using the technique outlined in Section 3.3.2. Since the assemblies under test comprised four couplers fabricated quasi-monolithically, it was only possible to assess insertion loss of the complete assembly. Under these conditions, the insertion loss was found to be below the limit of characterisation, and was thus estimated to be better than 0.004 dB.

4.2 SYSTEM TESTS

4.3.1 Test Assembly

Figure 1 shows schematically the test assembly utilised for characterisation of the breadboard Coded Sequence Generator. In use, the system was adjusted to deliver pulses 100 ps wide (FWHM), this width being used exclusively in the testing reported here. Equipment specifications have been noted in Section 3.2, above. Hard-copy records of output pulse train waveforms were obtained by photographing oscillopscope displays; these records were utilised as the data source for the system characterisation tests reported in the following sections.

4.3.2 Insertion Loss

System insertion loss, quantified by measuring link output pulse intensity with the system inserted and removed from the functioning test link as specified, was determined to be 0.85 dB. This represents the losses arising in 4 tuned couplers together with two FC/PC connectors.

4.3.3 Code Generation and Tunability

Figure 2 shows photographs of selected oscilloscope traces of output waveforms, demonstrating the inherent tunability of the pulse train. All of the 16 possible 4-bit waveforms, from 1111 to the trivial 0000, were capable of generation, not all being shown here.

4.3.4 Pulse Width

Pulse width can be readily quantified from the photographs of Figure 2. Statistical data for full width at half-maximum (FWHM), extracted from the photographic records, are tabulated in Table 1:

TABLE 1: PULSE WIDTH CHARACTERISTICS

Bit	Samples	Mean (ps)	Standard Deviation (ps)
Bit1	7	113.9	0.36
Bit2	6	111.8	0.56
Bit3	6	117.1	0.16
Bit4	7	118.4	0.31
Overall	26	115.4	0.45

Within the limits of accuracy of the determination, no significant difference in pulse width occurs across the pulse train; all output pulses, however, exhibit consistent broadening of the order of 15 ps over the 100 ps input pulse width. This broadening is directly attributable to the fibre components of the system and, in particular, implies a coupling region interaction length of the order of 3 mm, a dimension consistent with the known coupler geometry.

4.3.5 Dynamic Range

Dynamic range of the output pulse train was estimated from oscilloscope photographs. In the worst case observed, detected pulses of 10 nV were associated with a noise signal of the order of 0.5 nV peak to peak amplitude, equivalent to a dynamic range in excess of 13 dB. As readily seen from the sample pulse trains shown in Figure 2, output pulse quality is generally significantly better than this. Note that much of the lower amplitude signal structure was present on the input pulse, replicating directly into the output pulse train.

4.3.6 Inter-Pulse Interval

Determinations of the intrinsic inter-pulse interval provided by the system were made from oscilloscope photographs of a wide variety of output waveforms. The results derived from this data are summarised in Table 2, indicating excellent agreement with the design target of 500 ps.

TABLE 2: INTER-PULSE INTERVAL

Interval	Samples	Mean (ps)	Standard Deviation (ps)
Bit1-Bit2	7	502.5	0.25
Bit2-Bit3	8	507.8	0.13
Bit3-Bit4	7	500.0	0.23
Overall	22	503.5	0.35

4.3.7 Pulse Height Uniformity

It was initially planned to quantify pulse height uniformity by setting individual couplers to identical 10% coupling, with measurement of the corresponding output pulse heights. This approach proved impracticable, since mechanical hysteresis in the coupler tuning units prevented absolute calibration of coupling strength against tuner scale reading, a pre-requisite for this mode of determination. Operationally, it is preferable, anyway, to set the output pulse uniformity by direct reference to the generated waveform. The validity of this approach for setting uniform pulse trains can be seen from the figures; mechanically adjusted uniformity better than 3% (0.13 dB deviation), is readily achieved.

5. CONCLUSIONS

The foregoing results show that the performance of the assembled breadboard Coded Sequence Generator is in excellent agreement with design requirements, further demonstrating the viability of the annlytical design approach to coupler system parameter definition.

The quasi-monolithic construction approach adopted in this case represents a new departure for multiple coupler assemblies, permitting manufacture of multiple individual coupler elements on a single fibre length at separations considerably less than the mechanical dimensions of an individual mechanical assembly. Although an output pulse repetition rate of 2 GHz has been demonstrated here, based on an incremental fibre delay length of 103 mm, this dimension is obviously capable of significant further reduction; given current technology, it appears perfectly feasible to reduce the incremental delay by a factor of 10, to order 10 mm, giving an output pulse repetition rate of 20 GHz.

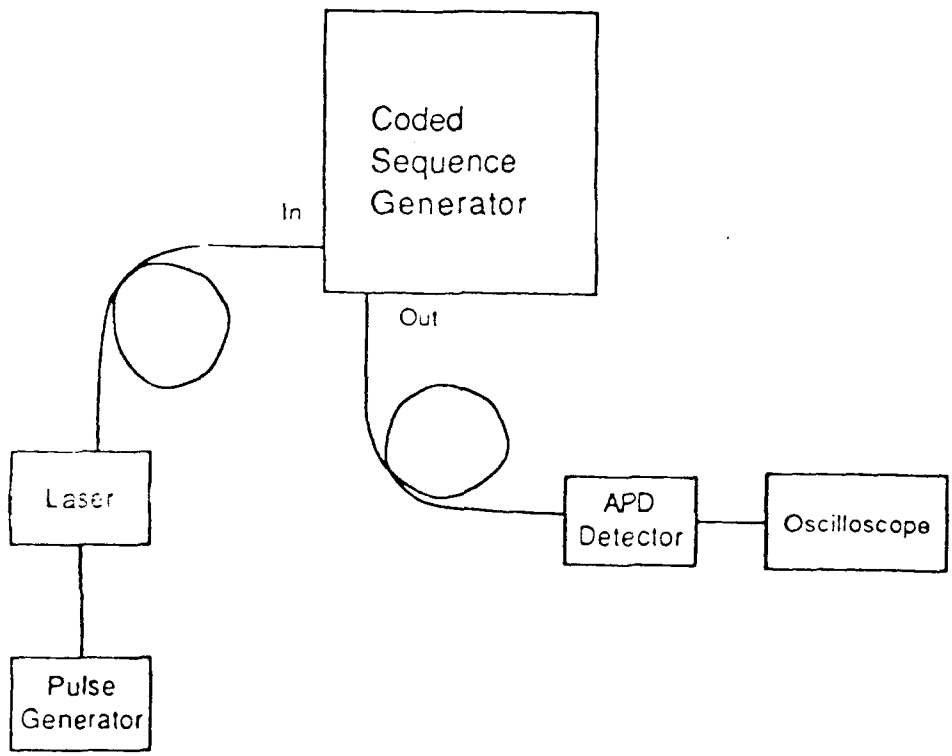

Figure 1. Coded Sequence Generator Test Arrangement

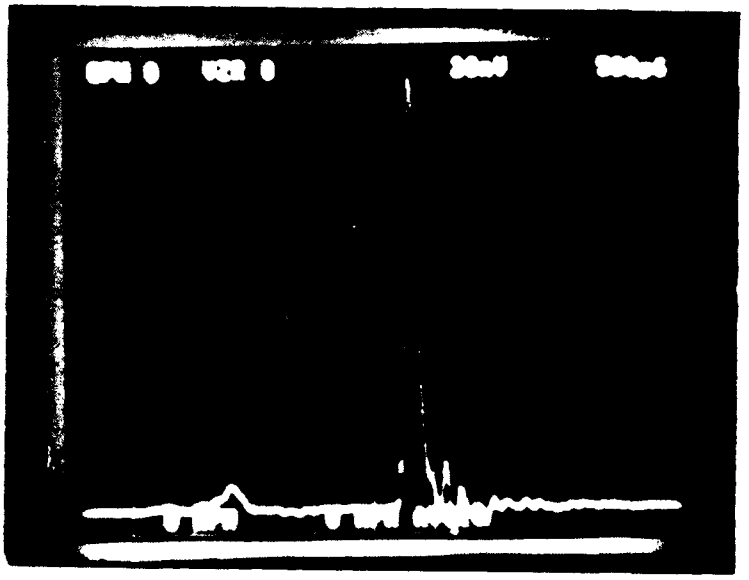

Input Pulse

Figure 2 (a). Input Pulse Waveform of the Coded Sequence Generator

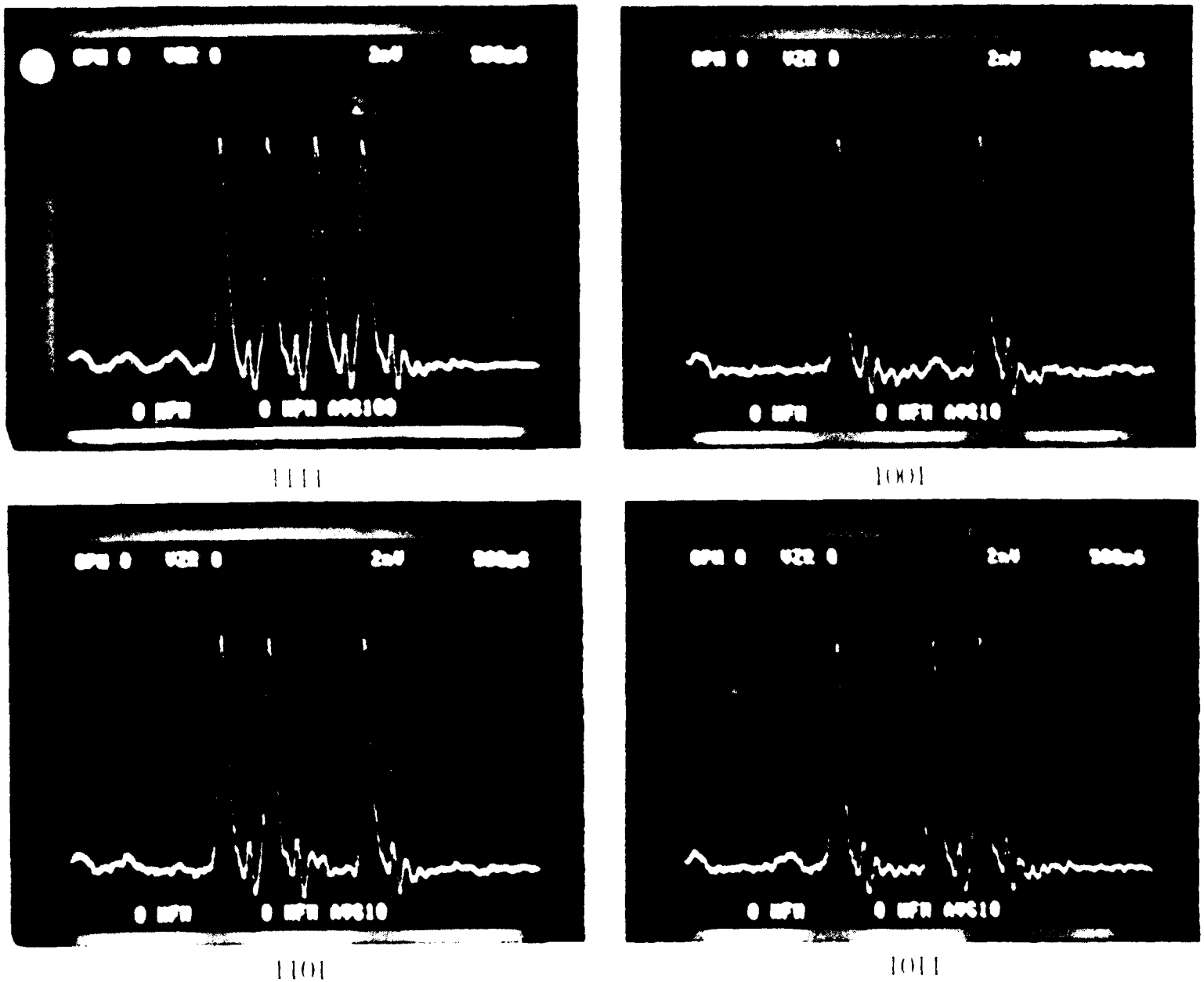

Figure 2 (b). Sample Output Waveforms from the Coded Sequence Generator

APPENDIX G

FIBER OPTIC BASED SIGNAL PROCESSING CODED SEQUENCE GENERATOR OPERATING INSTRUCTIONS AND USER'S NOTES

FIBRE OPTIC BASED SIGNAL PROCESSING

CONTRACT NO. F30602-87-C-0015

CODED SEQUENCE GENERATOR - OPERATING INSTRUCTIONS AND USER'S NOTES

Prepared by:

C J Groves-Kirkby
D C J Reid

January 22nd 1990

Plessey Research Caswell Limited
Allen Clark Research Centre
Caswell
Towcester
Northants NN12 8EQ
UK

1. INTRODUCTION

The Plessey Optical Fibre Coded Sequence Generator, Type CSG, comprises a quasi-monolithic, splice-free 4-stage optical fibre system, packaged in a robust enclosure. The system is interfaced to the outside world via four FC/PC bulkhead connectors; in addition, four FC/PC-to-biconic jump-lead adapters are provided to permit interfacing to optical fibre links configured with biconic couplers.

The system is designed to operate at an optical wavelength of 1.3 um and is configured to permit the generation of reconfigurable 4-bit pulse sequences, with a fixed pulse repetition rate of 2 GHz defined by the internal optical fibre delay line loops. The output pulse pattern is readily re-defined by manual adjustment of the mechanical tuning controls, as described more fully below.

2. PRINCIPLES OF OPERATION

The accompanying Figures outline the internal fibre delay line loop structure, indicating the principles of operation of the system. The structure comprises a pair of monomode fibres, coupled at regular intervals by evanescent-wave fibre couplers permitting optical power to transfer synchronously from one fibre to the other. The present system incorporates four couplers, defining three fibre stages, permitting the generation of a 4-bit code pattern from a single input pulse of appropriate parameters. By implementing the couplers in a mechanically tunable technology, manual reconfiguration of the output pulse train becomes possible. The further refinement of manufacturing the coupler arrays on single fibre lengths eliminates the need for inter-stage splices, considerably reducing optical attenuation.

As indicated in the Figure, pairs of adjacent couplers are separated by two optical fibres of differing lengths, with the length difference defining a relative optical propagation delay. The magnitude of this delay represents the inter-pulse interval of the resultant output coded bit stream, defined to be 500 ps in the present case and is incapable of alteration in the present design.

The relationship between the system components and individual bits of the pulse train is indicated schematically, the time axis being defined conventionally with time progressing to the right.

3. SYSTEM INSTALLATION

3.1 GENERAL

The Plessey Coded Sequence Generator System Type CSG comprises a sealed breadboard assembly comtaining 4 manually adjustable mechanically tuned evanescent-wave fibre couplers interconnected with fixed fibre delay loops. The system is contained in a sealed enclosure containing no electronic components and no user-servicable parts. Optical interface to the outside world is via 4 FC/PC bulkhead-mounted connectors, disposed as indicated in the accompanying Figures. For convenience in interfacing to optical links of US origin, a set of four FC/PC-Biconic adapter leads is provided. The system is most conveniently operated in a horizontal position, although the design of the mechanical assemblies is such that operation is any other attitude is generally possible.

In the normal mode of operation, the input pulse should be applied to the lower Input Port, representing the input to the shorter delay loop. The output pulses then represent the coupling strengths of the couplers a, b, c, d, appearing at the upper Output Port, longer delay loop, in the reverse order d, c, b, a. A signal representing the exact inverse of the output pulse train appears at the lower Output Port. The intrinsic mechanical and optical symmetry of the system permits equivalent operation in the complementary configuration with the input pulse applied to the Port labelled Output to give pulse outputs at the "Input" ports.

3.2 OPTICAL SOURCE

System design is optimised for operation at an optical wavelength around 1.3 um; operating range extends from fibre cut-off, around 1.2 um, to the region where bending loss becomes significant,

estimated to be around 1.6 um, although performance may be degraded at wavelengths remote from the design wavelength. In order to resolve output pulses with a separation of 500 ps, it is necessary to provide an input pulse with a width significantly narrower than this figure; experimental testing of the system was carried out using pulses of the order of 200 ps fwhm.

3.3 OPTICAL RECEIVER

The necessary Receiver characteristics are defined by the need to resolve the structure of the output pulse code sequence, together with the overall power budget of the link. With all couplers activated, giving the 1111 sequence output, and with couplers set for 10% coupling, the individual output pulse intensity will be degraded relative to the input pulse by at least -11.5 dB; for patterns containing fewer set bits, this figure will improve marginally, -10 dB being the theoretical degradation for a single bit pattern, eg 1000.

3.4 SETTING CODE PATTERN

The system has been prepared for delivery with all couplers mechanically set to 10% coupling, giving a 1111 output pulse train. Individual bits of this pattern can be cleared and reset by manually adjusting the appropriate coupler control through the portholes provided, a procedure best undertaken with the system inserted into a functional optical link, since this permits direct observation of the resultant output pulse train. As a general rule, anticlockwise rotation of the tuning control of any particular mechanical unit will result in the coupling strength of the associated coupler being reduced progressively from 10% to zero; since power is conserved within the system, such adjustment may result in an increase in absolute coupled power present in any individual output pulse (but not in relative coupling strength).

The coupling knob must remain within the region of the tuning shaft defined by the two coloured indicators at all times.

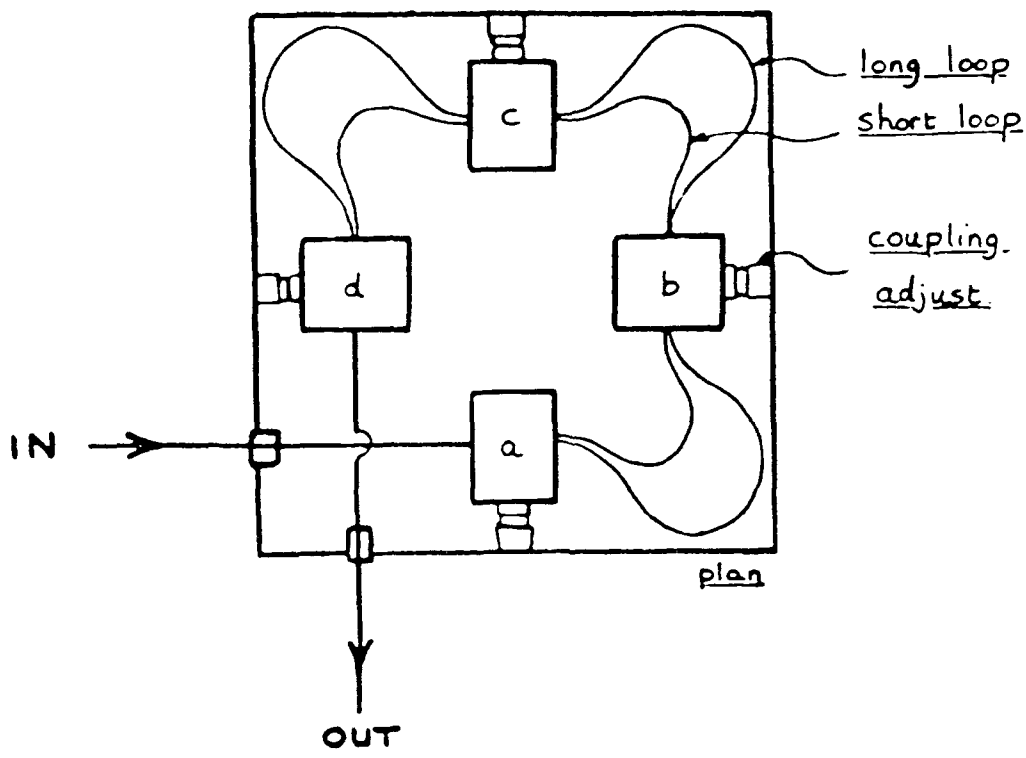

Figure 1. Internal Fiber Delay Line Loop Structure

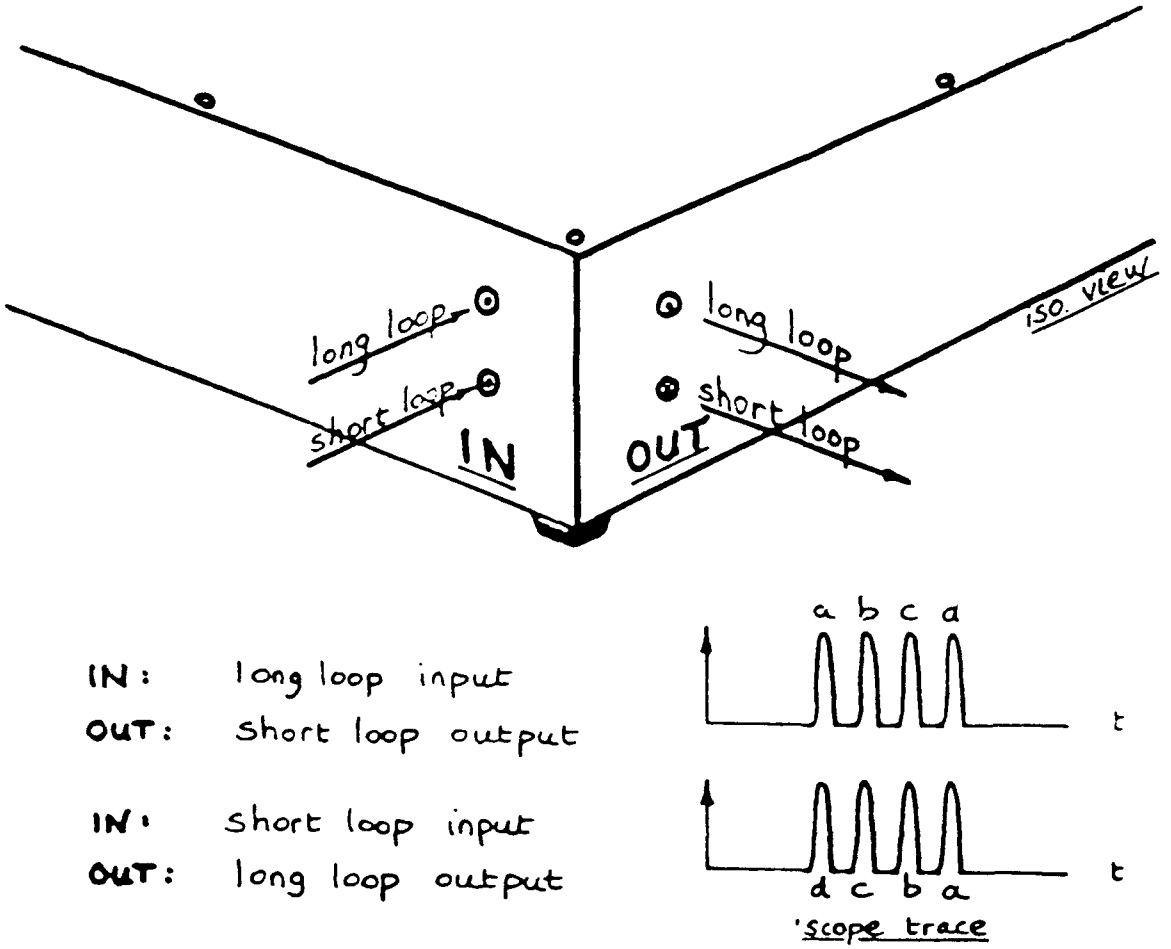

Figure 2. External Fiber Connection Arrangement

MISSION

OF

ROME LABORATORY

Rome Laboratory plans and executes an interdisciplinary program in research, development, test, and technology transition in support of Air Force Command, Control, Communications and Intelligence (C^3I) activities for all Air Force platforms. It also executes selected acquisition programs in several areas of expertise. Technical and engineering support within areas of competence is provided to ESD Program Offices (POs) and other ESD elements to perform effective acquisition of C^3I systems. In addition, Rome Laboratory's technology supports other AFSC Product Divisions, the Air Force user community, and other DOD and non-DOD agencies. Rome Laboratory maintains technical competence and research programs in areas including, but not limited to, communications, command and control, battle management, intelligence information processing, computational sciences and software producibility, wide area surveillance/sensors, signal processing, solid state sciences, photonics, electromagnetic technology, superconductivity, and electronic reliability/maintainability and testability.